The Geological Society of America
Special Paper 438
2008

The ancestral Cascades arc: Cenozoic evolution of the central Sierra Nevada (California) and the birth of the new plate boundary

Cathy J. Busby
Jeanette C. Hagan
Department of Earth Science, University of California, Santa Barbara, California 93106, USA

Keith Putirka
Department Earth and Environmental Sciences, California State University, Fresno, California 93710, USA

Christopher J. Pluhar
Department Earth Science, University of California, Santa Cruz, California 95064-1077, USA

Phillip Gans
Department of Earth Science, University of California, Santa Barbara, California 93106, USA

David L. Wagner
California Geological Survey, 801 K Street, Sacramento, California 95814-3500, USA

Dylan Rood
Steve B. DeOreo
Department of Earth Science, University of California, Santa Barbara, California 93106, USA

Ian Skilling
Department of Geology and Planetary Sciences, University of Pittsburgh, 200 SRCC, Pittsburgh, Pennsylvania 15260, USA

ABSTRACT

We integrate new stratigraphic, structural, geochemical, geochronological, and magnetostratigraphic data on Cenozoic volcanic rocks in the central Sierra Nevada to arrive at closely inter-related new models for: (1) the paleogeography of the ancestral Cascades arc, (2) the stratigraphic record of uplift events in the Sierra Nevada, (3) the tectonic controls on volcanic styles and compositions in the arc, and (4) the birth of a new plate margin.

Previous workers have assumed that the ancestral Cascades arc consisted of stratovolcanoes, similar to the modern Cascades arc, but we suggest that the arc was composed largely of numerous, very small centers, where magmas frequently leaked up strands of the Sierran frontal fault zone. These small centers erupted to produce andesite lava domes that collapsed to produce block-and-ash flows, which were reworked into paleocanyons as volcanic debris flows and streamflow deposits.

Busby, C.J., Hagan, J.C., Putirka, K., Pluhar, C.J., Gans, P., Wagner, D.L., Rood, D., DeOreo, S.B., and Skilling, I., 2008, The ancestral Cascades arc: Cenozoic evolution of the central Sierra Nevada (California) and the birth of the new plate boundary, *in* Wright, J.E., and Shervais, J.W., eds., Ophiolites, Arcs, and Batholiths: Geological Society of America Special Paper 438, p. XXX–XXX, doi: 10.1130/2008.2438(12). For permission to copy, contact editing@geosociety.org.

Where intrusions rose up through water-saturated paleocanyon fill, they formed peperite complexes that were commonly destabilized to form debris flows. Paleocanyons that were cut into Cretaceous bedrock and filled with Oligocene to late Miocene strata not only provide a stratigraphic record of the ancestral Cascades arc volcanism, but also deep unconformities within them record tectonic events.

Preliminary correlation of newly mapped unconformities and new geochronological, magnetostratigraphic, and structural data allow us to propose three episodes of Cenozoic uplift that may correspond to (1) early Miocene onset of arc magmatism (ca. 15 Ma), (2) middle Miocene onset of Basin and Range faulting (ca. 10 Ma), and (3) late Miocene arrival of the triple junction (ca. 6 Ma), perhaps coinciding with a second episode of rapid extension on the range front. Oligocene ignimbrites, which erupted from calderas in central Nevada and filled Sierran paleocanyons, were deeply eroded during the early Miocene uplift event. The middle Miocene event is recorded by growth faulting and landslides in hanging-wall basins of normal faults. Cessation of andesite volcanism closely followed the late Miocene uplift event.

We show that the onset of Basin and Range faulting coincided both spatially and temporally with eruption of distinctive, very widespread, high-K lava flows and ignimbrites from the Little Walker center (Stanislaus Group). Preliminary magnetostratigraphic work on high-K lava flows (Table Mountain Latite, 10.2 Ma) combined with new $^{40}Ar/^{39}Ar$ age data allow regional-scale correlation of individual flows and estimates of minimum (28,000 yr) and maximum (230,000 yr) time spans for eruption of the lowermost latite series. This work also verifies the existence of reversed-polarity cryptochron, C5n.2n-1 at ca. 10.2 Ma, which was previously known only from seafloor magnetic anomalies. High-K volcanism continued with eruption of the three members of the Eureka Valley Tuff (9.3–9.15 Ma). In contrast with previous workers in the southern Sierra, who interpret high-K volcanism as a signal of Sierran root delamination, or input of subduction-related fluids, we propose an alternative model for K_2O-rich volcanism.

A regional comparison of central Sierran volcanic rocks reveals their K_2O levels to be intermediate between Lassen to the north (low in K_2O) and ultrapotassic volcanics in the southern Sierra. We propose that this shift reflects higher pressures of fractional crystallization to the south, controlled by a southward increase in the thickness of the granitic crust. At high pressures, basaltic magmas precipitate clinopyroxene (over olivine and plagioclase) at their liquidus; experiments and mass-balance calculations show that clinopyroxene fractionation buffers SiO_2 to low values while allowing K_2O to increase. A thick crust to the south would also explain the sparse volcanic cover in the southern Sierra compared to the extensive volcanic cover to the north.

All these data taken together suggest that the "future plate boundary" represented by the transtensional western Walker Lane belt was born in the axis of the ancestral Cascades arc along the present-day central Sierran range front during large-volume eruptions at the Little Walker center.

Keywords: Cascades arc, Basin and Range, Sierra Nevada, latites, volcanic stratigraphy, paleomagnetism, magnetostratigraphy, geochronology.

INTRODUCTION

The Sierra Nevada is the longest and tallest mountain chain in the conterminous United States. It has also long been considered to be among the youngest, undergoing uplift through late Cenozoic tilting of a rigid block about faults along its eastern margin (Whitney, 1880; Lindgren, 1911; Christensen, 1966; Hamilton and Myers, 1966; Huber, 1981; Chase and Wallace, 1988; Unruh, 1991; Wakabayashi and Sawyer, 2001; Jones et al., 2004). More recent papers, however, have proposed a more complex uplift history for the Sierra Nevada, and some have argued for the antiquity of the range; these workers use different types of data sets, including U-Th-He thermochronology, fission-track analyses, paleobotanical studies, dating of cave sediments, oxygen isotope analysis of authigenic minerals, and analysis of relict landscape, to arrive at seemingly contradictory

models (Wolfe et al., 1997; House et al., 1998, 2001; Poage and Chamberlain, 2002; Horton et al., 2004; Stock et al., 2004; Clark et al., 2005; Cecil et al., 2006). Similarly, controversy abounds regarding the forces driving Cenozoic uplift, but possibilities include removal of a lithospheric root, passage of a slab window, upwelling asthenosphere, or surface uplift related to Basin and Range faulting (Ducea and Saleeby, 1998; Manley et al., 2000; Farmer et al., 2002; Saleeby and Foster, 2004; Clark et al., 2005; Le Pourhiet et al., 2006). Two major National Science Foundation (NSF) projects, the Sierra Nevada EarthScope Project and the Sierra Drip Continental Dynamics Project, are currently using dominantly geophysical techniques to understand the Sierra. However, some of the best constraints on our understanding of Sierran landscape evolution have come from field studies of dateable Cenozoic strata in the Sierra (Lindgren, 1911; Bateman and Wahrhaftig, 1966; Christensen, 1966; Huber, 1981, 1990; Axelrod, 1980; Unruh, 1991; Wakabayashi and Sawyer, 2001; Garside et al., 2005; Faulds et al., 2005). These Cenozoic strata were largely deposited and preserved within paleochannels or paleocanyons that crossed the present-day Sierra Nevada before Basin and Range faulting began there.

This paper summarizes the initial results of a multidisciplinary collaborative research project on Cenozoic volcanic and volcaniclastic rocks of the central Sierra Nevada. These rocks may have formed in response to a variety of events, including Cascadian subduction, hotspot magmatism, triple junction migration, Basin and Range extension, and Sierran root delamination (Fig. 1; McKee and Noble, 1976; Brem, 1977; Priest, 1979; Dickinson and Snyder, 1979; Glazner and Supplee, 1982; Christiansen et al., 1992; Wernicke et al., 1996; Ducea and Saleeby, 1996; Dickinson, 1997; Atwater and Stock, 1998; Ducea and Saleeby, 1998; Feldstein and Lange, 1999; Manley et al., 2000; Farmer et al., 2002; Stock et al., 2004; Saleeby and Foster, 2004; Jones et al., 2004; Busby et al., 2007; Garrison et al., this volume). However, prior to our work, very little was known about the spatial and temporal distribution and nature of Cenozoic magmatism in the central and northern Sierra Nevada. This gap in our understanding of western U.S. geology is particularly acute when the large volumes of well-preserved but poorly studied eruptive materials in the central and northern Sierra are compared with the small volumes of well-studied volcanic rocks in the southern Sierra.

We integrate new stratigraphic, structural, geochemical, geochronological, and magnetostratigraphic data on Cenozoic volcanic rocks in the central Sierra Nevada (Figs. 2 and 3) to address the following inter-related questions:

1. What can Neogene volcanic and intrusive rocks centers in the central Sierra Nevada tell us about the paleogeographic evolution of the ancestral Cascades arc?

Previous workers have assumed that the ancestral Cascades arc in the Sierra Nevada consisted of stratovolcanoes, similar to the modern Cascades arc, where dipping strata represent the eroded remnants of major edifices. However, we map dipping strata as slide sheets or growth-faulted strata (presented here), or small laccolithic structures (Roullet, 2006); we do not find the plumbing systems typical of stratovolcanoes. Instead, we suggest here that the arc consisted largely of numerous, very small centers, where magmas frequently leaked up strands of the Sierran frontal fault zone.

The possible controls of arc magmatism on Sierran uplift have not been evaluated, probably because so little was previously known about the arc. The Sierra Nevada are the ideal place to study the effects of volcanic arc initiation on continental crust, because the arc activity ceased within 10 m.y. of its birth here, so it is not heavily overprinted by intrusions or alteration.

2. What can Tertiary strata preserved in paleochannels tell us about the evolution of the central Sierran landscape, and how does its evolution compare with the rest of the range?

The geophysical and topographic expression of forces driving uplift are commonly transient, but the stratigraphic record is not. Sediments and the unconformities that divide them directly reflect surface conditions and thus provide the best possible record of landscape evolution. We use our preliminary data from paleochannels to propose that three episodes of Cenozoic uplift may have occurred in the central Sierra, corresponding to early Miocene onset of arc magmatism, middle Miocene onset of Basin and Range faulting, and late Miocene arrival of the triple junction.

3. What were the tectonic controls on volcanic styles and compositions in the arc?

We show here that the onset of Basin and Range faulting in the central Sierra coincided with the development of the only large center we identified within the andesite arc, a high-K volcanic center referred to as the Little Walker center (Noble et al., 1974; Priest, 1979). We report new $^{40}Ar/^{39}Ar$ and magnetostratigraphic age controls on the timing and duration of this volcanism, and we propose a new model for its petrogenesis. Previous workers have proposed that high-K volcanism in the Sierra records lithosphere delamination, or an arc-postarc transition through passage of the Mendocino triple junction (Manley et al., 2000; Farmer et al., 2002; Roelofs and Glazner, 2004). In our new model, a southward increase in crustal thickness, from Lassen to the southern Sierra, yields a southward increase in depths of magma stagnation (and therefore increased K_2O values) that is independent of time of eruption.

On the basis of preliminary structural work in the area, we propose that the Little Walker center formed at a releasing stepover on dextral transtensional faults at the western edge of the Walker Lane belt at its inception. We speculate that this fault system penetrated a lithospheric plate with a thick crustal section, tapping magmas generated at relatively great depths. If so, this high-K center records the birth of the future plate boundary.

CENOZOIC ROCKS OF THE SIERRA NEVADA

Early work in the central Sierra Nevada concluded that much of the Tertiary rock (gravels, volcanics, and volcaniclastics) were deposited into, and are preserved in, paleo-

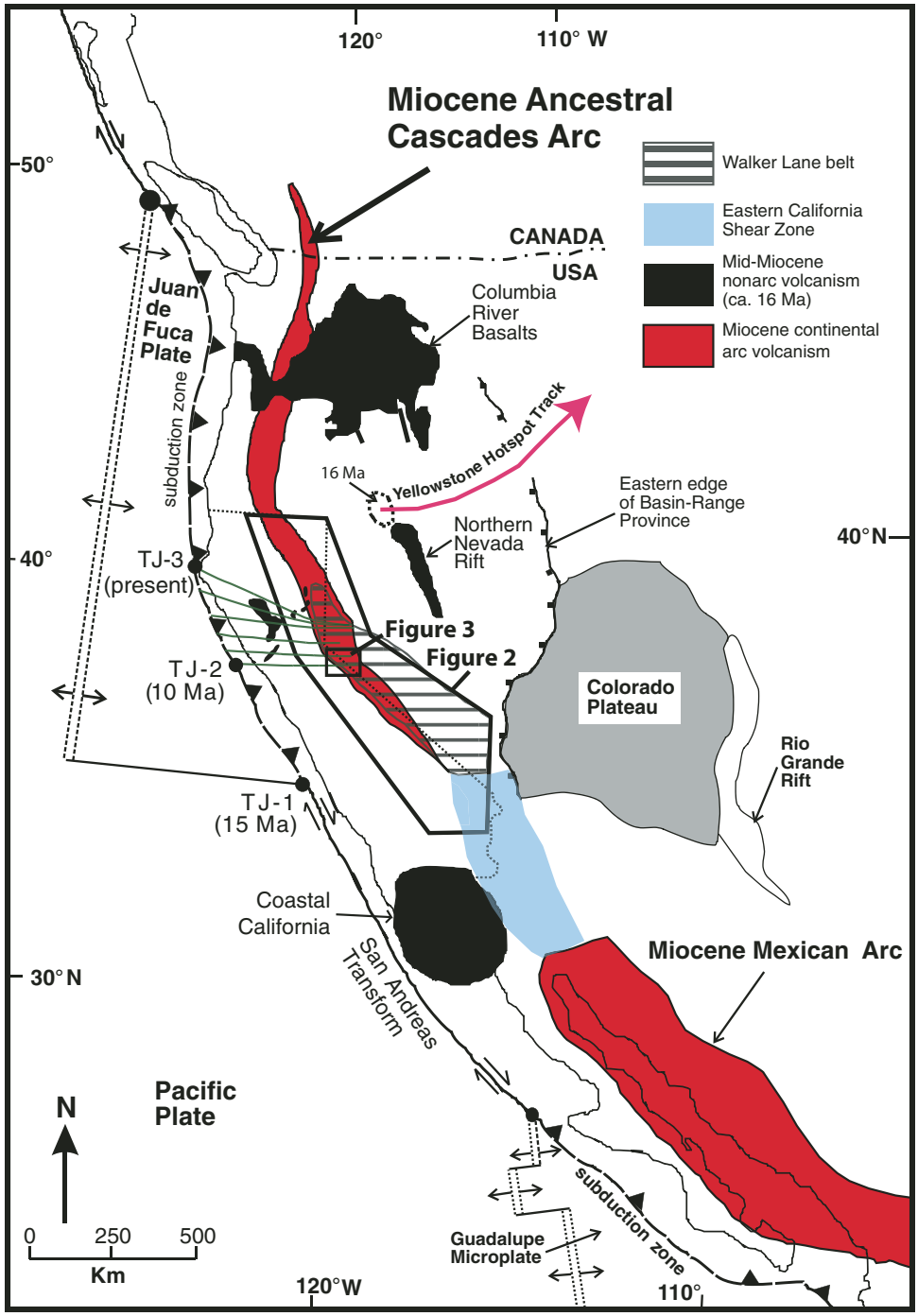

Figure 1. Palinspastic reconstruction of Miocene tectonic elements and magmatic provinces, modified after Dickinson (1997). Reconstruction depicts offshore ridge crests and transforms at ca. 16 Ma, with approximate positions of triple junction at 16 and 10 Ma (TJ-1 and TJ-2, respectively) (after Atwater and Stock, 1998). M—McDermitt caldera (of Snake River Plain–Yellowstone hotspot track, shown for reference). The segment of the ancestral Cascades described here (Fig. 2) is dominated by 14–6 Ma andesites (Fig. 3A) but also includes 10.3–9.2 Ma latitic (high-K trachyandesitic) volcanic rocks (Fig. 3B).

channels (Lindgren, 1911). Eocene paleochannel fill is present only in the lower reaches of the central Sierra and consists of "auriferous" river gravels (Lindgren, 1911). Oligocene paleochannel fill in the northern to central Sierra consists of silicic ignimbrites that originated from large calderas in present-day Nevada (Davis et al., 2000; Hinz et al., 2003; Faulds et al., 2005; Garside et al., 2005). Miocene paleochannel fill is composed of dominantly andesitic volcanic and volcaniclastic rocks, most of which (an estimated 620–1240 km^2) is preserved north of the Tuolumne River (Fig. 2; Curtis, 1954). Voluminous Miocene deposits accumulated in, and eventually buried, older bedrock river courses (Curtis, 1954; Wagner et al., 2000), causing many Miocene river channels to be cut into older Tertiary rocks rather than pre-Cenozoic basement rock. Miocene paleochannel fill of the central to northern Sierra Nevada is considered part of the ancestral Cascades arc (Fig. 1).

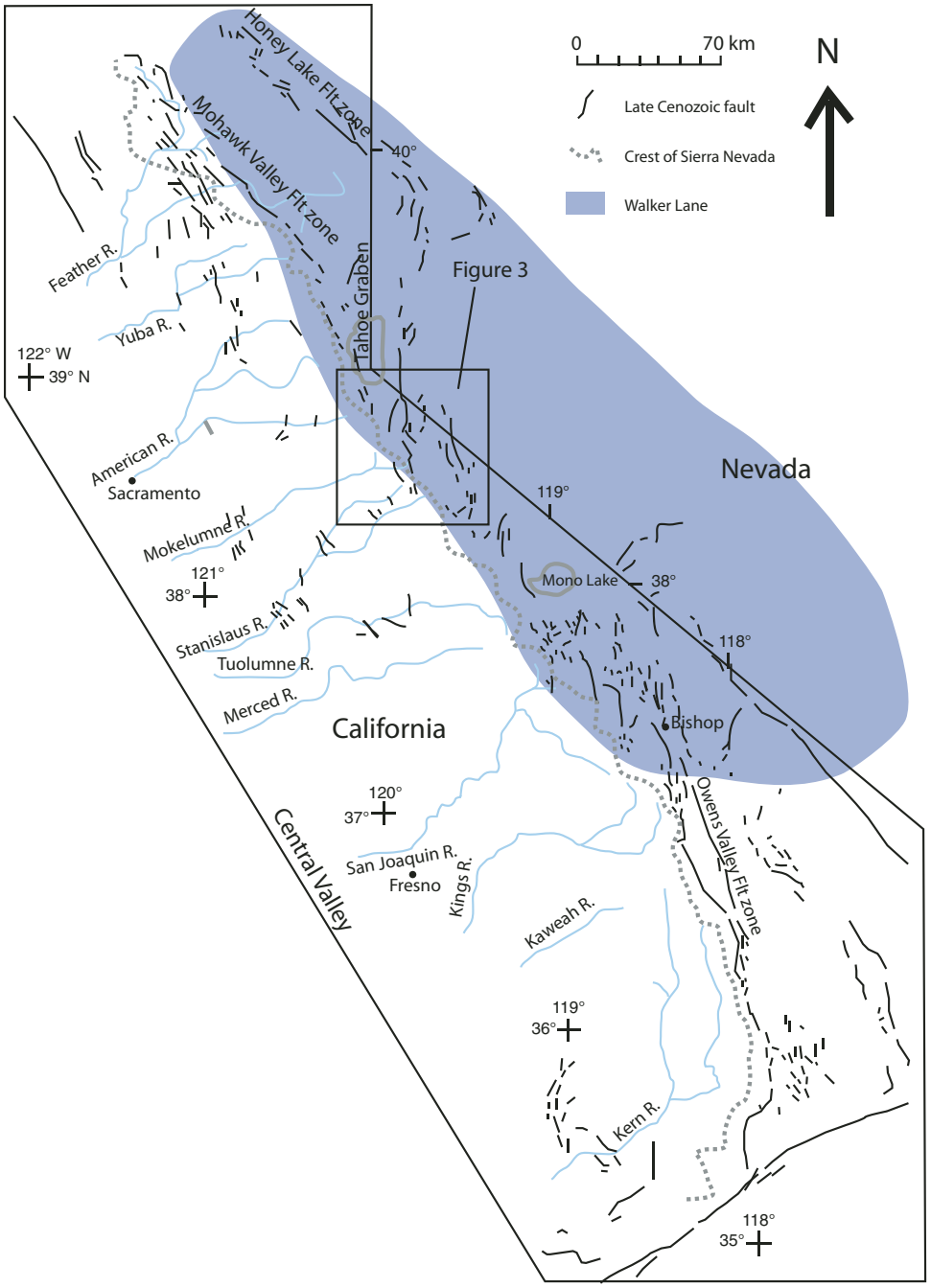

Figure 2. Generalized late Cenozoic fault map of the Sierra Nevada, modified from Wakabayashi and Sawyer (2001). Flt—fault.

Recent plate-tectonic reconstructions for the location of the migrating Mendocino fracture zone (Atwater and Stock, 1998) have suggested that subduction-related continental arc volcanism should have continued until ca. 10 Ma at the latitude of the central Sierra Nevada. Prior to our studies, however, there were very sparse age data on Miocene calc-alkaline intermediate volcanic rocks in the region. Only scattered K/Ar dates with relatively large errors existed for calc-alkaline and high-K volcanic rocks in the Sonora Pass to Ebbetts Pass area of the central Sierra (Dalrymple, 1963; Slemmons, 1966; Noble et al., 1974), and there were scattered K/Ar and $^{40}Ar/^{39}Ar$ ages on calc-alkaline volcanic rocks in adjacent parts of western Nevada (Golia and Stewart, 1984; John et al., 1999; Trexler et al., 2000; Castor et al., 2002). Our new $^{40}Ar/^{39}Ar$ age data, presented here and by Busby et al. (2007), suggest that arc magmatism in the central Sierra occurred from ca. 14 to 6 Ma.

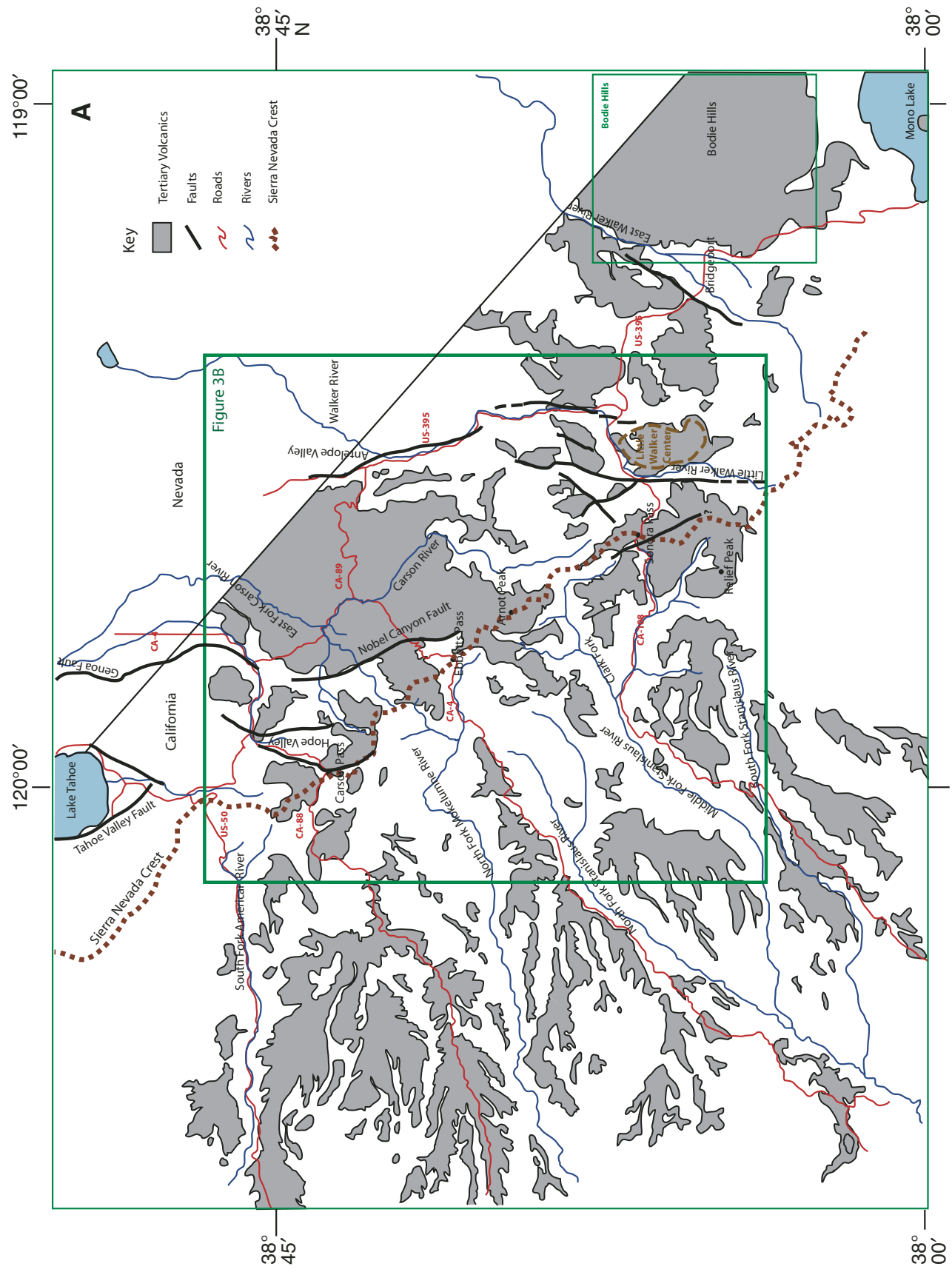

Figure 3 (*on this and following page*). (A) Distribution of Tertiary volcanic rocks in the central Sierra Nevada between Lake Tahoe and Bridgeport; localities described in text are shown here and in part B.

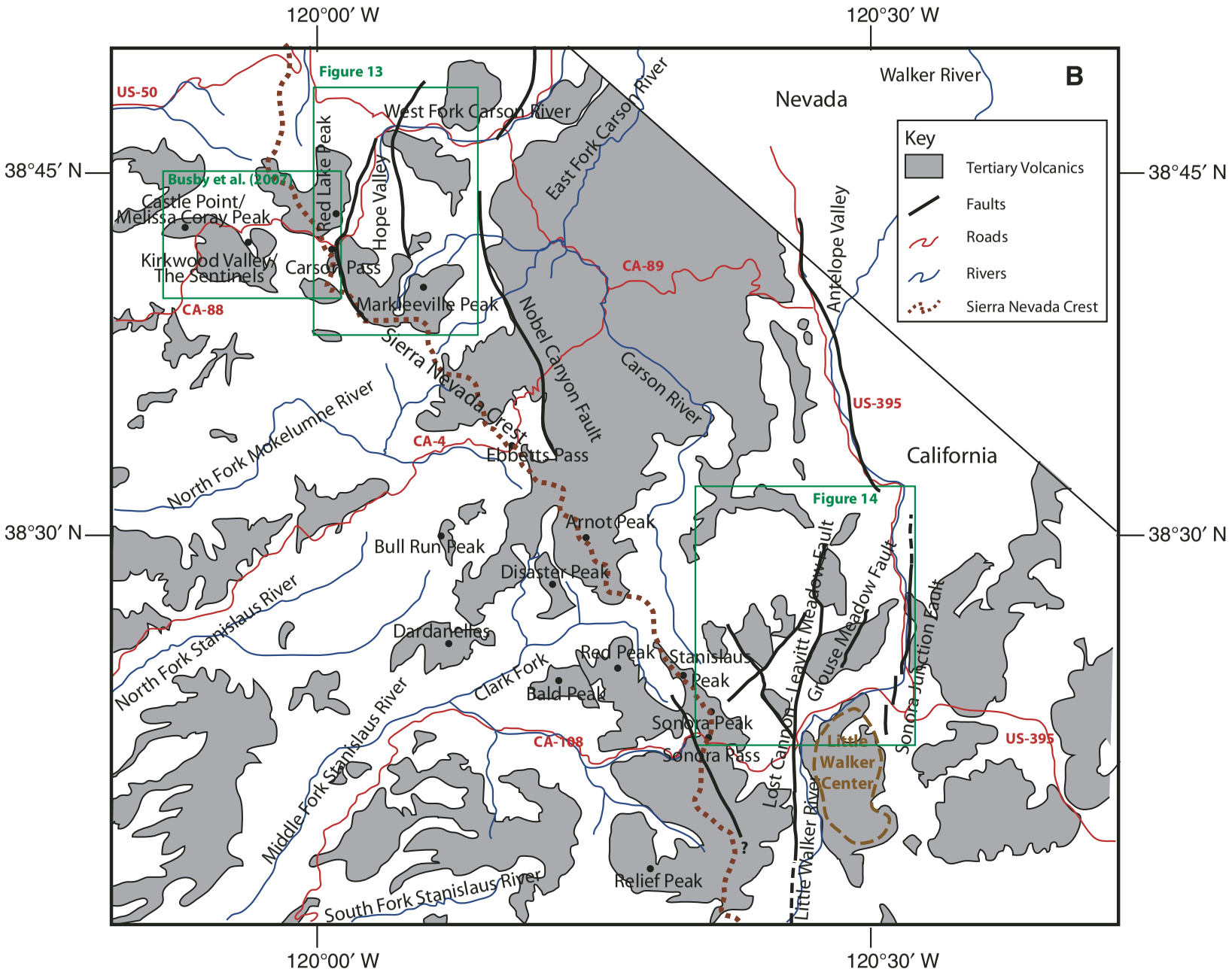

Figure 3 (*continued*). (B) Our work is concentrated along the range crest and range front between Carson Pass and Sonora Pass, where exposures are excellent and volcanic strata are abundant. The stratigraphy shown on Figure 4 is based on geologic mapping west of the modern crest, where strata are unfaulted (Carson Pass, box labeled Busby et al. 2007) to weakly faulted strata (Sonora Pass). Range front faults affect strata in the map areas shown in Figures 13 and 14.

STRUCTURAL SETTING OF THE MODERN SIERRA NEVADA

The modern Sierra Nevada lies within a microplate bounded to the west by the San Andreas fault and to the east by the Walker Lane belt, an ~150-km-wide belt of active seismicity along the western edge of the Great Basin (Figs. 1 and 2). The Walker Lane belt currently accommodates ~20%–25% of Pacific–North America plate motion (Bennett et al., 1999; Thatcher et al., 1999; Dixon et al., 2000; Oldow, 2000), and the Sierra Nevada block is currently moving 11–14 mm/yr toward the NW, in a more westerly direction than the trend of the Walker Lane belt and the Sierra Nevada frontal fault system (Dokka and Travis, 1990; Savage et al., 1990; Sauber et al., 1994). Much of the present-day to Quaternary displacement between the Sierra Nevada block and the rest of the Great Basin is being taken up along the western edge of the Walker Lane belt (Wallace et al., 1984; Eddington et al., 1987; Dokka and Travis, 1990; Dixon et al., 1995, 2000; Bennett et al., 1998; Thatcher et al., 1999; Oldow, 2003). The Sierra Nevada frontal fault zone lies at the westernmost margin of the Walker Lane belt (Figs. 1 and 2; Wakabayashi and Sawyer, 2001; Schweickert et al., 1999, 2000, 2004).

The eastern escarpment of the Sierra Nevada forms the boundary between the Basin and Range Province and the unextended Sierran block (Fig. 2), and it is one of the most prominent topographic and geologic boundaries in the Cordillera (Surpless et al., 2002). This boundary is relatively simple, straight, and narrow along the southern Sierra Nevada range front fault zone (Owens Valley fault zone, Fig. 2), but it becomes more complex in the central Sierra (between Bishop and Lake Tahoe, Fig. 2). There, it has been interpreted to form a northwest-trending zone of en echelon escarpments produced by normal or oblique faulting (Wakabayashi and Sawyer, 2001; Schweickert et al., 2004), and it has focal plane mechanisms suggestive of oblique normal faulting (Unruh et al., 2003).

The structural nature of the transition between the Basin and Range and the Sierran physiographic provinces has been investigated in detail in the southern Sierra (Jones and Dollar, 1986; Jones et al., 1994; Wernicke et al., 1996), although the long-term history of this segment is not well understood because Neogene volcanic rocks are generally lacking there. The long-term history of the northern transition zone is better understood where it has been studied in detail at the latitude of Lake Tahoe (Schweickert et al., 1999, 2000, 2004; Surpless et al., 2002). An ~110-km-long, E-W transect there shows that Basin and Range extension has encroached ~100 km westward into the former Sierran magmatic arc since the middle Miocene, along east-dipping normal faults that have accommodated >150% extension in the east (Surpless et al., 2002). In the west, the Genoa fault forms the east boundary of the Carson Range (Figs. 2 and 3) and records <10% extension (Surpless et al., 2002). The Carson Range locally contains west-tilted volcanic strata (Schweickert et al., 2000), but Tertiary strata useful for determining direction and timing of tilting are missing in much of the range. However, Surpless et al. (2002) modeled thermochronological data to infer a 15°W tilting of the Carson Range, between ca. 10 and 3 Ma. This supports the model that the Tahoe-Truckee depression is an asymmetric half graben bounded by the West Tahoe fault on the west side of the depression (Figs. 2 and 3; Lahren and Schweickert, 1995; Schweickert et al., 1999, 2000, 2004). This estimate for the timing of extension also broadly agrees with estimates that make use of Tertiary strata just to the north of the Carson range and the Tahoe-Truckee area, where a small-magnitude extensional episode occurred at ca. 12 Ma and significant extension began at ca. 3 Ma (Henry and Perkins, 2001).

The transition zone between the Basin and Range and the central Sierra had not been mapped and dated prior to our study. The central Sierra Nevada is ideal for determining the long-term history of the range front faults because it contains an areally extensive, dateable Neogene volcanic-volcaniclastic stratigraphy.

STRATIGRAPHIC FRAMEWORK FOR THE CENTRAL SIERRA NEVADA

Since the groundbreaking work of Ransome (1898), described further later in this paper, strata of the central Sierra have been little studied. Previous work in the Carson Pass to Ebbetts Pass area includes the Ph.D. research of Curtis (1951), the 1:62,500 Freel Peak quadrangle (Armin et al., 1984) and 1:62,500 Markleeville quadrangle (Armin et al., 1984), and an M.S. thesis in the Markleeville Peak area (Mosier, 1991). Previous work in the Sonora Pass to Ebbetts Pass area includes the research of Slemmons (1953, 1966, 1975), the 1:62,500 Carson-Iceberg Wilderness Map (Keith et al., 1982), and 15′ reconnaissance maps by Giusso (1981) and Huber (1981), and research largely to the east of Sonora Pass by Brem (1977) and Priest (1979). These previous workers grouped diverse volcanic-volcaniclastic and subvolcanic lithofacies into groups, formations, tuffs, and flows (Fig. 4), the ages of which were poorly determined by scattered K/Ar dates with relatively large uncertainties (Dalrymple, 1963; Slemmons, 1966; Noble et al., 1974). We follow their terminology because it is widely used in the literature.

Miocene andesitic volcanic and volcaniclastic rocks of the central Sierra Nevada are commonly referred to as the Merhten Formation (Fig. 4B; Piper et al., 1939; Curtis, 1951, 1954). In the Sonora Pass region, however, distinctive high-K volcanic rocks, referred to as the Stanislaus Group, lie within the andesite section (Fig. 4B); the underlying andesites are referred to as the Relief Peak Formation, and the overlying andesites are referred to as Disaster Peak Formation (Fig. 4B; Slemmons, 1953, 1966). Although this nomenclature works well where the high-K volcanic rocks are present, we recognize no distinction between the Relief Peak and Disaster Peak Formations that can be made on lithologic, mineralogic, or geochemical grounds. On the basis of our work in this and adjacent regions, we believe that the distinction between the Relief Peak Formation and Disaster Peak Formation can only made by reference to its stratigraphic or intrusive position relative to the Stanislaus Group. For example,

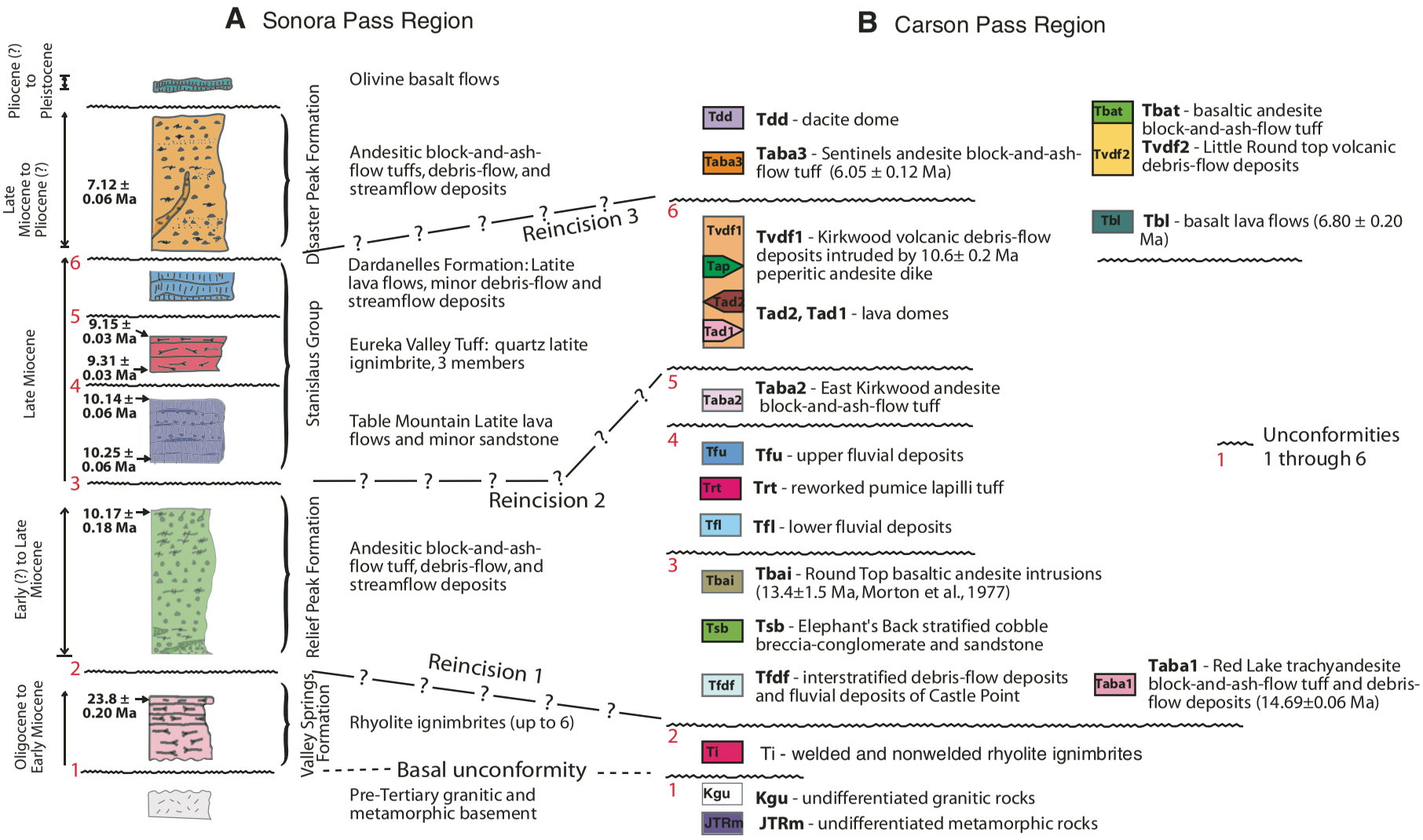

Figure 4. Generalized lithostratigraphic columns showing Tertiary volcanic rocks of the central Sierra Nevada. (A) Sonora Pass region: stratigraphic nomenclature of Slemmons (1953, 1966) and Brem (1977), where high-K volcanic rocks (Stanislaus Group) intervene between Miocene andesites of the Relief Peak Formation (below) and the Disaster Peak Formation (above). Shown here are new lithofacies interpretations (Figs. 5, 6, 7, 8, and 9) and $^{40}Ar/^{39}Ar$ ages (Fig. 11). (B) Carson Pass region: undivided strata of the Miocene Mehrten Formation (Curtis, 1954) between the Sierran crest and the Kirkwood Valley (Fig. 3) are here divided into lithofacies, using detailed mapping and $^{40}Ar/^{39}Ar$ ages presented in Busby et al. (2007). Basal Oligocene ignimbrites in the Sonora Pass area are referred to as Valley Springs Formation (Slemmons, 1953, 1966) and correlated with basal ignimbrites at Carson Pass. Mappable erosional unconformities between map units are recognized and numbered on both columns. Tentative correlations of the three deepest unconformities are given here, labeled reincision 1, 2, and 3.

rocks at Ebbetts Pass that have no demonstrated stratigraphic relation to the high-K rocks were referred to as Relief Peak Formation by Armin et al. (1984), even though they reported K/Ar dates similar to those of the Disaster Peak Formation. We therefore refer to those rocks, and to all andesites of the central Sierra Nevada that do not lie in stratigraphic continuity with the high-K volcanic rocks, as Merhten Formation (Fig. 4). Even in areas where Stanislaus Group is present, careful mapping must be done to distinguish Relief Peak Formation from Disaster Peak Formation where contact relations are complicated by paleotopographic effects, faults, or intrusions.

For the Sonora Pass region, we follow the stratigraphy defined by previous workers (Fig. 4A; Slemmons, 1953, 1966; Brem, 1977), even though the names do not all follow stratigraphic code, because this stratigraphy is firmly established in the literature, and it is useful. All the unconformities and their correlations (Figs. 4A and 4B) are proposed here on the basis of our mapping and dating. Basal Oligocene ignimbrites, widely referred to as Valley Springs Formation, are cut by a deep erosional unconformity that we refer to as reincision 1 (Fig. 4A). Overlying andesitic rocks of the Relief Peak Formation are in turn cut by a deep erosional and, in places, angular unconformity (reincision 2) below high-K volcanic rocks of the Stanislaus Group. The Stanislaus Group includes the Table Mountain Latite, the Eureka Valley Tuff, and the Dardanelles Formation, all separated by minor erosional unconformities. The Stanislaus Group is in turn cut by a deep erosional unconformity (reincision 3) that is overlain by the andesitic Disaster Peak Formation (Fig. 4A). Correlations of unconformities between the Sonora Pass and Carson Pass areas, and their significance, are discussed later.

The Stanislaus Group at Sonora Pass forms the type localities for "latite" and "quartz latite," as defined by Ransome (1898). The geochemistry and K/Ar geochronology of the Stanislaus Group were described by Noble et al. (1976). The Table Mountain Latite lava flows have distinctive large plagioclase with sieved textures, plus or minus large augite crystals (Ransome, 1898). The Eureka Valley Tuff consists of three mineralogically distinctive welded to nonwelded ignimbrites, referred to as members by Slemmons (1966; Fig. 4A). The Eureka Valley Tuff is described geochemically as quartz latite by Ransome (1898) and Noble et al. (1974, 1976) but plots in the trachyandesitic to trachydacitic fields of Le Bas et al. (1986) (Brem, 1977; Priest, 1979). It is inferred to have erupted from the Little Walker caldera (Fig. 3B; Noble et al., 1974), which we refer to here as the Little Walker center because we do not believe it has been proven to be a caldera. The Dardanelles Formation is defined as latitic volcanic and volcaniclastic rocks that overlie the Eureka Valley Tuff (Slemmons, 1953, 1966; Fig. 4A).

In this paper, we describe and interpret the lithofacies "building blocks" that make up the previously defined formations of the central Sierra Nevada (Figs. 5, 6, 7, 8, 9, and 10). We also emphasize the importance of erosional unconformities by numbering the major unconformity surfaces that bound the formations (Fig. 4). Additional erosional unconformities are also locally obvious between lithofacies, or between members within formations. We use unconformity surfaces as sequence boundaries without specifying a mechanism for their formation (e.g., Pekar et al., 2003; Bassett and Busby, 2005; Busby and Bassett, 2007), such as tectonics, base-level change, or climate change. It is impossible to map within these subaerially deposited volcanic-volcaniclastic successions without mapping the obvious, deep erosional unconformity surfaces that divide the strata into distinct packages. We further contribute to the stratigraphic framework by reporting new $^{40}Ar/^{39}Ar$ dates (Fig. 11) and new magnetostratigraphic data (Fig. 12).

LITHOFACIES DATA

Before the present study, most of the volcanic-volcaniclastic rocks of this area were undivided, and, in some instances, those that were divided were misidentified (e.g., intrusions were interpreted to be lava flows, block-and-ash-flow tuffs were called debris-flow deposits, sedimentary breccias were called volcanic rocks, and so on). For this reason, we give very detailed criteria for recognition of lithofacies present in the ancestral Cascades arc and believe that this will be useful to other workers in arc terranes. The volcanic-volcaniclastic terminology used in this paper largely follows that of Fisher and Schmincke (1984), Heiken and Wohletz (1985), and Sigurdsson et al. (2000). Lithofacies names are assigned based on mineralogy and/or chemical compositions, depositional structures and textures, and inferred volcanic or sedimentary eruptive and depositional processes. The mineralogy of these lithofacies is based on visual examination of about three-hundred thin sections by the first author; the geochemistry of selected samples is described in a following section.

Ignimbrites of the Valley Springs Formation form the oldest strata along the central Sierran crest (Figs. 4A and 4B), so those are briefly described first. Andesite lithofacies are described second; except for minor interstratified basalts, these make up all of the Merhten, Relief Peak, and Disaster Peak Formations. Lithofacies of the high-K Stanislaus Group (Fig. 4) are described next, in order to point out how they differ from the andesites. Basalt lava flows, though rare, occur within all the andesitic formations as well as the high-K section, so they are described last. Chemical compositions are described later.

The geographic distribution of each lithofacies is included in its description in this section (with reference to Fig. 3B), and in the last section, we integrate these data with geochronological, magnetostratigraphic, geochemical, and structural data (Figs. 11, 12, 13, 14, 15, and 16) to provide a preliminary paleogeographic and tectonic reconstruction of the ancestral Cascades arc in the central Sierra Nevada (Fig. 17). Lithofacies descriptions and interpretations are based on detailed mapping at Carson Pass, both west of the crest (Busby et al., 2007) and east of it (Fig. 13), on Busby's unpublished reconnaissance mapping at Ebbetts Pass, on Busby and Rood's unpublished mapping west of the crest at Sonora Pass, and on mapping east of the crest at Sonora Pass (Fig. 14).

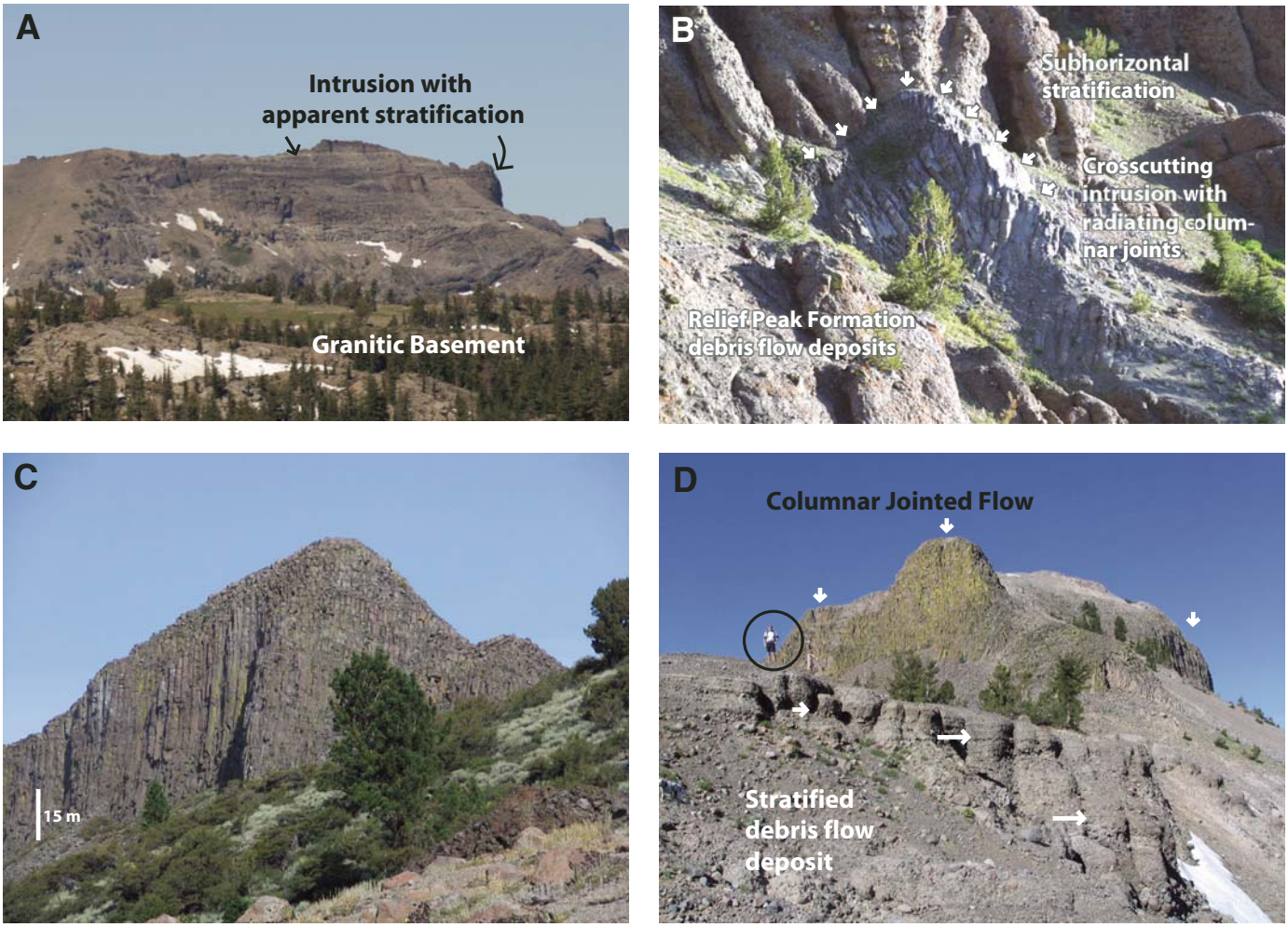

Figure 5 (*on this and following page*). Photographs of intrusive and lava-flow lithofacies. Geographic localities are labeled on Figure 3B. (A) At a distance, this intrusion appears to be stratified, but it is composed entirely of homogeneous, massive intrusive hornblende andesite (southern spur of Round Top, the Sisters, Carson Pass area). (B) Small andesite intrusion crosscutting nearly flat-lying debris-flow deposits, with columnar joints perpendicular to the boundaries of the intrusive body (height of tree in center of photo is ~5 m). Debris-flow deposits are Relief Peak Formation on the west flank of the Sonora Peak–Stanislaus Peak ridge (Fig. 14). (C) Columnar jointed plug, Picket Peak; map relations (Fig. 13) indicate that this crosscuts debris-flow deposits (not visible in this photo). (D) Erosional remnant of a columnar jointed lava flow, forming Bull Run Peak (Ebbetts Pass area). Map relations cannot be used to determine an intrusive versus extrusive relationship with debris-flow deposits (foreground), but the basal contact consists of a laterally persistent flow breccia. Person for scale.

Valley Springs Formation (Rhyolite Ignimbrites)

The Oligocene(?)–early Miocene Valley Springs Formation consists of up to three to four petrographically distinctive silicic welded to nonwelded ignimbrites (Slemmons, 1953; Mosier, 1991; Busby et al., 2007). They consist of pumice lapilli and lesser lithic fragments set in a groundmass of vitric tuff, with less than 15% quartz, 1%–10% sanidine, and 1%–15% plagioclase crystals. Welded ignimbrites have flattened pumices (fiamme) and sintered bubble-wall shards, and locally are columnar jointed, with basal vitrophyres. The ignimbrites are generally poorly exposed and occur as deeply incised erosional remnants on the walls or floors of paleocanyons.

In the Carson Pass region, basal ignimbrites occur on the floor of the Carson Pass–Kirkwood paleocanyon (Busby et al., 2007), where they are discontinuously exposed along the north side of the modern Kirkwood Valley, west of the modern Sierran crest (Fig. 3). This paleocanyon is inferred to branch up the paleocurrent direction into two tributary paleocanyons that lie east of the modern crest, as discussed next. The southern of these two tributary paleocanyons (Fig. 13) contains basal ignimbrites as well, although they are intruded by sills emanating from the Markleeville intrusion.

In the Sonora Pass region west of the modern range crest, ignimbrites form part of the lower slopes of the Dardanelles (Fig. 4B) and are overlain by the Relief Peak Formation and

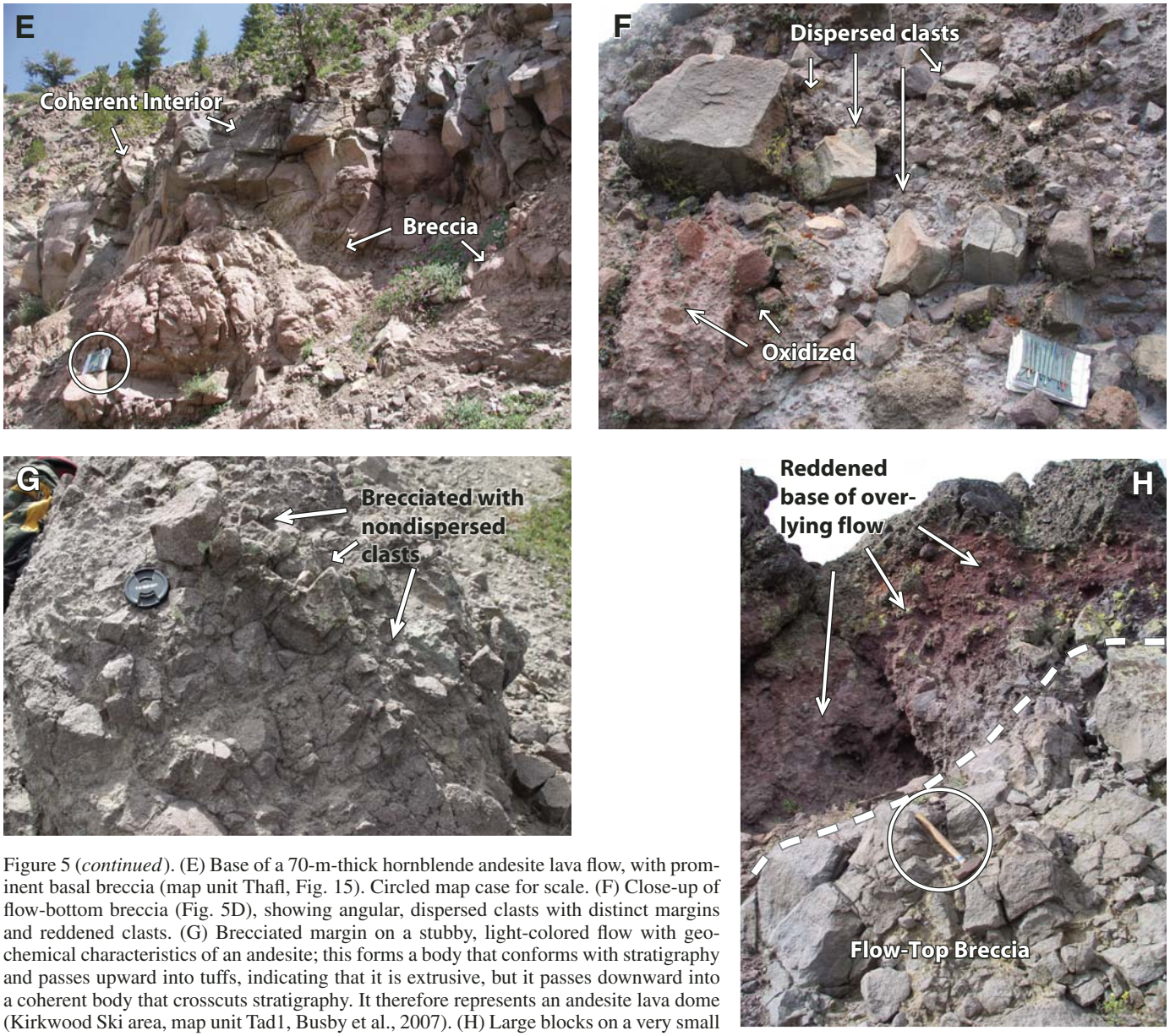

Figure 5 (*continued*). (E) Base of a 70-m-thick hornblende andesite lava flow, with prominent basal breccia (map unit Thafl, Fig. 15). Circled map case for scale. (F) Close-up of flow-bottom breccia (Fig. 5D), showing angular, dispersed clasts with distinct margins and reddened clasts. (G) Brecciated margin on a stubby, light-colored flow with geochemical characteristics of an andesite; this forms a body that conforms with stratigraphy and passes upward into tuffs, indicating that it is extrusive, but it passes downward into a coherent body that crosscuts stratigraphy. It therefore represents an andesite lava dome (Kirkwood Ski area, map unit Tad1, Busby et al., 2007). (H) Large blocks on a very small (less than 100 m diameter) andesite lava dome, with a coherent base that crosscuts strata (not shown); circled hammer for scale; northeast face of Red Lake Peak.

Stanislaus Group, likely defining a paleocanyon there. On the south flank of Red Peak (Fig. 3B), ignimbrites are very well exposed along steps high on the paleocanyon wall that follow joints in the granite basement. In the Sonora Pass region east of the modern range crest, ignimbrites occur at the base of the paleocanyon fill east of the Leavitt Meadow–Lost Cannon fault (Fig. 14). They have also been mapped beneath the Relief Peak Formation east of the Grouse Meadow fault by Priest (1979), but we reinterpret those ignimbrites as avalanche slabs within debris-flow deposits of the Relief Peak Formation; these also occur within the Relief Peak Formation in the hanging-wall basin of the Leavitt Meadow–Lost Cannon fault (Fig. 14). As discussed later, we recognize widespread avalanche deposits at the top of the Relief Peak Formation in the Sonora Pass area.

Merhten Formation, Relief Peak Formation, and Disaster Peak Formation (Andesite Volcanic-Volcaniclastic Rocks)

Lithofacies within the Merhten Formation (Fig. 4B) and the Relief Peak and Disaster Peak Formations (Fig. 4A) are andesites or clastic rocks composed entirely of andesite detritus, except for sparse granitic basement clasts and rare basalt lava flows

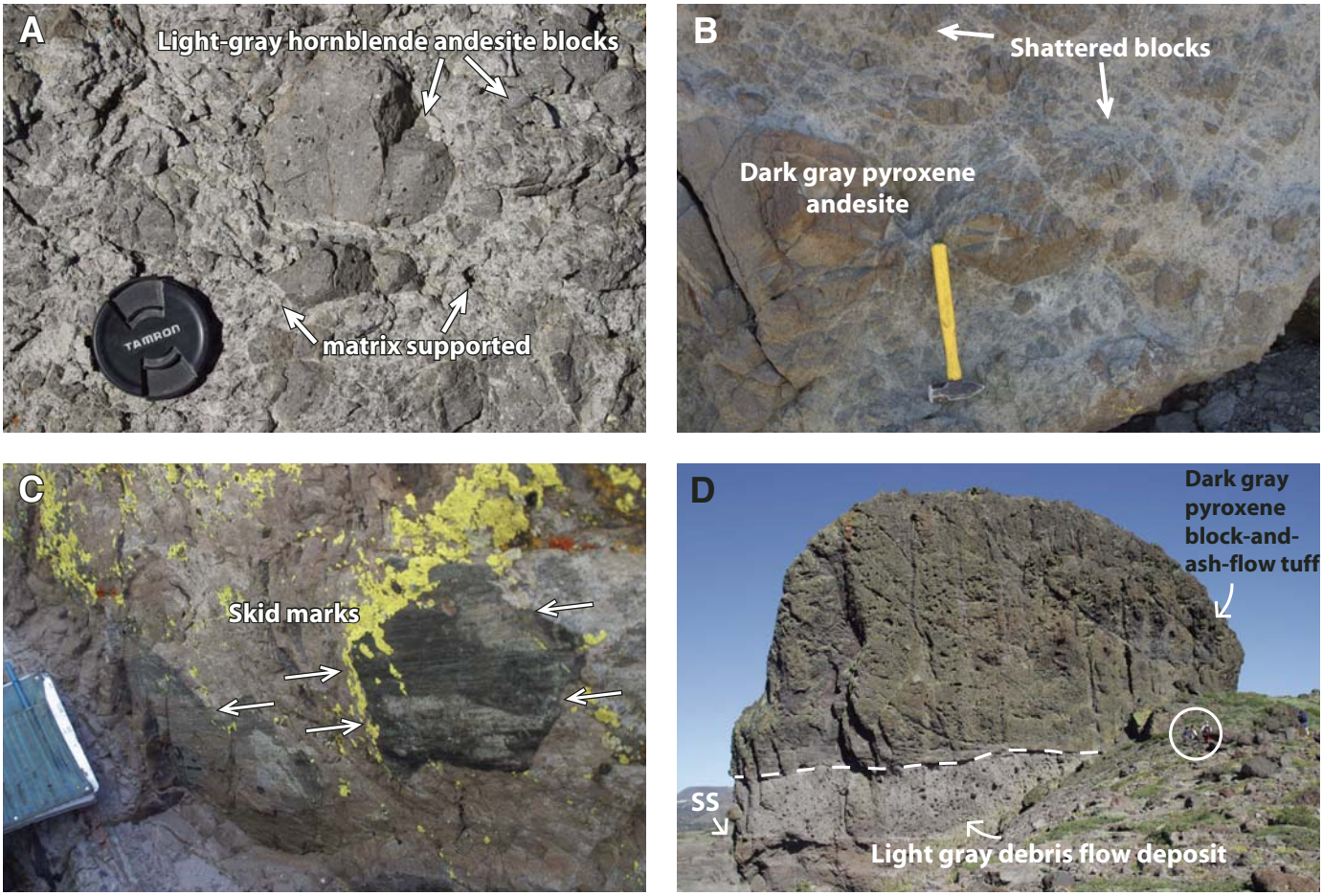

Figure 6. Photographs of block-and-ash-flow tuff lithofacies. Geographic localities are labeled on Figure 3B. (A) Block-and-ash-flow tuff interfingering with andesite lava dome deposits, Kirkwood Ski area (map unit Tad2 of Busby et al., 2007; lens cap for scale), showing typical matrix-supported deposit of unsorted, angular, monomict andesite. (B) Sentinels block-and-ash-flow tuff at Melissa Corey Peak, showing shattering of blocks, typical of hard-rock avalanches in general. (C) "Skid marks" on the base of the Sentinels block-and-ash-flow tuff at Melissa Corey Peak (pen for scale). (D) Heterogeneous volcanic debris-flow deposit overlain by more homogeneous block-and-ash-flow tuff on The Sentinels, above Kirkwood Ski area (Carson Pass; ss—sandstone interbed). People circled for scale.

(described later). Previous workers largely divided andesites of the area into intrusions and strata, in places incorrectly, and most of the andesitic strata were lumped together as "breccias." In this section, we show how these "breccias" can be divided into several mappable lithofacies, which can then be used to reconstruct the paleogeography and structure of the region.

Plagioclase is commonly the most abundant phenocryst phase, followed by hornblende and/or clinopyroxene, and, less commonly, orthopyroxene. Biotite occurs rarely in extrusive rocks, although it is present in some intrusions (Fig. 15). Some rocks are aphyric and therefore are only tentatively included in the andesites. Rocks bearing olivine are described under basalts in a subsequent subsection.

Lithofacies within the Merhten, Relief Peak, and Disaster Peak Formations include nonfragmental rocks, interpreted as intrusions and flows (Fig. 5); monomict fragmental rocks, interpreted as flow breccias and block-and-ash-flow tuffs (Fig. 6); and polylithic andesite fragmental rocks, interpreted as debris-flow, debris-avalanche, and fluvial deposits (Figs. 7 and 8). These lithofacies interfinger laterally and repeat vertically, so they cannot be described in order of relative age. Instead, we describe them in order of inferred vent-proximal to vent-distal settings, and then we describe avalanche deposits, which are important at the top of the Relief Peak Formation in the Sonora Pass area.

Hypabyssal Intrusions and Lava Flows

It can be extremely difficult to distinguish between intrusions and lava flows in the stratigraphic record, so these two lithofacies are described together in order to highlight the differences between them. It is important to be able to distinguish between them because lavas can flow large distances from the vent, particularly if they are basaltic andesites or basalts. Intrusions mark the sites of vents, and their chemistry can be used to infer mantle and crustal magma genesis processes directly beneath the site.

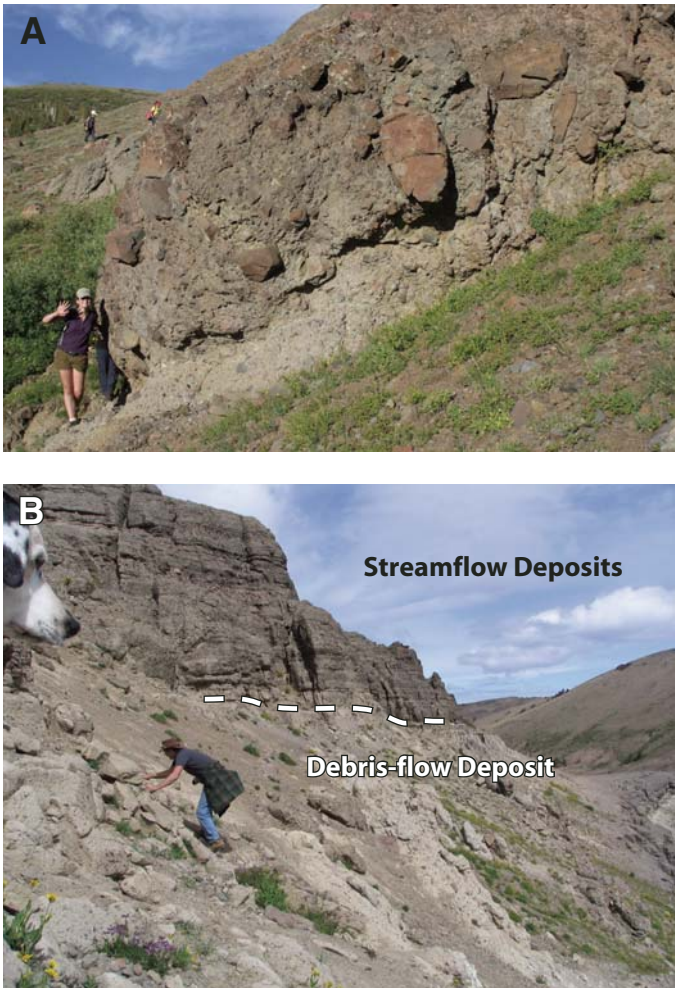

Figure 7. Photographs of debris-flow lithofacies. Geographic localities are labeled on Figure 3B. (A) Massive, very poorly sorted andesite clast debris-flow deposits. This forms part of a nonstratified accumulation >200 m thick that fills an E-W–trending paleochannel (1 km north of St. Mary's Pass near Sonora Pass). (B) Massive debris-flow deposit (bottom half) overlain by stratified fluvial deposits. The massive debris-flow deposit has a higher proportion of sandstone matrix than that shown in A and is thus less resistant (Merhten Formation north of Red Lake Peak). (C) Jointed block in a debris-flow deposit, suggesting that the debris flow was fed by, or minimally reworked from, a block-and-ash flow (Relief Peak Formation at Grouse Meadow, see Fig. 17).

Intrusions are easiest to recognize when they are large, wholly coherent (i.e., nonfragmental) bodies, with no internal stratification. A massive, nonlayered intrusion, however, may pass laterally into a body with well-developed layering that can, from a distance, be mistaken for multiple flows, when it is in actuality merely the product of flow banding or jointing within an intrusion (Fig. 5A). For example, a cliff and bench topography on the north face of Markleeville Peak (locality shown on Fig. 3B) was interpreted by Mosier (1991) to represent multiple lava flows, but closer examination shows the peak to be a single massive intrusion (discussed later). A further difficulty in recognizing intrusions is that they may have fragmental textures, although the fragments commonly have indistinct margins. It is easier to discern crosscutting relations and columnar joints oriented perpendicular to intrusive contacts on the outcrop scale (Fig. 5B) than it is on the map scale (Fig. 5C). Plugs and volcanic necks are generally thicker and less aerially extensive than lava flows (Fig. 5C), but lava flows may be ponded (e.g., in a paleocanyon); when these are preserved as erosional remnants on modern peaks and ridges, they appear to be plugs unless their basal contact is examined in detail (Fig. 5D). If the body has a basal flow breccia, this is evidence for an extrusive origin; however, basal flow breccias may be thin (<0.5 m) and laterally discontinuous. Many flows, however, completely lack breccias along their bases or tops, and contacts between flows may be marked only by subtle features like vesiculation horizons; these must be mapped out and shown to be horizontal and continuous because some of the hypabyssal intrusions have lenticular flat vesicular horizons. Lava flows may be misidentified as intrusions if they appear to crosscut stratigraphy, when in fact they have infilled a complex paleotopography; this may even include infilling of undercut channel reaches (Garrison et al., this volume).

Fortunately, most andesite lava flows are easily identified by their coherent interiors sandwiched between thick flow-top and flow-bottom breccias (Figs. 5E and 5F). Flow breccia clasts do not have jigsaw textures, but they do have more distinct edges and are more dispersed than is typical of brecciated intrusions. Reddened clasts are also typical of extrusive breccias (Fig. 5F).

Some of the andesite flows map out as thick, short bodies with an aspect ratio (height to lateral extent) of less than 1:10 and are light in color (Figs. 5G and 5H); for these reasons, we called them dacites in the field, but they are geochemically all andesites (described later). These commonly map continuously

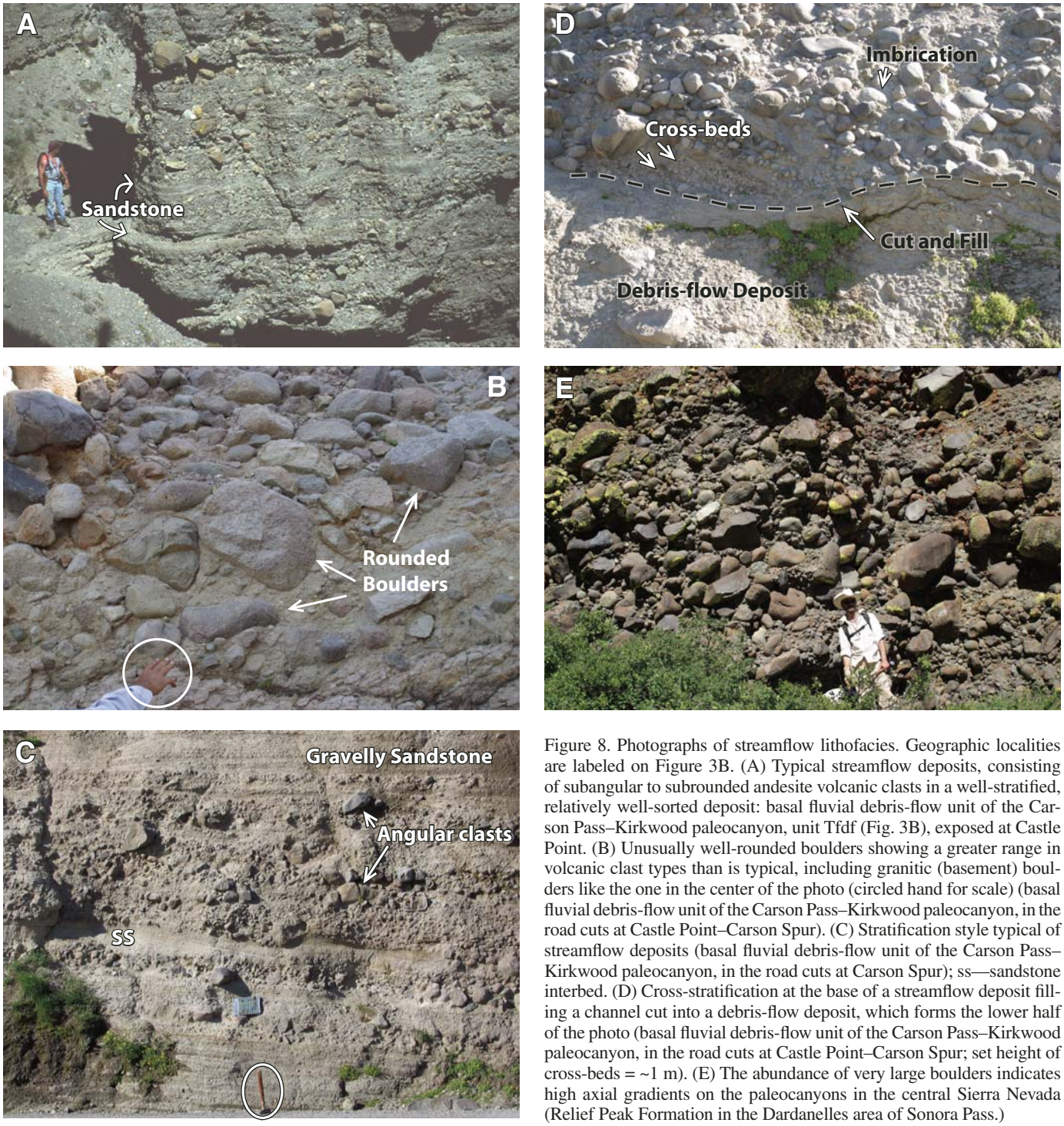

Figure 8. Photographs of streamflow lithofacies. Geographic localities are labeled on Figure 3B. (A) Typical streamflow deposits, consisting of subangular to subrounded andesite volcanic clasts in a well-stratified, relatively well-sorted deposit: basal fluvial debris-flow unit of the Carson Pass–Kirkwood paleocanyon, unit Tfdf (Fig. 3B), exposed at Castle Point. (B) Unusually well-rounded boulders showing a greater range in volcanic clast types than is typical, including granitic (basement) boulders like the one in the center of the photo (circled hand for scale) (basal fluvial debris-flow unit of the Carson Pass–Kirkwood paleocanyon, in the road cuts at Castle Point–Carson Spur). (C) Stratification style typical of streamflow deposits (basal fluvial debris-flow unit of the Carson Pass–Kirkwood paleocanyon, in the road cuts at Carson Spur); ss—sandstone interbed. (D) Cross-stratification at the base of a streamflow deposit filling a channel cut into a debris-flow deposit, which forms the lower half of the photo (basal fluvial debris-flow unit of the Carson Pass–Kirkwood paleocanyon, in the road cuts at Castle Point–Carson Spur; set height of cross-beds = ~1 m). (E) The abundance of very large boulders indicates high axial gradients on the paleocanyons in the central Sierra Nevada (Relief Peak Formation in the Dardanelles area of Sonora Pass.)

inward and downward into coherent intrusions, so we refer to them as lava domes (Figs. 5G and 5H).

The andesite lava domes show complete lateral gradation from flow breccia (Fig. 5G) to hot block avalanche deposits (Fig. 5H) to block-and-ash-flow tuffs (Fig. 6), with shattered clasts encased in a lapilli-to-ash–sized matrix of the same composition.

Block-and-Ash-Flow Tuffs

Block-and-ash-flow tuffs are small-volume pyroclastic flow deposits characterized by dense to moderately vesicular juvenile blocks supported in a massive, unsorted, medium- to coarse-ash matrix of the same composition (Fig. 6A). Shattered blocks with "jigsaw" texture are common in block-rich

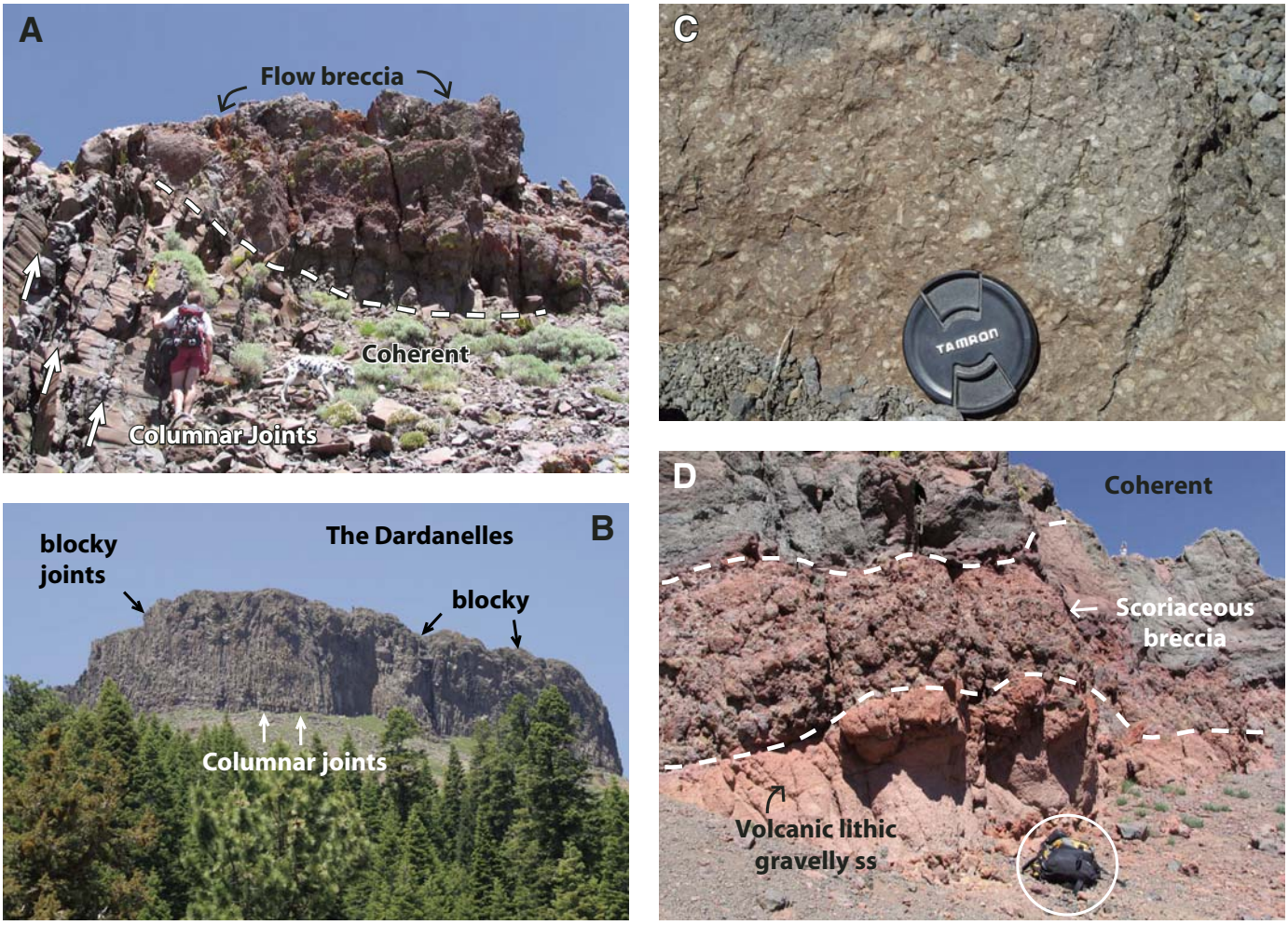

Figure 9 (*on this and following page*). Photographs of the high-K rocks, all in the Sonora Pass area. Geographic localities are labeled on Figure 3B. (A) Typical latite lava flow with coherent base passing upward into flow-brecciated top (Fig. 10A). Columnar and horizontal jointing is well developed (Sonora Peak section, Fig. 10A). (B) Well-developed columnar jointing; upper part shows blocky jointing typical of flow tops quenched by running water or ice (The Dardanelles; height of cliff face = ~80 m). (C) Large skeletal plagioclase typical of the latite lava flows. Augite is also present but is quite variable in size. Flows are rarely aphyric. (Lens cap for scale.) (D) Scoriaceous breccia, overlain by coherent latite lava flow and underlain by stratified volcanic lithic sandstone (ss); lies within Sonora Peak flow section (Fig. 10A). Circled day pack for scale.

deposits (Fig. 6B). Block-and-ash-flow tuffs occur in units that are meters to tens of meters thick, and they may show very crude stratification on the multimeter scale, including matrix-poor vesicular block horizons. They show evidence for hot emplacement, including bread-crust bombs, prismatically jointed blocks, and plastically deformed clasts, similar to those described by workers in modern deposits (Fisher, 1984; Freundt et al., 2000; Miyabuchi, 1999). Charred wood fragments are locally present. The block-and-ash-flow tuffs at Carson Pass are commonly cut by complexly brecciated dike-like bodies of the same composition, interpreted to be peperites (Busby et al., 2007; Skilling et al., 2004). The block-and-ash-flow tuffs commonly interfinger with lithic lapilli tuffs of the same composition, which in places form mappable units. These may be massive or occur in multimeter thick beds like the block-and-ash-flow tuffs, or they may be better stratified, with bedding on the meter scale.

The block-and-ash-flow tuff that forms the Sentinels above the Kirkwood ski area (Figs. 6B, 6C, and 6D) has particularly abundant, well-preserved bread-crust and prismatically jointed blocks, as well as abundant peperitic intrusions, suggesting it is a near-vent deposit. On nearby Melissa Coray Peak (Fig. 3B), some of the meter-scale blocks at the base of the block-and-ash-flow tuff have basal surfaces composed of homogeneous glass, in a layer up to 1 cm thick, with lineations that all show the same trend (Fig. 6C). We interpreted these as friction marks (or "skid marks"), similar to those described from the bases of andesite block-and-ash-flow deposits at Soufriere Hills volcano in Montserrat (Grunewald et al., 2000).

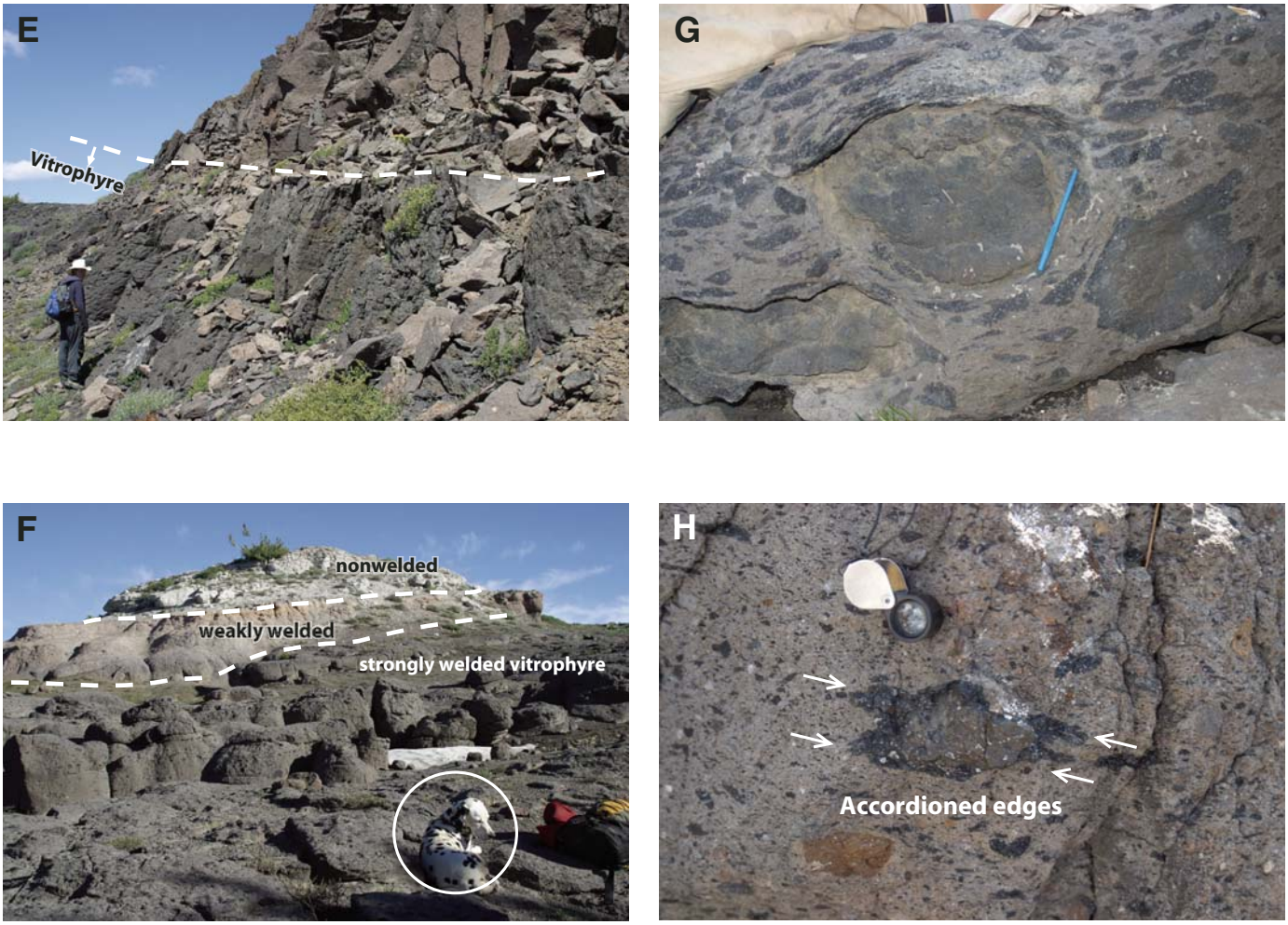

Figure 9 (*continued*). (E) Basal vitrophyre on the By Day Member of the Eureka Valley Tuff (Red Peak area). (F) Welding zonation in the Tollhouse Flat Member of the Eureka Valley Tuff (Bald Peak). Dalmatian for scale. (G) Highly flattened and plastically deformed obsidian mixed with rigid, vesicular bombs cored by obsidian. This is a distinctive characteristic of both the Tollhouse Flat and By Day Members of the Eureka Valley Tuff (photo taken by Bald Peak). Pen for scale. (H) Accordion edges on obsidian clast, attesting to its origin as flattened pumice (Tollhouse Flat Member of Eureka Valley Tuff near Bald Peak). Hand lens for scale.

Eruption mechanisms for block-and-ash flows include gravitational or explosive collapse of lava domes (Fisher and Heiken, 1982; Camus et al., 2000; Voight et al., 2000) or collapse of Vulcanian eruption columns (Fisher et al., 1980; Freundt et al., 2000). We found no evidence for explosive volcanism in the form of pumiceous/scoriaceous flow or fall deposits within the andesite sections of the central Sierra. We therefore infer that fragmentation in the central Sierra was accomplished by lava dome collapse, in some cases augmented by magma–wet sediment interaction (Skilling et al., 2004; Busby et al., 2007). The Unzen block-and-ash-flow tuffs pass distally into lithic lapilli tuffs (Miyabuchi, 1999) that are like those described here, supporting the interpretation that the lithic lapilli tuffs in the Sierra are distal equivalents of block-and-ash-flow tuffs.

The block-and-ash-flow tuffs are commonly interstratified with volcanic debris-flow deposits (Fig. 6D). Evidence for soft-sediment mixing between the two lithofacies includes open slump folds involving the two lithofacies types, as well as reworking of block-and-ash-flow deposits as irregularly shaped megaclasts within debris-flow deposits, described further later.

Debris-Flow Deposits

Debris-flow deposits are thick- to very thick-bedded (Fig. 7A) or massive (Fig. 7B) unsorted deposits of angular to subangular volcanic clasts set in a pebbly-sandstone matrix. Blocks may be monolithic or polylithic, but the matrix is polylithic, consisting of pebbly sandstone and numerous andesitic volcanic rock fragment types of varying mineralogy. The proportion of clasts to matrix varies considerably (Figs. 7A and 7B). The coarse grain size and range in clast compositions of all of the debris-flow deposits (nearly all andesite) indicate restricted source areas.

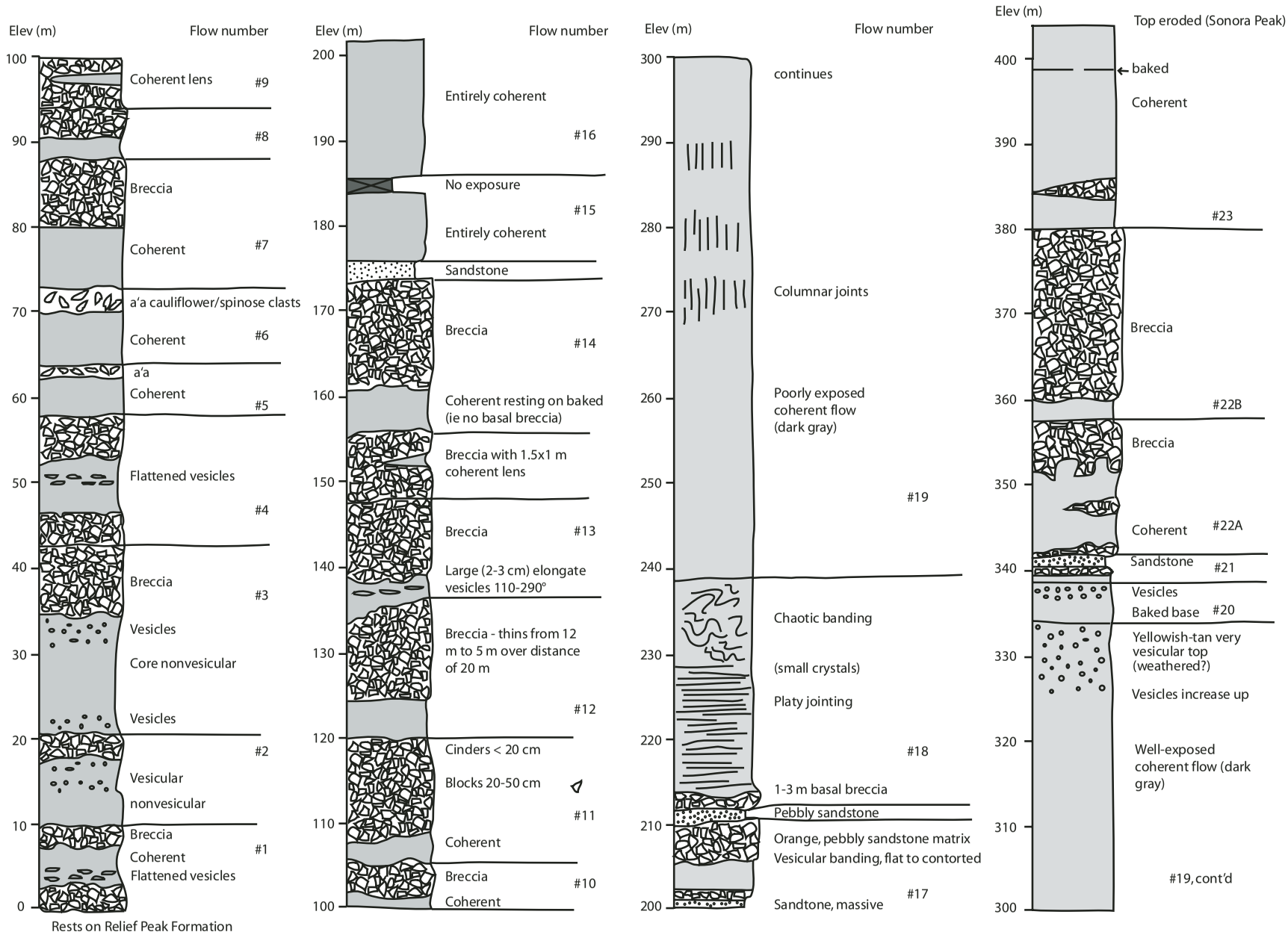

A Latite flows, Sonora Peak section

Figure 10 (*on this and following page*). Measured sections through the latite lava flows at (A) Sonora Peak (location in Fig. 3B), and (B) Grouse Meadow (location on Fig. 15). The magnetostratigraphy of these flows is presented in Figure 12.

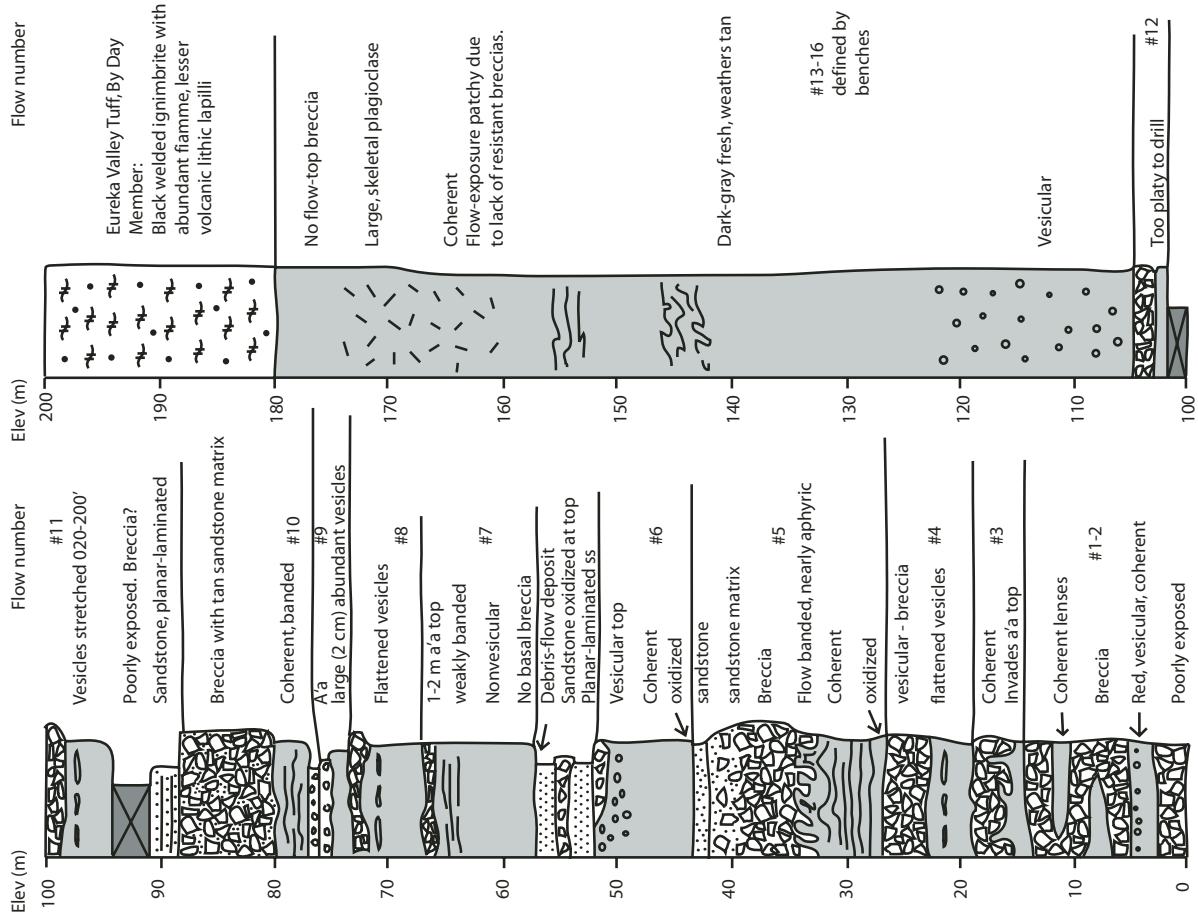

B Latite flows, Grouse Meadow section

Figure 10 (*continued*).

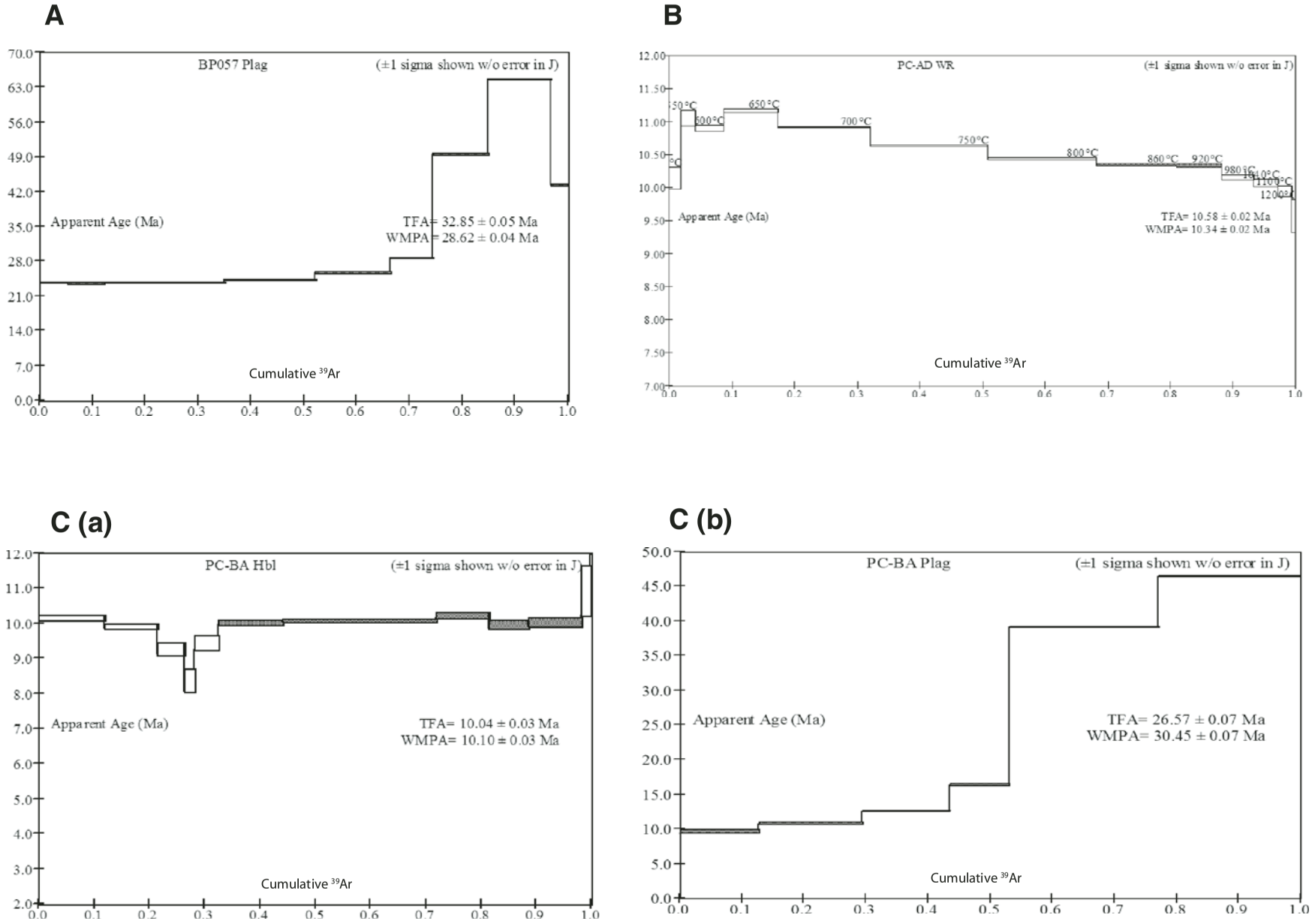

Figure 11 (*on this and following three pages*). $^{40}Ar/^{39}Ar$ spectra of samples from the Sonora Pass area; data and GPS localities given in Table 1. (A) Plagioclase from the youngest welded ignimbrite in the Valley Springs Formation near Red Peak. Plateau age is interpreted to be 23.8 ± 0.2 Ma. (B) Whole rock age on a hornblende andesite dike that intrudes the Relief Peak Formation at Sonora Peak, with an interpreted age of 10.35 ± 0.25 Ma. (C) Block and ash flow tuff from the top of Relief Peak Formation at Sonora Peak: (a) A hornblende separate yielded a plateau age of 10.10 ± 0.06 Ma and an isochron age of 10.17 ± 0.18 on 66% of the gas released. We believe the error is more robust for the isochron age and prefer it. (b) A plagioclase separate yielded an age spectrum that climbs from 10 Ma to 46 Ma, suggesting xenocrystic contamination.

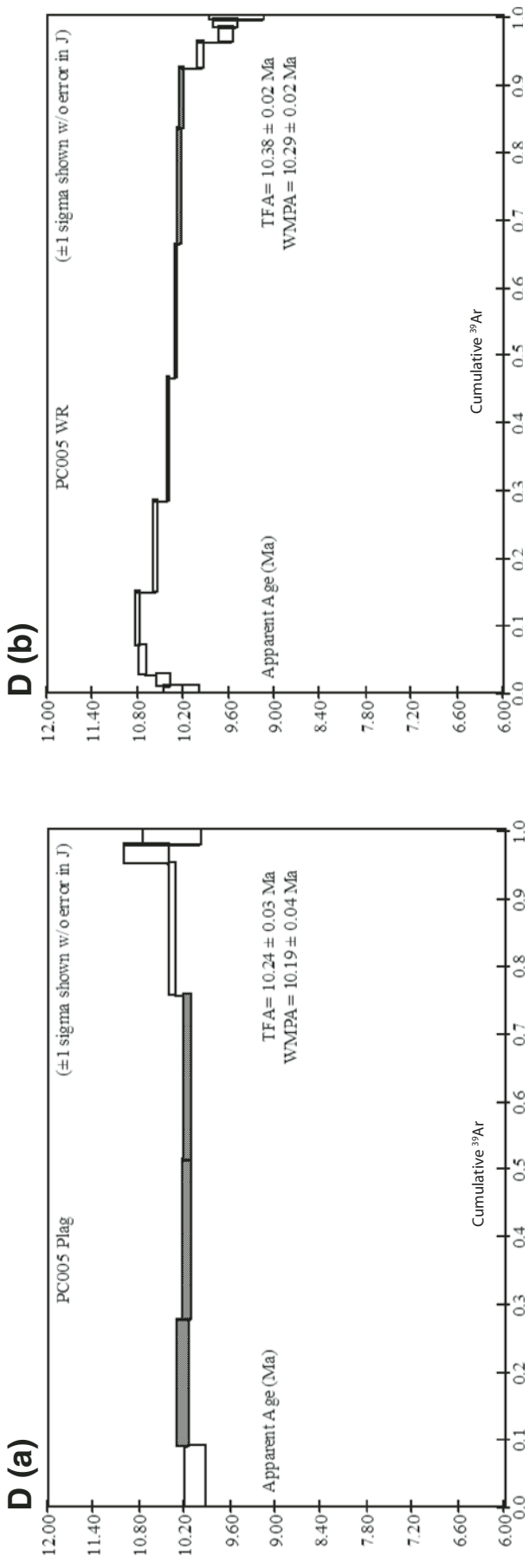

Figure 11 (*continued*). (D) Basal lava flow of the Table Mountain Latite at Sonora Peak: (a) plagioclase plateau age of 10.25 ± 0.06 Ma; (b) interpreted age on same whole-rock sample of 10.3 ± 0.1 Ma. (E) Top lava flow of the Table Mountain Latite at Sonora Peak: (a) plagioclase plateau age of 10.14 ± 0.06 Ma; (b) interpreted age of 10.0 ± 0.1 Ma on whole rock.

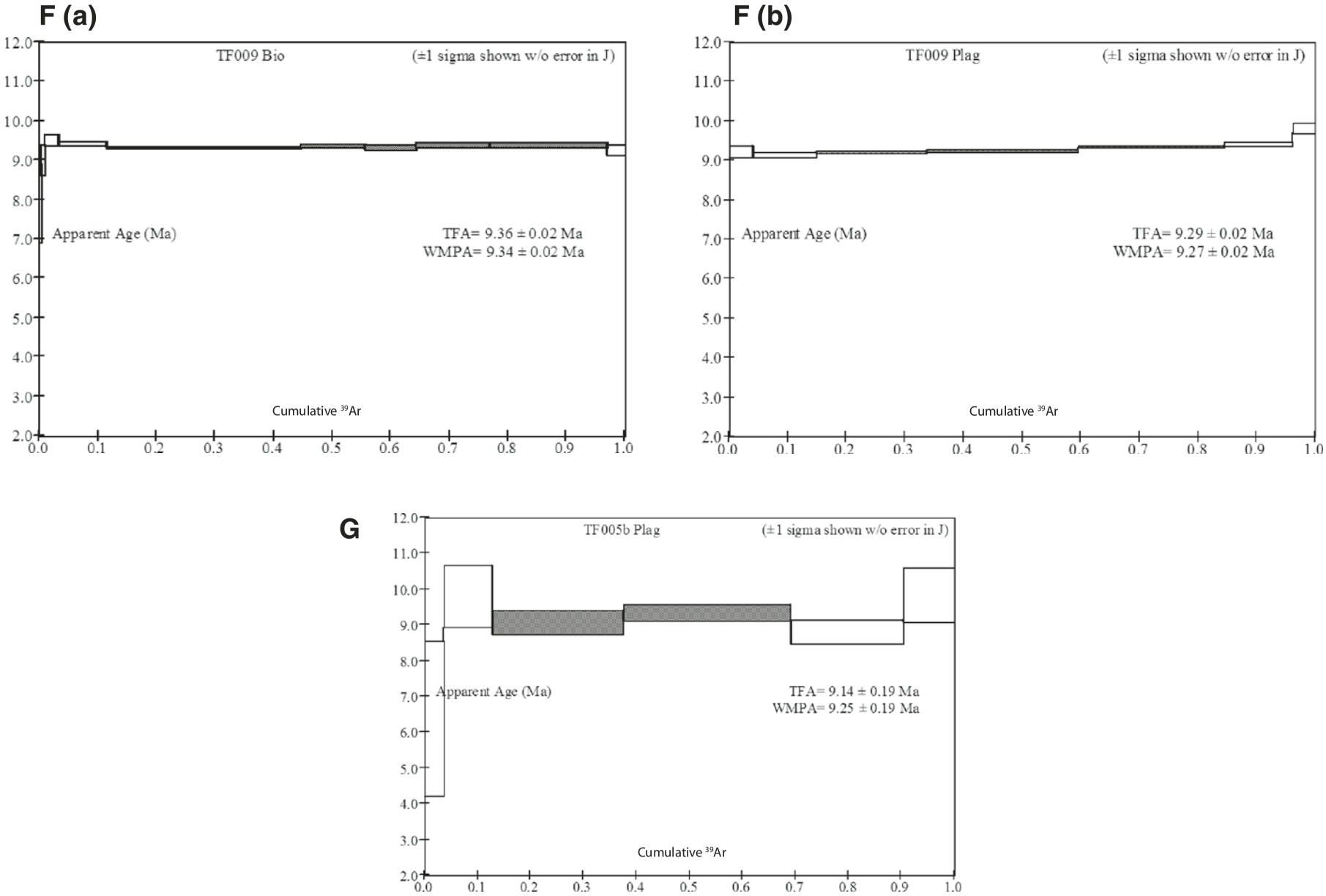

Figure 11 (*continued*). (F) Tollhouse Flat Member of the Eureka Valley Tuff in its type section at Tollhouse Flat (Fig. 3): (a) age of 9.34 ± 0.04 Ma based on biotite spectra with an excellent plateau; (b) plagioclase dates showing an age of 9.27 ± 0.04 Ma with an excellent plateau. (G) Plagioclase separate from the By Day Member of the Eureka Valley Tuff at Tollhouse Flat. Six steps in the middle of the spectrum yield an age of 9.2 ± 0.3 Ma.

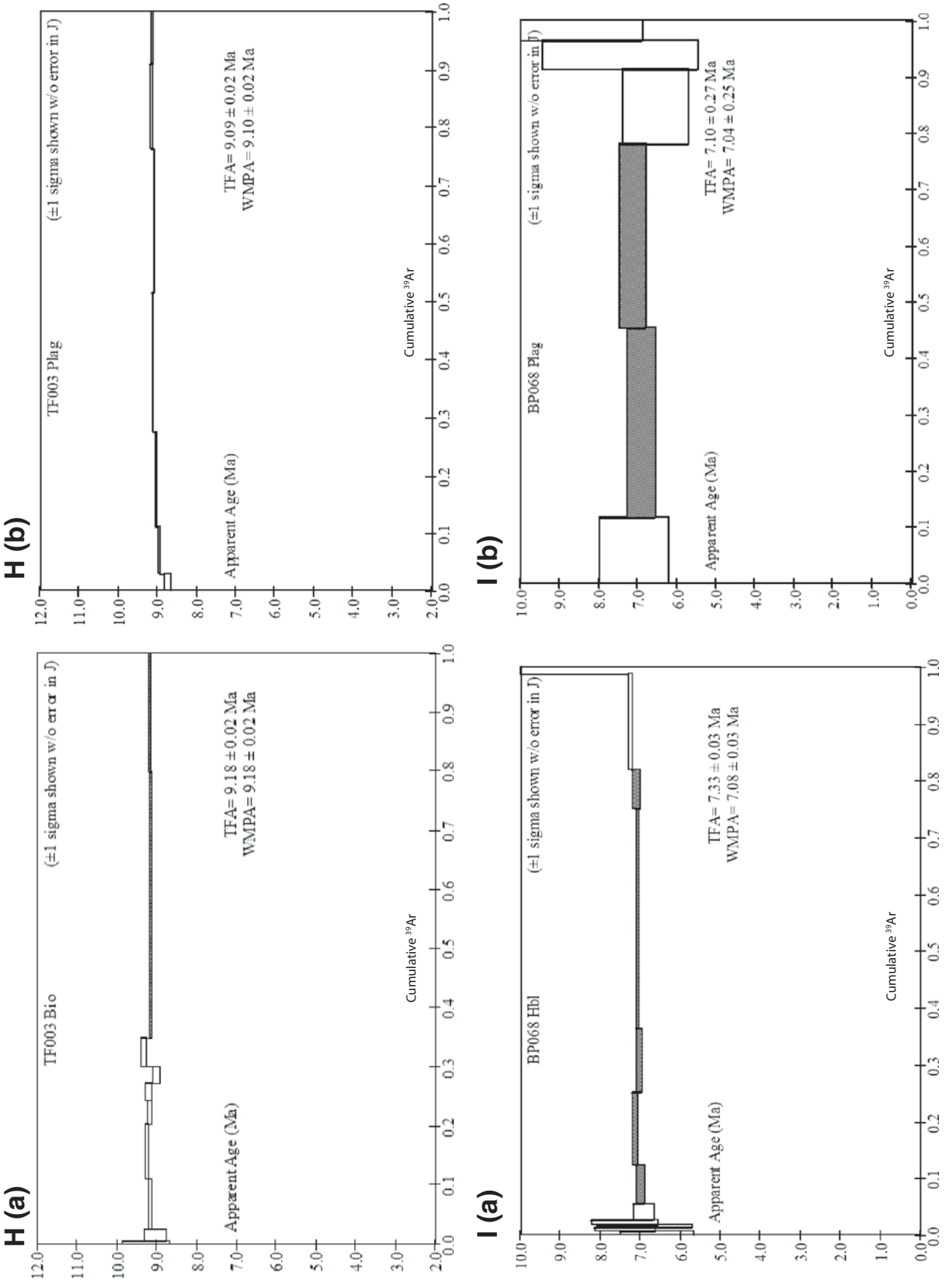

Figure 11 (*continued*). (H) Upper member of the Eureka Valley Tuff in its type section at Tollhouse Flat (Fig. 3): (a) biotite yielded an interpreted age of 9.18 ± 0.04 Ma; (b) plagioclase yielded an excellent plateau with an age of 9.14 ± 0.04 Ma. (I) Andesite plug cutting Stanislaus Group northeast of Bald Peak, representing the intrusive equivalent of the Disaster Peak Formation: (a) hornblende separate yielded a plateau age of 7.12 ± 0.06 Ma; (b) plagioclase from the same sample yielded a pseudo-plateau age of 7.0 ± 0.5 Ma.

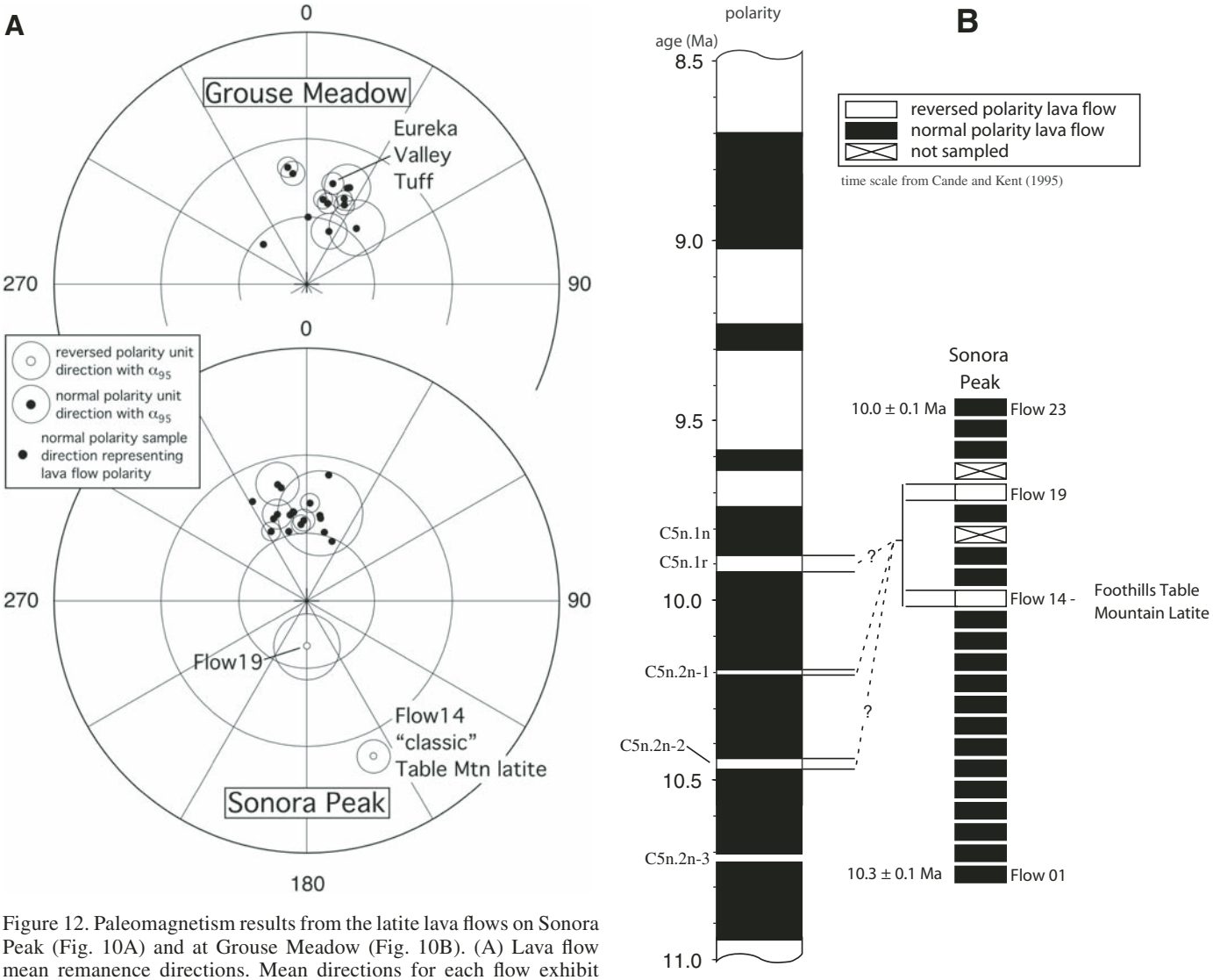

Figure 12. Paleomagnetism results from the latite lava flows on Sonora Peak (Fig. 10A) and at Grouse Meadow (Fig. 10B). (A) Lava flow mean remanence directions. Mean directions for each flow exhibit some secular variation, which results in statistically differing directions amongst the flows. Units of interest are indicated: reversed polarity flow 19 at Sonora Peak and the Eureka Valley Tuff at Grouse Meadow. The difference in directions between the two localities indicates either incorrect tilt-correction, original dips, vertical-axis rotation, or a combination of these. (B) Correlation of Sonora Peak section to the magnetic polarity time scale. $^{40}Ar/^{39}Ar$ age constraints (Fig. 11) are indicated. Correlation of flow 19 to a proposed cryptochron near 10.2 Ma explicitly agrees with the $^{40}Ar/^{39}Ar$ data and their analytical errors. Two alternate correlations are also indicated.

Some debris-flow deposits show features that indicate they were evolved directly from block-and-ash flows or were reworked from block-and-ash-flow deposits with minimal transport. Debris-flows deposits do not typically contain prismatically jointed blocks or bread-crust bombs because these are too fragile to survive resedimentation (Fisher, 1984), but they are locally present in the volcanic debris flows of the central Sierra (Fig. 7C). Many debris-flow deposits are dominated by one clast type, such as red scoria clasts, or clasts that are uniform in phenocryst type and abundance. Irregularly shaped clasts of block-and-ash-flow tuff, several meters in size, are also present within many of the debris-flow deposits. The basal andesitic unit at Carson Pass (Table 1, Fig. 4B) consists of polymict debris-flow and monomict, glassy block-and-ash-flow tuff, intimately mixed together in irregularly shaped lenses and patches on the multimeter scale, with no relict stratification. We infer that the two distinct types of deposits were complexly "stirred" by slumping or avalanching of soft material, perhaps on a steep apron surrounding a lava dome, or within a steep paleocanyon, perhaps aided by seismicity during eruption of the lava dome that fed the block-and-ash flows.

Debris-flow deposits interfinger with hyperconcentrated-flood-flow deposits, which exhibit crude stratification defined by flat clast alignment or flat lamination, and these interfinger with well-stratified streamflow deposits.

Streamflow Deposits

The streamflow deposits are well-stratified, relatively well-sorted clast-supported deposits composed dominantly of subrounded andesitic volcanic clasts (Fig. 8A) and minor granitic boulders (Fig. 8B). They include coarse-grained sandstones and pebbly sandstones, and cobble to boulder conglomerate, in thin to thick beds, and they are flat-laminated to massive (Fig. 8C), with local cut-and-fill structures and cross-lamination (Fig. 8D). The common presence of large boulders (Fig. 8E) indicates high axial paleogradients on the paleocanyons that contain these strata. Large, flat-lying log casts are aligned parallel to the trend of the Carson Pass–Kirkwood paleocanyon at the base of one fluvial unit there (Busby et al., 2007). Unlike the debris=flow deposits, the cobble- to boulder-sized clasts in the fluvial deposit are nowhere monolithic; however, the restricted range in clast types, as well as general angularity of clasts, suggests that andesite source areas were not very far away.

Map units composed entirely of streamflow deposits, with no interbeds of debris-flow deposits, form the most resistant outcrops of the central Sierra, besides the hypabyssal intrusions; for this reason, both the Kirkwood Valley (Fig. 8F) and the Bear Valley ski areas lie partly within this type of deposit. In contrast, map units consisting of interstratified streamflow and debris-flow deposits (Fig. 8G) are less resistant. We suspect that this is because the well-sorted streamflow deposits were more permeable and thus became better cemented.

Streamflow deposits in the Dardanelles Cone area (locality on Fig. 3B) have been the subject of intense scrutiny because they contain uranium associated with organic deposits. These studies include a drilling program in the 1970s and ongoing remediation studies by the U.S. Geological Survey (USGS).

Avalanche Deposits

Avalanche deposits are an important feature of the Relief Peak Formation along the range front fault system in the Sonora Pass area. These landslide deposits are concentrated at the top of the Relief Peak Formation, just below the Table Mountain Latite, and they are one of our lines of evidence for onset of faulting just before eruption of the Table Mountain Latite (the other being growth faulting, discussed in the structure section). For this reason, the relationship of the landslide deposits to the faults is discussed in the structure section. In terms of lithofacies characteristics, the landslide deposits are of two types.

In the first type, shattered slabs of welded ignimbrite (derived from the Oligocene Valley Springs Formation), several meters to several tens of meters in size, are interstratified with debris-flow deposits of the Relief Peak Formation. These represent hard-rock avalanches, probably from active fault scarps, although some of the interstratified debris-flow deposits have intervals that are very rich in rhyolite pumice and crystals, suggesting that nonwelded parts of the ignimbrite sections were shed from scarps by debris flow.

In the second type, crudely stratified to well-stratified sections of the Relief Peak Formation show chaotic bedding orientations. These represent soft-rock avalanches of volcaniclastic materials that were consolidated enough (perhaps by early zeolite formation) to hold together in blocks and megablocks. Strata within the blocks include crudely stratified debris-flow deposits and block-and-ash-flow tuffs, as well as distinctly stratified streamflow conglomerates and sandstones. Stratification in many of the avalanche blocks is far too steep to represent depositional dips (greater than 40°) or dips rotated about normal faults (greater than 70°). One semicoherent block is so large (~1.6 km in length, Fig. 14) that it could be interpreted as stratigraphy rotated to dips of ~50° about a normal fault; however, dips do not flatten upward, as they should in a growth fault (Fig. 14); instead, the semicoherent block is underlain by a deposit in which block size progressively decreases away from the megablock.

We know of no way to recognize avalanche blocks derived from a nonstratified, homogeneous volcaniclastic source area (such as proximal block-and-ash-flow tuffs).

Stanislaus Group

As described already, the late Miocene Stanislaus Group is a suite of high-K, volcanic and volcaniclastic rocks that consists of three formations, all bounded by erosional unconformities (Slemmons, 1966; Fig. 4): Table Mountain Latite, the Eureka Valley Tuff, and the Dardanelles Formation. We do not believe it is possible to distinguish between flows of the Table Mountain Latite and the Dardanelles member in the field, unless the Eureka Valley Tuff intervenes; however, our new age data (presented here) indicate that flows of the Table Mountain Latite and the Dardanelles member must be at least 1 m.y. different in age.

Table Mountain Latite

The Table Mountain Latite is a thick, extensive sequence of lava flows and flow breccias (Fig. 10). The typical latite lava flow has a coherent base and a flow-brecciated top (Figs. 9A and 10), although a few flows have basal breccias (e.g., flows 1 and 4, Fig. 10A). Some flows lack flow-top breccias. Entirely coherent flows marked by prominent vesicular tops represent more fluidal flows, such as pahoehoe (e.g., flows 19 and 20, Fig. 10A). Entirely coherent flows that lack a vesicular top may represent erosional remnants of flows that may or may not have originally had brecciated tops (e.g., flows 15, 16, 18, and 25, Fig. 10A; flow 13, Fig. 10B). Columnar jointing is present in some flows (Figs. 9A and 9B) but is not common (Fig. 10). The latite flows are very distinctive because they commonly contain large (to 1 cm) disequilibrium sieve-textured plagioclase phenocrysts (Fig. 9C) and augite of varying sizes. Flows with small crystals (flow 18, Fig. 10A) are rare. Most of the flow-top breccias are composed of angular blocks, but some flow tops have smaller, more spinose or cauliflower-shaped clasts, referred to as a‘a (e.g., flows 5 and 6, and top of flow 11, Fig. 10A). Flow banding is present in a few flows in the Grouse Meadow section (flows 5, 7, 10, and 13, Fig. 10B) but is absent from the Sonora Peak section (Fig. 10A). Platy jointing occurs rarely (e.g., flow 18, Fig. 10A; flow 12, Fig. 10B).

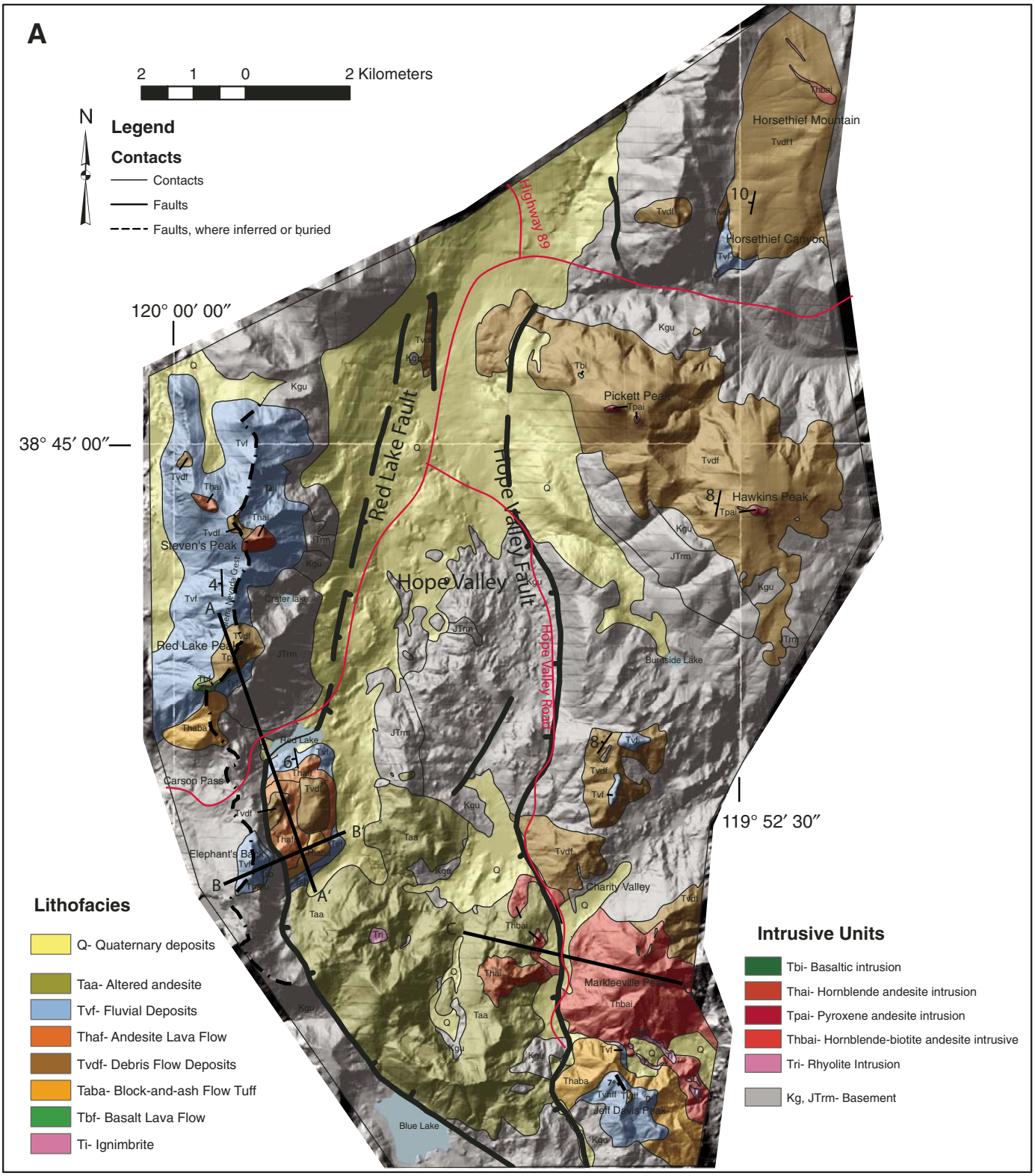

Figure 13 (*on this and following page*). Preliminary geologic map (A) and cross sections (B) of the Carson Pass segment of the central Sierra Nevada range front (locality on Fig. 3) based on our new mapping, with intrusions and parts of the faults modified from Armin et al. (1984). Hagan's Tertiary map units are grouped into lithofacies and intrusions, divided by mineralogy. We interpret the dominant range front structure to be a full graben that is largely postvolcanic.

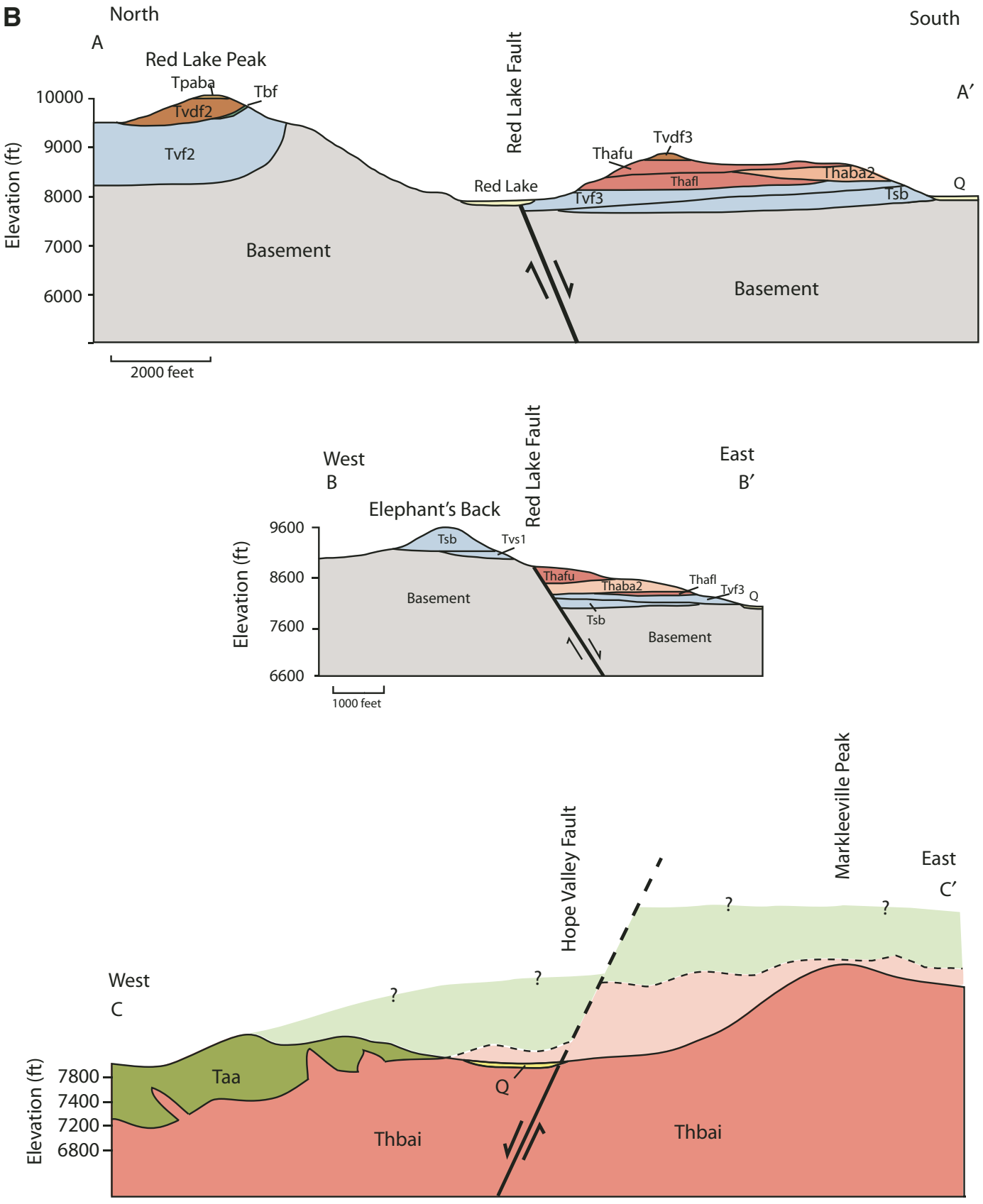

Figure 13 (*continued*).

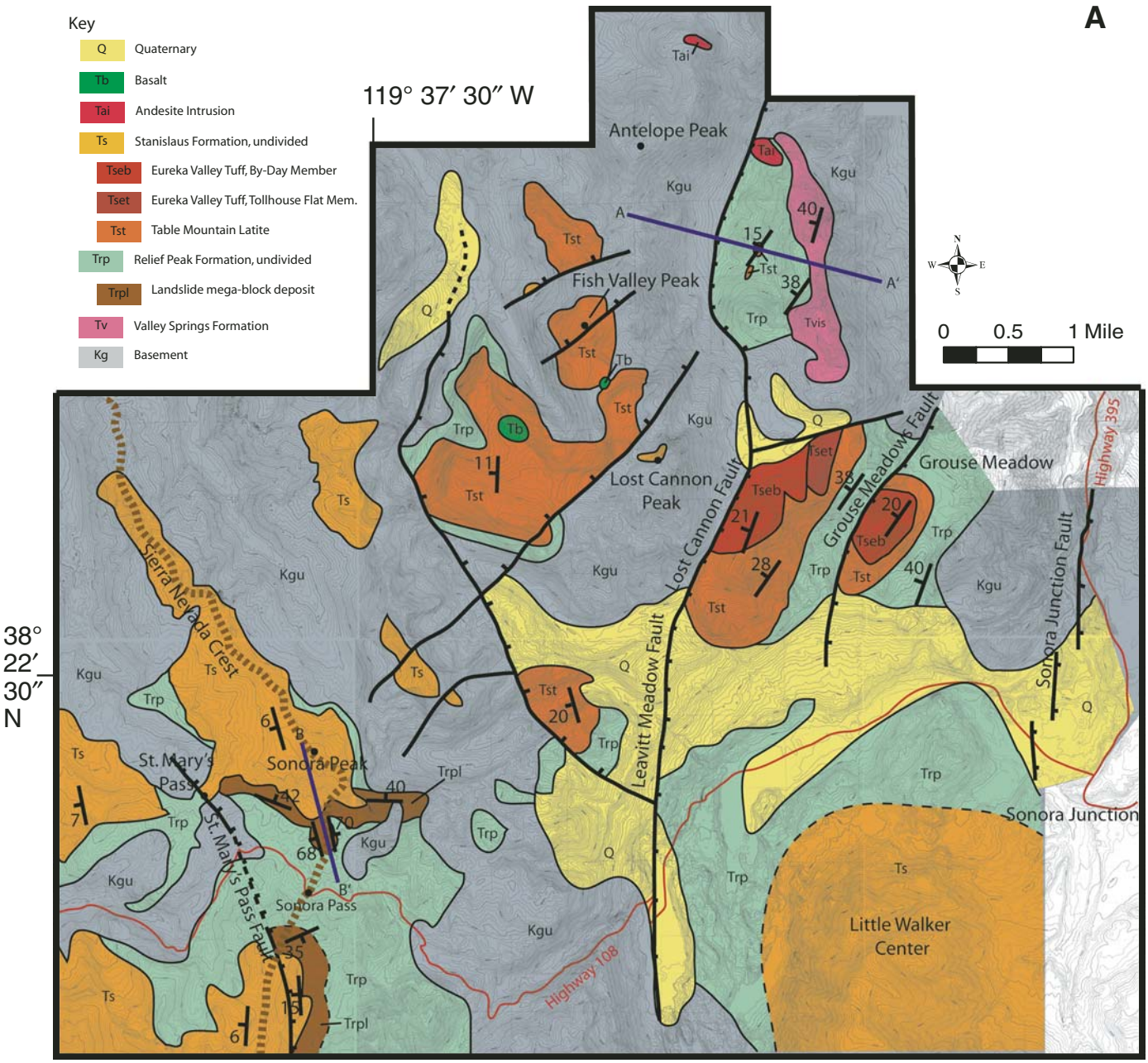

Figure 14 (*on this and following page*). Preliminary geologic map (A) and cross sections (B) of the Sonora Pass segment of the central Sierra Nevada range front, showing faults previously mapped by Priest (1979) and Slemmons (unpublished map archived at the California Geological Survey). We interpret the dominant range front structure here to be down-to-the-east half grabens. Cross-section A–A′ shows evidence for the onset of normal faulting along the Lost Cannon fault during eruption of the Table Mountain Latite. Cross-section B–B′ shows evidence for landsliding onto the hanging-wall block of the St. Mary's Pass fault immediately prior to eruption of the Table Mountain Latite. Together, these relations (and others described in the text) suggest that the onset of range front faulting triggered high-K volcanism at the Little Walker center.

Interbeds of scoriaceous sandstone and scoriaceous lapilli tuff (Figs. 9D, 9E, and 10) are generally massive to very weakly stratified. These may represent debris avalanching off the fronts of flows, perhaps mixing with water. Massive to planar-laminated, moderately well-sorted volcanic lithic sandstones record periods of fluvial reworking (Figs. 9F and 10). These fluvial sandstones are generally less than 4 m thick (Fig. 10), but one sandstone horizon thickens from 10 m to over 60 m toward the footwall of the Leavitt Meadow–Lost Cannon Peak fault (Fig. 14A), which also shows fanning dips (Fig. 14B, discussed later).

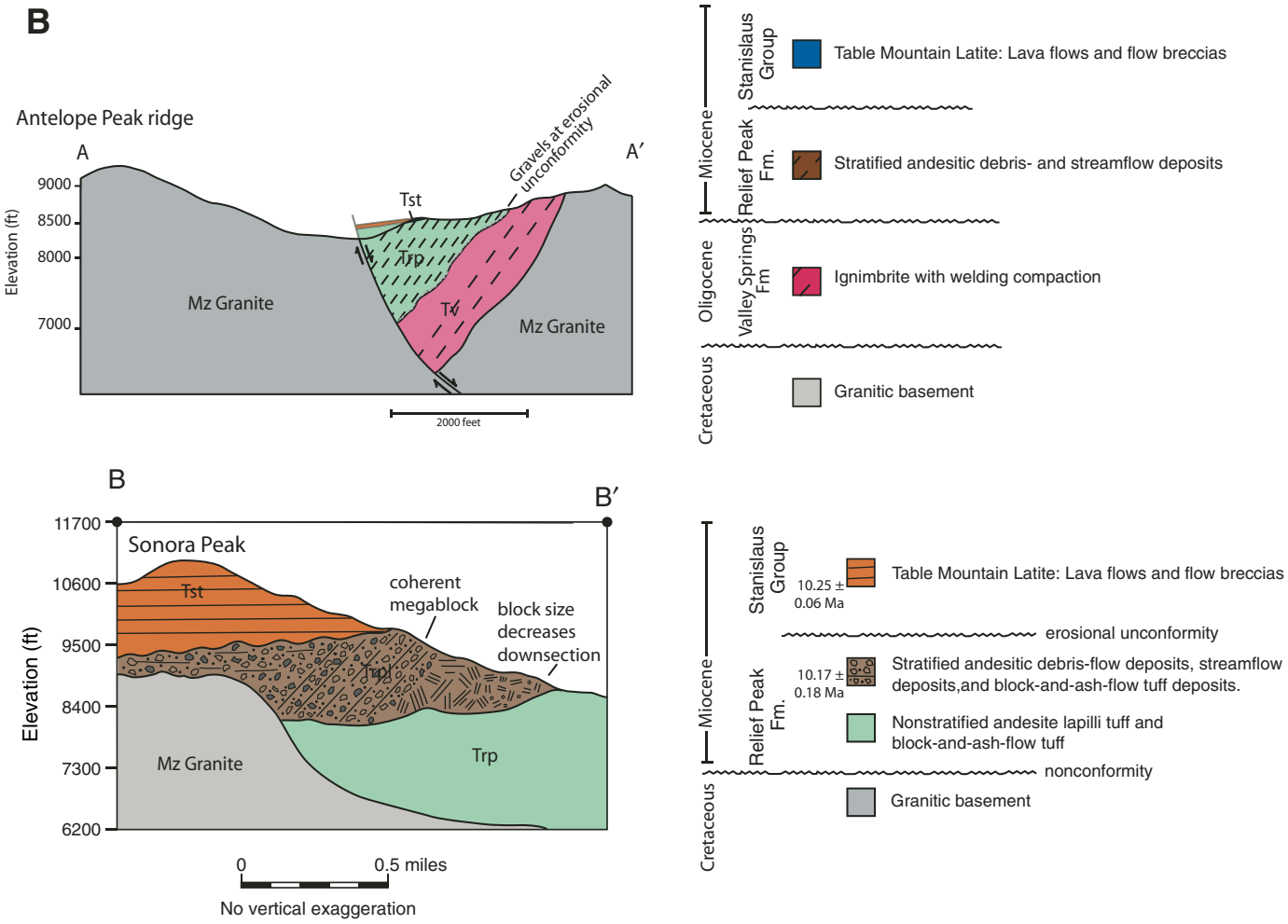

Figure 14 (*continued*).

Eureka Valley Tuff

We recognize two of the three members of the Eureka Valley Tuff in the Sonora Pass area: the biotite-rich Tollhouse Flat Member and the overlying By Day Member, which has much fewer and smaller biotite crystals. Both of these ignimbrites show strong welding zonation, from a basal vitrophyre, through weakly welded dark-gray tuff, to nonwelded white tuff (Figs. 9E and 9F). The nonwelded, biotite-bearing upper member, which occurs at the type section along the Little Walker River (Fig. 3), appears to be absent from the Sierra Nevada. The welded facies of the Eureka Valley Tuff is characterized by highly flattened and plastically deformed obsidian; in places, these plastic clasts wrap around rigid angular blocks of obsidian (Fig. 9G). Accordion edges on the edges of some flat obsidian clasts attest to their origin as flattened pumices (Fig. 9H). Pebble-sized rock fragments are present throughout the Tollhouse Flat and By Day Members. Like most ignimbrites, the Eureka Valley Tuff members make excellent stratigraphic markers and strain markers.

Dardanelles Formation

The Dardanelles Formation consists of latite lava flows, latite clast–bearing debris-flow deposits, and minor latite clast–bearing volcaniclastic streamflow deposits. The Dardanelles Formation can only be recognized in the field by its stratigraphic position above the Eureka Valley Tuff because its latite lava flows appear identical to Table Mountain Latite. It forms some of the highest peaks and ridges in the Sonora Pass to Ebbetts Pass area. The Dardanelles Formation has not, to our knowledge, been dated.

Disaster Peak Formation

The Disaster Peak Formation has previously been mapped as andesite strata that overlie the high-K rocks of the Stanislaus Formation (Keith et al., 1982). In contrast, we find that many of these andesites are intrusions that crosscut the Stanislaus Formation, holding up the highest peaks, including Arnot Peak and Disaster Peak (Fig. 3). Furthermore, most of the strata that overlie the Stanislaus Formation consist of streamflow and debris-flow deposits with polylithologic andesite clasts. Primary andesite volcanic

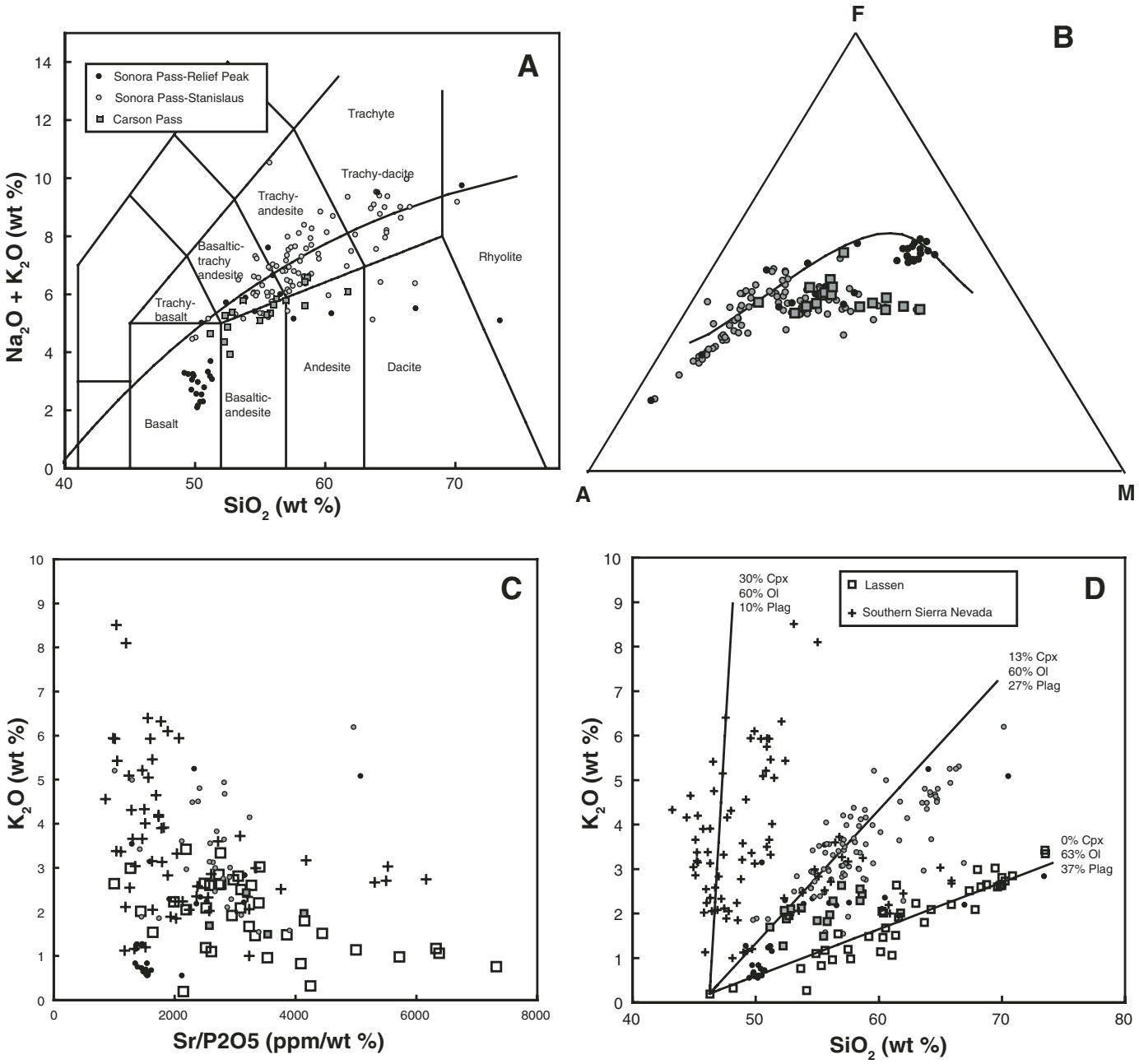

Figure 15. (A) Alkali-silica (Le Bas, 1986) and (B) AFM (A = Al_2O_3 – 3 K_2O, F = FeO and M = MgO; Irvine and Baragar, 1971) classification diagrams for the Central Sierra Nevada Ancestral Cascades arc (CSNAC) province volcanics. These volcanics are dominated by intermediate rock compositions but evolve to higher alkali contents (i.e., higher K_2O) compared to most Cascade volcanic centers. (C) K_2O is compared to Sr/P_2O_5, a positive indicator of slab fluid input at Lassen. Notably, K_2O contents do not positively correlate with Sr/P_2O_5 or other putative slab-derived components such as Ba/Rb. (D) K_2O-SiO_2 diagram, illustrating the remarkable latitudinal variation of K_2O within the Sierra Nevada, shifting from low-K_2O volcanics of the Lassen volcanic center to the north, through intermediate-K_2O rocks of the Carson and Sonora Pass regions, to ultrapotassic volcanics in the southern Sierra Nevada. Mass-balance calculations show that increases in the proportion of clinopyroxene (cpx) relative to olivine (ol) and plagioclase (plag) in a fractional crystallization assemblage can explain K_2O-SiO_2 variations. Greater extents of clinopyroxene fractionation are expected at high pressures and are proposed to be controlled by an increase in crustal thickness to the south.

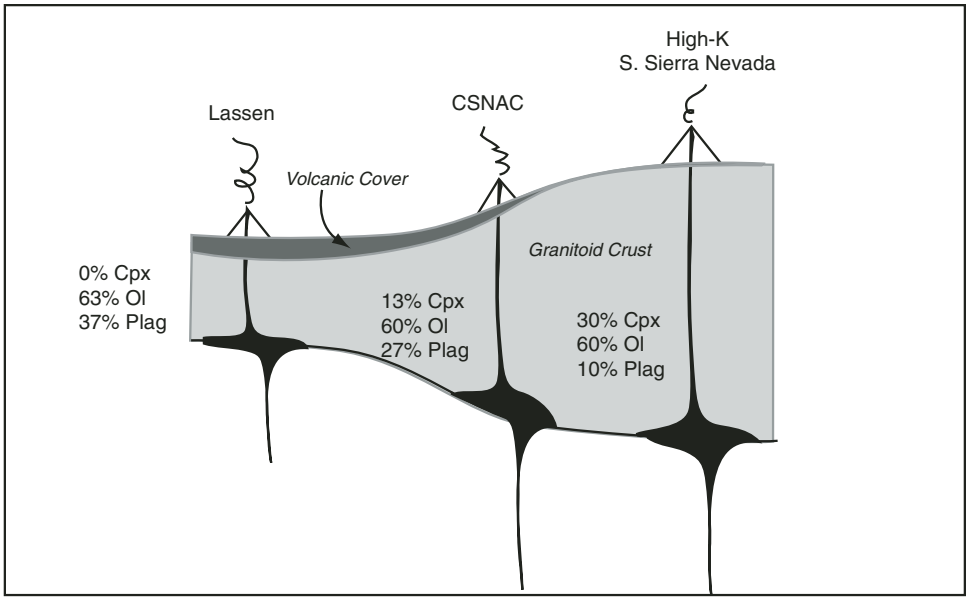

Figure 16. Geochemical model to explain latitudinal shifts in K_2O-SiO_2 and variations in volcanic cover within the Sierra Nevada. Here, crustal thickness controls the depth of fractional crystallization and, in consequence, the relative amounts of clinopyroxene, olivine, and plagioclase in a fractional crystallization mineral assemblage. Crustal thickness might also control the extent of volcanic cover in the Sierra Nevada. Thin volcanic cover in the southern Sierra may reflect an inhibition of magma transport due to the presence of a thick, low-density granitic crustal "cap." In the southern Sierra, volcanic rocks are probably trapped at great depth, precipitating relatively larger amounts of clinopyroxene. Such rocks might only be erupted if they are highly differentiated, i.e., after they have achieved sufficiently high concentrations of volatiles so as to allow bulk magma densities that allow transport through a thick, low-density crust.

rocks are rare and appear to be restricted to lenses of block-and-ash-flow tuff within the debris-flow–streamflow sections. We have found no andesite lava flows in the Disaster Peak Formation. This contrasts with age-equivalent strata of the Merhten Formation in the Carson Pass area, which include andesite lava flows (Fig. 13) as well as abundant block-and-ash-flow tuffs (units Taba3 and Tbat, Fig. 4B; Busby et al., 2007). Therefore, mapping and dating of intrusive suites in the Sonora Pass area may hold the key to characterizing the geochemical evolution of that segment of the arc after the high-K volcanism ended there.

Basalt Lava Flows (Merhten Formation, Relief Peak Formation, and Stanislaus Group)

Basalt lava flows are sparse in the central Sierra Nevada, but they occur at all stratigraphic levels in the Miocene section. This is important because their geochemistry holds the key to understanding mantle processes through time. Because of their importance, we describe the localities and stratigraphic relations of the basalt lava flows geochemically analyzed in this paper. Basalt intrusions would also be useful for geochemical work if they were also shown to cover a time span similar to that of the lava flows, but as yet, we have not had the funding to date them.

The basalt lava flows are black to dark-gray, glassy to crystalline flows that are aphyric or have phenocrysts or microphenocrysts (<20% olivine, <20% plagioclase, <10% clinopyroxene). Most flows are entirely coherent and have microvesicular columnar jointed interiors and coarse stretched-vesicle horizons marking the tops of flows; these represent pahoehoe flows. Some flows have rubbly tops and irregular lobes of the coherent interior injected into the rubble, representing a'a flows.

We identified a series of at least five basalt lava flows along the crest at Carson Pass between Red Lake Peak and Little Round Top (Fig. 3B), dated at 6.75 ± 0.15 Ma (unit Tbl, Fig. 4B; Busby et al., 2007). Chemical compositions are described later. Small olivine basalt intrusions also lie along the crest at Carson Pass and to the east of it in the Hope Valley area (Fig. 13), but these have not been dated, so it is not known if they represent the intrusive equivalents of the 6.75 Ma lava flows.

Basalt lava flows also occur in the Sonora Pass area (Fig. 3B), and in this paper, we present geochemical results from basalts within the Relief Peak Formation and the Stanislaus Group (Figs. 15 and 16). Further field and geochemical work on the Disaster Peak Formation is in progress.

We recognized basalts lava flows of the Relief Peak Formation at the Dardanelles (Fig. 3B), where an up to 150-m-thick section with up to 10 flows (or more) rests on granitic basement or Valley Springs Formation. The basalts are largely overlain by the latite lava flows that make up the Dardanelles (Fig. 9B), although they are locally overlain by debris-flow deposits of the Relief Peak Formation.

Basalt lava flows occur at three stratigraphic levels within the Stanislaus Group: (1) The lowest basalt section lies within a section of Table Mountain Latite lava flows (on Bald Peak, Fig. 3B). The latite section underlies the Tollhouse Flat Member of the Eureka Valley Tuff, which is in turn overlain by latite lava flows of the Dardanelles Formation. The basalt is a 55-m-thick single (ponded?) flow with vesicular base and top. (2) The next highest basalt section rests upon the Tollhouse Flat Member of the Eureka Valley Tuff and is overlain by latite-clast debris-flow deposits of the Dardanelles Formation (on Dardanelles Cone, Fig. 3B). It consists of an ~35-m-thick section of

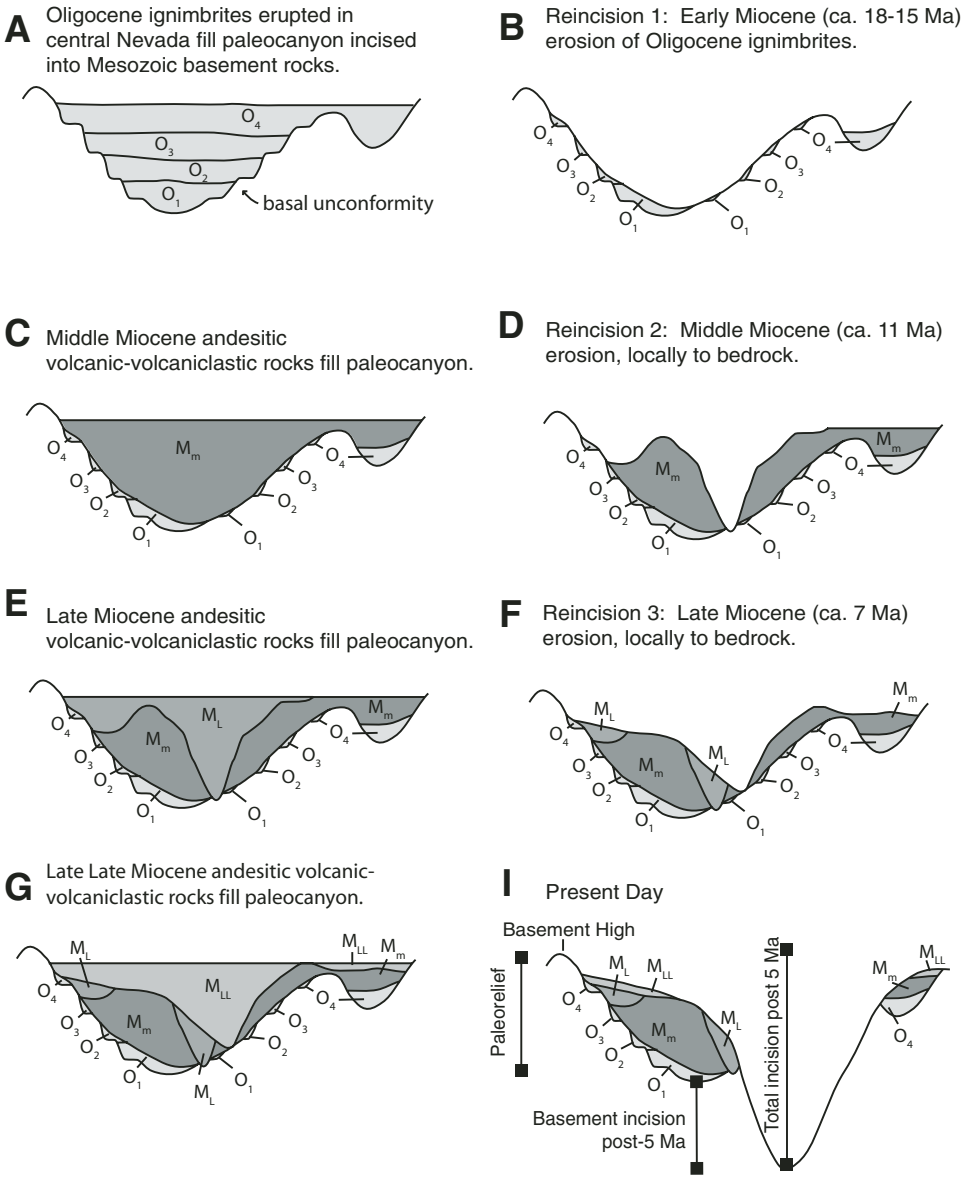

Figure 17. Model for the Cenozoic topographic evolution of the central Sierra Nevada, from Busby et al. (2007). Reincision events are inferred from deep and steep-sided unconformities shown on Fig. 4. Reincision event 1 corresponds to unconformity 2; reincision event 2 corresponds to unconformity 3; and reincision event 3 corresponds to unconformity 6. We interpret reincision 1 event one to record uplift associated with the onset of arc magmatism in the Sierra Nevada at about 15 Ma. Reincision 2 is interpreted to record the onset of Walker Lane transtension. Reincision 3 may record renewed uplift at the arrival of the triple junction at about 7 Ma, followed by cessation of arc volcanism at about 6 Ma.

at least two basalt flows. (3) The highest basalt section occurs within the Dardanelles Formation, above a latite lava flow that in turn overlies the Tollhouse Flat Member of the Eureka Valley Tuff (on the first prominent unnamed peak east of Red Peak). The top of this section is eroded.

$^{40}Ar/^{39}Ar$ GEOCHRONOLOGY AND GEOLOGIC RELATIONS OF SAMPLES FROM THE SONORA PASS AREA

In this section, we present new $^{40}Ar/^{39}Ar$ data from the Sonora Pass area (Fig. 11; Table 1) and describe the geologic context of the samples. The $^{40}Ar/^{39}Ar$ geochronology of the Carson Pass–Kirkwood area is described in a separate paper (Busby et al., 2007).

Analytical Methods

Standard density and magnetic separation techniques were used to generate groundmass and mineral separates. Separates were irradiated in a cadmium-lined tube at the TRIGA (Training, Research, Isotopes, General Atomics) reactor at Oregon State University and were analyzed in the $^{40}Ar/^{39}Ar$ geochronology laboratory at the University of California–Santa Barbara using the general procedures and system described by Gans (1997). The flux monitor used for all irradiations was Taylor Creek Rhyolite with an assigned age of 27.92 Ma (Duffield and Dalrymple, 1990). For comparison, we obtained an age of 27.60 Ma on Fish Canyon Tuff sanidine (another widely used standard) using this flux monitor. All errors given for our estimated (preferred) ages as reported throughout the text and in

TABLE 1. SUMMARY OF $^{40}Ar/^{39}Ar$ GEOCHRONOLOGY RESULTS FOR SAMPLES FROM THE SONORA PASS REGION

Sample	Packet	Mat	Geological context	Experiment	Pref. age (Ma)	Est ± 2σ	TFA	WMPA	39p (%)	IsoA	39i (%)	MSWD	40/36i	K/Ca	Rad (%)	Lat (°N)	Long (°W)
BP068	SB51-51	Hbl	Hbl andesite plug, Disaster Peak FM	13 step heat	7.12	0.06	7.33	7.12 ± 0.06	99	7.26 ± 0.16	99	0.97	289.9 ± 3.0	0.063–0.067	30–60	38.37609	119.76975
BP068	SB51-50	Plag	Hbl andesite plug, Disaster Peak FM	6 step heat	7.00	0.50	7.1	7.04 ± 0.50	66	6.83 ± 0.94	100	0.28	300.9 ± 5.6	0.011–0.013	14–48	38.37609	119.76975
TF003	SB51-57	Plag	Upper Member, Eureka Valley Tuff, Stanislaus Gp	7 step heat	9.15	0.03	9.09	9.11 ± 0.04	89	9.10 ± 0.08	89	2.06	300.6 ± 11.9	0.25–0.26	89–94	38.43096	119.44792
TF003	SB51-58	Bio	Upper Member, Eureka Valley Tuff, Stanislaus Gp	10 step heat	9.18	0.04	9.18	9.18 ± 0.04	65	9.20 ± 0.04	76	1.02	294.3 ± 1.4	8.5–108	73–83	38.43096	119.44793
TF005b	SB51-59	Plag	By Day Member, Eureka Valley Tuff, Stanislaus Gp	6 step heat	9.20	0.30	9.14	9.19 ± 0.32	96	9.10 ± 0.52	95	1.28	299.3 ± 7.3	0.074–0.077	42–71	38.43041	119.44805
TF009	SB51-60	Plag	Tollhouse Flat Member, Eureka Valley Tuff, Stanislaus Gp	7 step heat	9.27	0.04	9.29	9.27 ± 0.04	70	9.30 ± 0.10	95	1.93	288.8 ± 5.5	0.077–0.060	72–92	38.42891	119.44841
TF009	SB51-61	Bio	Tollhouse Flat Member, Eureka Valley Tuff, Stanislaus Gp	9 step heat	9.31	0.03	9.36	9.35 ± 0.04	86	9.32 ± 0.06	86	0.26	296.9 ± 0.4	24–125	35–81	38.42891	119.44842
PC032	SB51-54	Plag	Uppermost Table Mtn Latite Flow, Stanislaus Gp	8 step heat	10.14	0.06	10.02	10.14 ± 0.06	94	10.15 ± 0.08	94	0.67	295.2 ± 0.5	0.072–0.077	28–81	38.35378	119.63440
PC032	SB51-55	WR	Uppermost Table Mtn Latite Flow, Stanislaus Gp	13 step heat	10.00	0.10	10.12	9.98 ± 0.04	46	10.02 ± 0.08	46	1.36	273 ± 13.2	0.7–2.5	55–95	38.35378	119.63441
PC005	SB51-52	Plag	Lowermost Table Mtn Latite Flow, Stanislaus Gp	7 step heat	10.25	0.06	10.24	10.19 ± 0.08	100	10.30 ± 0.16	100	1.89	292.6 ± 3.7	0.046–0.048	51–81	38.34641	119.63263
PC005	SB51-53	WR	Lowermost Table Mtn Latite Flow, Stanislaus Gp	13 step heat	10.30	0.10	10.38	10.29 ± 0.04	46	10.35 ± 0.14	46	1.86	253.4 ± 43.3	0.5–1.9	62–96	38.34641	119.63264
PC-AD	SB51-45	WR	Subalkalic andesite dike, Upper Relief Peak Fm	13 step heat	10.35	0.25	10.58	10.34 ± 0.04	20	NA	NA	NA	NA	0.5–0.79	70–95	38.34641	119.63265
PC-BA	SB51-62	Hbl	Block-and-ash-flow tuff, Upper Relief Peak Fm	12 step heat	10.17	0.18	10.04	10.10 ± 0.06	66	10.17 ± 0.18	66	1.41	289.7 ± 6.5	0.02–0.4	27–80	38.34427	119.63404
PC-BA	SB51-63	Plag	Block-and-ash-flow tuff, Upper Relief Peak Fm	6 step heat	Ca. 10	NA	26.57	NA	NA	NA	NA	NA	NA	0.26–1.9	20–82	38.34427	119.63405
BP057	SB51-13	Plag	Uppermost welded ignimbrite, Valley Springs Fm	10 step heat	23.80	0.20	32.85	NA	35	NA	NA	NA	NA	0.26–1.4	95–98	38.37824	119.74298

Note: Mat—Material, TFA—Total Fusion Age, WMPA—weighted mean plateau age , IsoA—Inverse Isochron Age, MSWD—mean squared weighted deviation, Rad—% Radiogenic, 39(%)—% of cumulative 39Ar used in plateau (p) or isochron (i) calculation, Lat—Latitude, Long—Longitude, Hbl—Hornblende, Plag—Plagioclase, Bio—Biotite, WR—Whole Rock.

Table 1 are ±2σ (95% confidence), whereas uncertainties on weighted mean plateau ages (WMPA) and total fusion ages (TFA) on the spectra of Figure 11 are, by convention, ±1σ. Preferred ages for each unit are summarized on Figure 4.

Valley Springs Formation

We dated the youngest of the four Valley Springs Formation ignimbrites recognized by Slemmons (1953) in order to determine the age of the top of the formation in the Sonora Pass area. A $^{40}Ar/^{39}Ar$ age spectrum on plagioclase separate yielded discordant data that suggest the unit is no older than ca. 24 Ma. The age spectrum climbs sharply from a fairly flat low-temperature segment, with a mean age of 23.8 ± 0.20 Ma, to high-temperature ages as old as 65 Ma (Fig. 11A). The increase correlates with climbing K/Ca ratios, all of which are too high to be a volcanic plagioclase (Table 1), suggesting that the volcanic plagioclase is contaminated by minor amounts of older (Cretaceous) granitic K-feldspar. The simplest interpretation of the data is that the juvenile plagioclase is younger than 23.8 Ma, and the xenocrystic contamination is older than 65 Ma.

Relief Peak Formation

The Relief Peak Formation in the Sonora Pass area is dominated by andesitic volcanic debris-flow and fluvial deposits and lacks the andesite lava flows and domes present in the Carson Pass area. For this reason, the most primary andesitic deposit we could find was block-and-ash-flow tuff at the top of the Relief Peak Formation, which we sampled at the base of Sonora Peak (Fig. 3). When we collected this sample, we originally interpreted it to be part of a section that was tectonically tilted prior to eruption of the overlying Table Mountain Latite, but we now believe it lies within a very large avalanche megablock (1.6 km long, Fig. 14). The block-and-ash-flow tuff could have thus been substantially older than the avalanche deposit, but it is not, as shown here.

A hornblende separate from the block-and-ash-flow tuff yielded a plateau age of 10.10 ± 0.06 Ma and an isochron age of 10.17 ± 0.18 on 66% of the gas released (Fig. 11C, a). A plagioclase separate from the block-and-ash-flow tuff yielded discordant results, giving an age spectrum that climbs from 10 Ma to 46 Ma and K/Ca ratios that climb from 0.26 to 1.9, suggesting xenocrystic contamination (Fig. 11C, b). We believe the error is more robust for the isochron age and prefer it (Fig. 4). The age of the block-and-ash-flow tuff overlaps with the age of the overlying basal Table Mountain Latite (within error). This means that the megablock was derived from the upper part of the Relief Peak Formation, consistent with our observation that block-and-ash-flow tuffs are restricted to the top of the Relief Peak Formation in areas not affected by significant faulting, west of the modern crest (in the stable Sierran block, Fig. 2).

We also collected a hornblende andesite dike that intrudes the block-and-ash-flow tuff that we dated. This vertical dike abruptly ends at the contact between the Relief Peak Formation and the overlying Table Mountain Latite, so it was collected to provide further constraints on the age of this contact. A whole-rock sample from the dike yielded a disturbed spectrum that is typical of reactor-induced recoil, with no clear plateau or isochron age and apparent ages that decrease monotonically from 11.2 to 10.0 Ma. A reasonable assessment of the age of this sample is provided by the mean age of the gas released in the moderate- to high-temperature steps and is interpreted to be ca. 10.35 ± 0.25 Ma (Fig. 11B; Table 1). It therefore provides no useful age constraints on the contact. We do not know whether the dike was emplaced in situ (after deposition of the avalanche deposit), or if it was transported as part of the proposed avalanche megablock; because it is vertical, either interpretation is viable. However, we prefer the interpretation that it was emplaced in situ because it strikes N-S, parallel to the regional trend of dikes and faults in the ancestral Cascades arc.

Our age data from the Relief Peak Formation indicate that very little time (0–140 k.y.) is recorded by the erosional unconformity between it and the overlying Table Mountain Latite lava flows (age data described later).

Stanislaus Group

The thickest section of Table Mountain Latite that we are aware of lies on Sonora Peak (Figs. 3 and 10A), so we dated the base and top of that section. The type section of the Eureka Valley Tuff along the Little Walker River (Fig. 3), where all three members occur, had only been previously dated by the K/Ar method (see previous work). We redated the all three members at the type section by the $^{40}Ar/^{39}Ar$ method.

Table Mountain Latite

Plagioclase from the basal lava flow of the Table Mountain Latite on Sonora Peak (Figs. 3 and 10) yielded a plateau age of 10.19 ± 0.08 Ma and an isochron age of 10.30 ± 0.16, for which we report the mean. A whole-rock separate from the same flow yielded a recoil-type spectrum (Figs. 11D and 11E) with a well-developed high-temperature miniplateau of 10.30 ± 0.1 Ma (Table 1). Since all three ages are concordant, we take the weighted mean age of 10.25 ± 0.06 as the best estimate of the age for the lowest flow (Fig. 4; Table 1). Similarly, plagioclase from the highest flow yielded concordant plateau and isochron ages of 10.14 ± 0.06 and 10.15 ± 0.08 Ma, and a more disturbed whole-rock recoil-type spectrum suggesting an age of ca. 10.0 ± 0.2 Ma. We prefer the plateau age for this sample (Fig. 4), and use the combined data to demonstrate that the entire Table Mountain Latite succession of lava flows on Sonora Peak spans no more than 230 k.y., and could be as little as only a few thousand years. Paleomagnetic data discussed later provide additional constraints on the minimum amount of time spanned by the Sonora Peak latite section.

Eureka Valley Tuff

The Eureka Valley Tuff (Tollhouse Flat Member) yielded excellent concordant plateau and isochron ages on biotite of 9.35 ± 0.04 and 9.32 ± 0.06 and on plagioclase of

9.27 ± 0.04 and 9.30 ± 0.10 Ma, respectively (Fig. 11F). We take the grand weighted mean of all these analyses to indicate an age of 9.31 ± 0.03 Ma for the unit (Fig. 4, 11F).

A plagioclase separate from the middle member of the Eureka Valley Tuff (By Day Member) yielded a reasonably flat spectrum but had somewhat larger errors due to the lower radiogenic yields (Fig. 11G) with concordant plateau (9.19 ± 0.32) and isochron ages (9.10 ± 0.52) (Table 1). For this unit, we report an age of 9.2 ± 0.3 Ma, which overlaps with the ages of both the overlying and underlying members.

A biotite separate from the upper member of the Eureka Valley Tuff yielded concordant plateau and isochron ages of 9.18 ± 0.04 and 9.20 ± 0.06 Ma (Fig. 11H). A plagioclase separate from the same sample yielded a slightly climbing spectrum with concordant plateau and isochron ages of 9.11 ± 0.04 and 9.10 ± 0.08 Ma. These analyses overlap (barely) within 2σ uncertainty, and we use the weighted mean of all these ages to infer an emplacement age of 9.15 ± 0.03 Ma for the upper member of the Eureka Valley Tuff (Fig. 4).

In summary, the ages of the three members of the Eureka Valley Tuff suggest that it was erupted over an ~160 ± 60 k.y. time span between ca. 9.3 and 9.15 Ma.

Disaster Peak Formation

The only age we have on rocks younger than the Stanislaus Formation is from a hornblende andesite plug on Bald Peak (Fig. 3). This plug intrudes the Stanislaus Group and thus may represent the intrusive equivalent of the Disaster Peak Formation. As stated previously, we found very few localities where primary volcanic strata are preserved on the peaks above the Stanislaus Group. Our age data from the Carson Pass area (Busby et al., 2007) indicate that andesite volcanism there persisted until at least 6 Ma.

A hornblende separate from the plug at Bald Peak yielded a plateau age of 7.12 ± 0.06 Ma (Fig. 4, 11I; Table 1). A plagioclase separate from the same sample did not release much gas, so errors are much larger, yielding an age of 7.0 ± 0.5 Ma (Fig. 11I). These data provide a minimum estimate for reestablishment of andesitic magmatism after the end of high-K volcanism.

PALEOMAGNETISM RESULTS FROM TABLE MOUNTAIN LATITE FLOWS

Paleomagnetism Methods

We collected oriented paleomagnetism samples from most lava flows shown on the measured sections described previously, on Sonora Peak (Fig. 10A) and at Grouse Meadow (Fig. 10B). At least six independently oriented samples were collected from the coherent part (Fig. 10) of each flow unit. Samples were distributed both along and through each flow so that individual slump blocks or lightning strikes would affect at most only one or two samples each. For all lava samples, sun compass or sight point corrections were applied to account for local magnetic anomalies. Pluhar conducted paleomagnetic analyses using the University of California–Santa Cruz DC-SQUID 2G Enterprises magnetometer housed in a shielded room. Samples were subdivided into specimens and were stepwise demagnetized in an alternating field (AF demagnetization) up to 180 mT. AF demagnetization is our preferred method for removing secondary components from lightning strikes, which commonly affect lavas at high altitudes and mountaintops. The data are summarized in Table 2.

Bedding attitude tilt-correction was applied to sample data assuming original horizontality. For lava flows, this is clearly a simplification, since they flow by virtue of being emplaced upon an existing slope. Hence, some error in direction will result from unrecognized "initial dip" of the lavas. This error can be reduced if the local paleoslope direction is known. For the Grouse Meadow section, intercalated lithic sandstone–wackestone permitted precise tilt correction to be applied for that locality.

Sample demagnetization data were analyzed using principal component analysis (PCA) (Kirschvink, 1980; Cogné, 2003) to reveal best-fit primary magnetization directions, also called characteristic remanent magnetization (ChRM). For some samples with very large overprint directions, the maximum applied AF field was insufficient to fully reveal the ChRM, in which case, great circle analysis was applied to the demagnetization paths. Initially, we analyzed one sample per flow to get an overall sense of the magnetostratigraphy and then analyzed more samples from selected flows that formed the top and bottom of the section, that bracketed reversals within the section, or that otherwise might have indicated the overall secular variation recorded at each locality. Mean directions were calculated (Fisher, 1953) from the sample ChRMs and great circles for flows from which we analyzed multiple samples. Future work will see the complete analysis of six or more samples from each flow in order to completely characterize the secular variation within (and thus time spanned by) the latites at each locality sampled.

Paleomagnetism Results

Sample demagnetization paths typically exhibited univectorial decay to the origin, unless they had been affected by a large randomly oriented secondary component, probably resulting from lightning-induced isothermal remanence magnetization. Samples probably suffered little magnetization from baking by emplacement of overlying flows because flows were typically capped by thick flow breccia (Fig. 10), which would have insulated the coherent part of the lavas from baking by flows above. MAD (maximum angular deviation) of best-fit PCA-derived ChRMs was typically less than 5° and often less than 1°, usually yielding flow mean directions with α_{95} values less than 10°.

Flow mean directions exhibit some scatter, and many are statistically distinguishable from one another (Fig. 12A), indicating that the sections at both Sonora Peak and Grouse Meadow sample significant secular variation. Indeed, an approximate (approximate because not all flows have been fully analyzed) mean direc-

TABLE 2. PALEOMAGNETIC DATA

Lava flow or sample ID	Data Used[†]	*n* (samples or steps)	Geographic		Tilt corrected		MAD (°)	k	α_{95} (°)	Comment	Applied tilt correction[‡]
			Declination (°)	Inclination (°)	Declination (°)	Inclination (°)					
Grouse Meadow Locality											
GM flow 17	Both	8	45.1	33.7	14.5	45.2	–	176.1	4.2	By Day Eureka Valley Tuff	193°/37°W
GM flow 16	Great circles	3	63.8	30.4	35.8	53.8	–	–	8.4	Flow	193°/37°W
GM flow 15	N.S.	N.S.	N.S.	N.S.	N.S.	N.S.	N.S.	N.S.	N.S.		
GM flow 14	N.S.	N.S.	N.S.	N.S.	N.S.	N.S.	N.S.	N.S.	N.S.		
GM flow 13	N.S.	N.S.	N.S.	N.S.	N.S.	N.S.	N.S.	N.S.	N.S.		
GM flow 12	Both	3	69.1	30.9	41.6	57.0	–	156.5	11.6	Flow	193°/37°W
GM flow 11	ChRMs	3	67.6	42.5	22.7	64.4	–	257.7	7.7	Flow	193°/37°W
GM1005A	15–180 mT	11	52.7	39.1	14.5	53.3	4.2	–	–	Sample	193°/37°W
GM0905A	45–180 mT	7	53.7	32.3	23.6	49.3	3.2	–	–	Sample	193°/37°W
GM0806A	45–180 mT	7	25.1	43.2	350.8	39.7	3.8	–	–	Sample	193°/37°W
GM0707B	15–180 mT	11	49.7	40.1	10.9	52.2	3.8	–	–	Sample	193°/37°W
GM0602	20–180 mT	10	50.1	28.6	23.9	44.5	0.9	–	–	Sample	193°/37°W
GM0506	25–180 mT	9	29.2	43.7	352.9	42.3	4.6	–	–	Sample	193°/37°W
GM0403A	25–180 mT	9	55.1	48.9	1.2	60.1	0.3	–	–	Sample	193°/37°W
GM0304	20–180 mT	10	59.6	71.3	312.9	63.7	1.0	–	–	Sample	193°/37°W
GM flow 2	ChRMs	3	56.6	33.1	25.3	51.6	–	913.6	4.1	Flow	193°/37°W
GM flow 1	ChRMs	5	49.8	29.5	22.8	45.0	–	75	8.9	Flow	193°/37°W
Sonora Peak Locality											
So Flow 23	Both	7	355.8	56.3	355.8	56.3	–	242.7	3.9	Flow	0°/0°
So2204A	NRM–180 mT	15	175.1	38.4	175.1	38.4	7.9[‡]	–	–	[§]	0°/0°
So2106	ChRMs	2	358.0	54.6	358.0	54.6	–	3088.6	4.5	[#]	0°/0°
So Flow 20	N.S.	N.S.	N.S.	N.S.	N.S.	N.S.	N.S.	N.S.	N.S.		
So flow 19	Both	5	179.7	–69.6	179.7	–69.6	–	37.1	14.5	Reversed flow	0°/0°
So1806	80–180 mT	5	345.5	58.3	345.5	58.3	0.5	–	–	Sample	0°/0°
So Flow 17	N.S.	N.S.	N.S.	N.S.	N.S.	N.S.	N.S.	N.S.	N.S.		
So1606	10–180 mT	12	9.9	36.4	9.9	36.4	0.8	–	–	Sample	0°/0°
So flow 15	ChRMs	4	346.0	39.3	346.0	39.3	–	133.6	8.0	Flow	0°/0°
So flow 14	Both	6	156.8	–22.4	156.8	–22.4	–	182.4	5.2	Correlates to classic latite	0°/0°
So flow 13	Both	3	8.8	52.2	8.8	52.2	–	72.8	17.1	Flow	0°/0°
So1201	10–180 mT	12	23.0	61.3	23.0	61.3	0.4	–	–	Sample	0°/0°
So1105	15–180 mT	11	351.7	51.0	351.7	51.0	0.6	–	–	Sample	0°/0°
So1001	10–180 mT	12	331.4	41.8	331.4	41.8	0.2	–	–	Sample	0°/0°
So0902	05–180 mT	13	14.4	58.7	14.4	58.7	0.4	–	–	Sample	0°/0°
So0804B	15–180 mT	11	9.6	53.4	9.6	53.4	0.4	–	–	Sample	0°/0°
So0708A	80–150 mT	4	338.1	51.4	338.1	51.4	1.1	–	–	Sample	0°/0°
So0602	20–180 mT	10	332.9	55.7	332.9	55.7	3.9	–	–	Sample	0°/0°
So0505	30–180 mT	8	1.9	47.7	1.9	47.7	3.7	–	–	Sample	0°/0°
So0402	15–180 mT	11	347.3	40.7	347.3	40.7	0.2	–	–	Sample	0°/0°
So0305	15–180 mT	11	349.1	51.8	349.1	51.8	0.4	–	–	Sample	0°/0°
So0201	30–180 mT	8	351.4	50.7	351.4	50.7	0.3	–	–	Sample	0°/0°
So flow 1	ChRMs	7	341.3	50.3	341.3	50.3	–	104.3	5.9	Flow	0°/0°

Note: Lava flows are indicated in italic. All other data derives from single samples. MAD—maximum angular deviation. N.S.—not sampled.

[†]Data types: for individual samples, the demagnetization steps used for least squares fit through origin, "ChRMs" for mean flow directions using ChRM directions, "great circles" for means using great circles only, and "both" for means determined using ChRMs and great circles.

[‡]At Grouse Meadow, this was determined from attitude of intercalated sediments. At Sonora Peak, 6°W dip of lavas was interpreted to be initial/original dips. Thus, no tilt-correction was applied to Sonora Peak results.

[§]Great circle fit heading toward normal polarity.

[#]Mean direction from two specimens from same sample.

tion (declination = 353.8°, inclination = 52.4°, α_{95} = 5.0°) for the Sonora Peak locality is indistinguishable from the expected mean direction for this latitude at the time of lava emplacement. On the other hand, the mean direction of the Grouse Meadow locality is clockwise deflected from the expected mean, suggesting (1) insufficient time spanned by the section to fully average secular variation, or (2) clockwise vertical-axis rotation of the fault-bounded block(s) on which the Grouse Meadow locality rides. Further study will resolve this issue.

The magnetostratigraphy at Grouse Meadow is entirely normal polarity, while Sonora Peak exhibits two reversed polarity zones with normal polarities above, between, and below (Fig. 12B). The upper reversed zone at Sonora Peak is composed of one very thick latite flow, flow 19 (Fig. 10A). The lower reversed zone, also composed of a single flow, flow 14, exhibits a direction statistically distinct from but very similar to the unusual paleomagnetic direction of the classic Table Mountain Latite of the Sierra Foothills (Pluhar and Coe, 1996). We tentatively correlate Sonora Peak flow 14 with the Table Mountain Latite that flowed all the way to Knight's Ferry at the edge of the Great Valley and attribute the difference in directions between the foothills and Sonora Peak to (1) unrecognized tilt, (2) tectonic rotation, or (3) extremely fast secular variation during the period of emplacement of this large flow.

The $^{40}Ar/^{39}Ar$ dates suggest that flows 14 through 19 at Sonora Peak represent proposed cryptochron C5n.2n-1 (10.197–10.205 Ma), which, to date, is only known from seafloor magnetic anomalies that suggest its existence (Cande and Kent, 1995). If

so, then C5n.2n-1 exhibits more complex field behavior than previously suggested—two closely spaced subchrons with normal polarity in between, instead of one subchron. The rest of the Sonora Peak section falls within the normal polarity chron C5n.2n (9.920–10.949 Ma). An alternate hypothesis is that flows 14 and 19 may correlate to the reversed subchron at 9.880–9.920 Ma or another proposed cryptochron at 10.446–10.470 Ma (Cande and Kent, 1995) or that one flow belongs to one of the cryptochrons and the other flow to another. All of these alternate hypotheses require a loose interpretation of the $^{40}Ar/^{39}Ar$ geochronology for this locality and are not preferred.

The four magnetic reversals (between flows 13 and 14, 14 and 15, 18 and 19, and 19 and 20) evident at Sonora Peak permit a lower bound to be assigned for the duration of emplacement of that locality's latites. Clement (2004) showed that the duration of the last four magnetic reversals averaged ~7000 yr. If we assume that the four reversals recorded at Sonora Peak are typical reversals, then the Sonora Peak latite section must represent at least 28,000 yr.

STRUCTURAL CONTROLS ON VOLCANOLOGY AND STRATIGRAPHY

In this section, we show how we used the stratigraphy in unfaulted (Fig. 4B) to weakly faulted (Fig. 4A) terranes of the stable Sierran block, west of the modern crest, to determine the nature and timing of range front faulting relative to ancestral Cascades arc magmatic events. We present preliminary results from two contrasting segments of the range front fault system: (1) the Hope Valley graben at Carson Pass, which is a largely postarc volcanic full graben that down-drops the Carson Pass–Kirkwood paleocanyon along normal faults with no apparent strike-slip offset (Fig. 13); and (2) the series of synarc volcanic to postarc volcanic half grabens that extend from Sonora Pass to the Little Walker center (Fig. 14), which have a possible strike-slip component of deformation. We discuss the postarc full graben first, in order to emphasize the features we used to identify structures active during arc magmatism. These data will be incorporated into the paleogeographic and tectonic reconstruction of the arc after geochemical data are presented.

Hope Valley Graben: Largely Postarc Full Graben Initiated within the Active Arc

At Carson Pass (Fig. 3), we traced the stratigraphy mapped and dated in the completely unfaulted terrane west of the modern Sierran crest (Fig. 4B; Busby et al., 2007) into range front faults at the modern crest (Fig. 13). Rocks there include lava flows, block-and-ash-flow tuffs, debris-flow and fluvial deposits, and four intrusive suites, including a hornblende-phyric andesite, a 2-pyroxene andesite, a hornblende-biotite andesite, and small basalt intrusions (Tbi) (Fig. 13).

The map is split down the middle by the Hope Valley graben (Fig. 13A). Two major volcanic ridges, one on the east and one on the west side of the map area, are cut by normal faults that down-drop the valley in the middle. The modern N-S river drainages of Hope Valley and Charity Valley are controlled by this structure. Tertiary stratigraphic units are almost flat-lying and have a slight (3–10°) westerly dip throughout the entire mapped area (similar to dips on the stable Sierran block), and the dips do not change as the units approach faults (Fig. 13B).

The west side of the Hope Valley graben is bounded by a previously unnamed, east-dipping normal fault that we refer to as the Red Lake fault (Fig. 13); we infer that this fault largely, but not entirely, postdates the 15–6 Ma arc magmatism in the Carson Pass–Kirkwood area from the crest westward (Fig. 4B). The Red Lake fault lies along a prominent topographic escarpment (Fig. 13A) and down-drops Cenozoic volcanic rocks against Mesozoic granitic basement; it also offsets volcanic units that we correlate here. In the E-W cross section (section A, Fig. 13B), we show a stratified conglomerate-breccia (map unit Tsb) that outcrops on both sides of the fault and is offset ~1300 ft (400 m). In the N-S cross section (section B, Fig. 13B), we show a fluvial unit (Tvf) that is widespread on the stable Sierran block (Tvf, Fig. 4B; Busby et al., 2007) and correlate that with a fluvial unit within the graben east of Elephant's Back (Tvf), suggesting a minimum offset along the fault of ~1000 ft (300 m). There is no apparent ponding of the lava flows (Thafu and Thafl) against the fault, and all of the units are flat-lying; they do not dip or thicken toward the fault, unlike in the Sonora pass region (Fig. 17B). However, where the Red Lake fault is well exposed cutting granitic basement, just southeast of Elephant's Back (Fig, 13), it consists of a 15-m-wide zone of brecciated granite invaded by an andesite plagioclase porphyry. This indicates that range front faulting began within the active arc.

The east side of the Hope Valley graben is bounded by a previously unnamed, west-dipping normal fault that we refer to as the Hope Valley fault; we infer that this fault has approximately the same offset as the Red Lake fault, although constraints are not as good. The Hope Valley fault is marked by a prominent 1200 ft (380 m) west-facing escarpment within granitic rocks, or is hidden by Quaternary deposits, but it cuts volcanic rocks at its south end, along the Charity Valley. There, the Hope Valley fault places heavily altered volcanic rocks (map unit Taa) against the hornblende biotite andesite intrusion that forms Markleeville Peak (map unit Thbai, Fig. 15A). The heavily altered volcanic rocks west of the fault also have small intrusions of the Markleeville Peak hornblende biotite andesite (Fig. 15A); we interpret these to represent apophyses of the Markleeville Peak intrusion, which is thus shown lying at depth west of the fault on the cross section (Fig. 15A, cross-section C). We interpret the heavily altered rocks (map unit Taa) to represent the roof rocks to the Markleeville Peak intrusion, which have been down-dropped along the Hope Valley fault (Fig. 15A, cross-section C). While we realize that the top of an intrusion is uneven, we make a crude estimate of at least 1200 ft (380 m) of offset along the Hope Valley fault using the inferred offset between the base of the altered unit and the top of the intrusion (Fig. 15A, c). This estimate matches the height of the granite escarpment.

We propose that the Carson Pass–Kirkwood paleocanyon can be traced eastward from the Sierran crest into the Red Lake Peak–Steven's Peak area (Fig. 13), where it appears to branch into two paleotributaries: (1) a northern paleotributary, defined by thick Miocene strata in the Pickett Peak–Horsethief Mountain area, and (2) a southern paleotributary, defined by Oligocene to Miocene strata in the Jeff Davis Peak–Red Lake (although the southern branch is partly intruded out by the Markleeville Peak intrusions). If this interpretation is correct, the paleocanyon does not show any dextral offset across the normal faults that displace it, suggesting that geodetic data for the central Sierra are not everywhere consistent with the long-term displacement history.

While these field relations show that most of the faulting in the Hope Valley graben postdated volcanism, two lines of evidence suggest that incipient faulting controlled the ascent of magmas. First, thick hornblende andesite lava flows occur on the graben floor along the Red Lake fault, only a few hundred meters north of exposures of the fault-brecciated granite that has been invaded by an andesite plagioclase porphyry. Second, the graben is the site of one of the biggest intrusions and alteration zones within the ancestral Cascades arc of the central Sierra (Markleeville center).

The timing of magmatism and faulting in the Hope Valley graben is constrained to be younger than ca. 11 Ma, and perhaps as young as ca. 7 Ma. The andesite flows could be just slightly younger than the fluvial deposits they overlie (correlated with unit Tfu of Fig. 4B, between 14.7 and 10.6 Ma), or the flows could be just slightly older than the debris-flow unit that overlies them (tentatively correlated with unit Tvdf of Fig. 4B, which is between 6.8 and 6.05 Ma in age). A K-Ar date of 6.9 ± 0.7 reported by Mosier (1991) from the Markleeville Peak intrusion supports the interpretation that the graben structure is younger than ca. 7 Ma. This age is also consistent with the inferred age of the Tahoe graben just to the north (Surpless et al., 2002), so we prefer it.

Sonora Pass–Little Walker Half Grabens: Evidence for Transtensional Walker Lane Faulting within the Arc Axis

The widespread and distinctive nature of the various units in the high-K volcanic section (Stanislaus Group, Fig. 4A) makes them extremely useful as strain markers in range front faults of the Sonora Pass area. Early mapping by Priest (1979) and Slemmons (unpublished map from the 1970's provided to the authors by B. Slemmons in 2001) shows a series of faults, roughly subparallel to the modern range front, that drop Tertiary volcanic-volcaniclastic rocks down to the east against granite. Our preliminary map and cross sections of the area (Fig. 14) show a series of half grabens, with strata dipping toward faults. At least one of these faults, the Sonora Junction fault, is still active and has N-S–trending scarps that cut Pleistocene deposits (Rood et al., 2005). In this section, we present new evidence that faulting began just before eruption of the high-K volcanic rocks, presumably from the Little Walker center. This evidence includes fanning dips (i.e., hanging-wall strata that dip toward normal faults, with dips that flatten upsection), thickening of strata toward footwalls, and avalanche deposits just below the high-K volcanic rocks. The presence of avalanche deposits at the top of the Relief Peak Formation in the range front at Sonora Pass is significant because they do not occur on the stable Sierran block, nor do they occur in the postvolcanic Hope Valley graben. We interpret them as paleolandslides that were shed from active faults.

The longest fault in the Sonora Pass–Little Walker center area is the Leavitt Meadow–Lost Cannon fault (Fig. 14). The Relief Peak Formation, Table Mountain Latite, and Eureka Valley Tuff are dropped down at least 3000 ft (~900 m) against granitic basement along this fault and dip toward it. This section is repeated to the east by the Grouse Meadow fault, with lesser offset (Fig. 14; Busby et al., 2006). Avalanche blocks of welded ignimbrite (described previously) are present in the Relief Peak Formation of the Grouse Meadow block. At the latitude of Grouse Meadow, dips in the volcanic rocks do not fan dramatically, but they do appear to flatten somewhat between the Table Mountain Latite and the Eureka Valley Tuff. More dramatic is the rapid thickening of Table Mountain Latite toward the Lost Cannon fault, and even more pronounced thickening of a fluvial sandstone within the Table Mountain Latite (not shown at the scale of Fig. 14), which thickens from ~<10 m to >30 m toward the fault. At the north end of the map, strata clearly fan toward the Lost Cannon Peak fault, which shows at least 4100 ft (~1240 m) of normal offset (section A–A′, Fig. 14). The Valley Springs Formation welded ignimbrites and the Relief Peak Formation debris-flow and lesser streamflow deposits dip ~45° toward the fault, but the Table Mountain Latite dips only 15° toward the fault. We did not see depositional dips greater than ~5–7° on the Table Mountain Latite in the stable Sierran block (which is tectonically tilted ~2°), so we infer that it was tilted when it was down-dropped against granitic basement. We interpret the dips on the strata beneath to record greater offset along the fault, prior to eruption of the latite. One could argue that dips in the Relief Peak Formation were originally steep (although 45° is not reasonable), but the welding compaction fabric in the underlying welded ignimbrites uniformly dips the same way, providing a reliable paleohorizontal indicator. Furthermore, the Relief Peak Formation has large shattered avalanche slabs of ignimbrite just below the Table Mountain Latite. Taken together, we interpret these features to record the onset of faulting just before eruption of the Table Mountain Latite.

We also recognize landslide deposits in the top of the Relief Peak Formation on the hanging wall of the St. Mary's Pass fault, beneath Table Mountain Latite (Fig. 14). These are the soft-rock avalanches of bedded volcaniclastic sections described previously. The St. Mary's Pass fault shows minor offset after eruption of the Table Mountain Latite: it drops Table Mountain Latite ~200 ft (~60 m) down to the east against Relief Peak Formation at St. Mary's Pass, and south of Sonora Pass, it drops the latite down 300 ft (~90 m), and the latite dips toward the fault a bit more steeply (15°) than the regional westward dip of the

latites (less than 5–7°). Much more impressive, however, is the thickness of the avalanche deposit below the latite along the east margin of the fault (Fig. 14). It is at least 500 m thick, suggesting that it was shed from a prominent topographic feature, and the distribution of the deposit along the fault suggests deposition in a hanging-wall basin. As described already, the age of a block-and-ash-flow tuff within the 1.6-km-long landslide megablock is 0–140 k.y. older than the Table Mountain Latite (using analytical uncertainties described previously). Thus, the timing of inferred landsliding off the St. Mary's Pass fault is also within 0–140 k.y. of the onset of high-K volcanism.

We have preliminary evidence for a strike-slip component to the normal faulting at Sonora Pass. Faults of this area step right around the north end of the Little Walker center (Fig. 3B), and some individual faults also appear to step right (e.g., Sonora Junction fault, Fig. 14). Releasing stepovers in strike-slip faults produce much bigger volcanic centers than releasing bends (Busby and Bassett, 2007), consistent with the position of the Little Walker center (Figs. 3B and 14). Our preliminary paleomagnetic results from the Table Mountain Latite in the Grouse Meadow block (described previously) are suggestive of clockwise rotation. A plug in the footwall of the Lost Cannon Peak at the north end of the map (where the normal component of offset is estimated at 4100 ft [~1242 m]) appears to have been "decapitated" by the fault, with a strike-slip offset component of ~1500–2000 ft (~455–606 m). Along the east side of the St. Mary's Pass fault, between Sonora Peak and Sonora Pass (Fig. 14), the Relief Peak Formation is cut by steeply dipping shear zones that do not penetrate the overlying Table Mountain Latite. Kinematic indicators are not well-developed in the soft-rock avalanche blocks there, but the vertical dike that cuts them has Riedel shears suggestive of strike-slip deformation. As discussed already, the dike may have been transported along with the megablock it intrudes, so the shallowly plunging shears may be rotated 50° about a horizontal E-W axis, but we prefer the interpretation that the dike was emplaced in situ because its orientation fits regional trends.

In summary, our new data strongly support the interpretation that the onset of faulting immediately preceded the onset of high-K volcanism within the ancestral Cascades arc of the Sonora Pass area. Preliminary evidence is suggestive of a dextral strike-slip component of movement on the normal faults, and development of the major Little Walker center on a releasing stepover. Thus, this faulting and attendant high-K volcanism may record the birth of Walker Lane transtensional deformation.

GEOCHEMICAL RESULTS: SIGNIFICANCE OF HIGH-K_2O VOLCANISM

High-K_2O Magmatism and Tectonics

Since Hatherton and Dickenson (1969) first proposed that K_2O in volcanic rocks increases with depth to the underlying subducted slab, there has been considerable interest in using K_2O either to infer paleosubducted plate behavior (e.g., Lipman et al., 1972), or to connect K_2O in some way to tectonic processes. Volcanic rocks from the Carson and Sonora Pass regions, which include the type locality for "latite" and "quartz latite" (Ransome, 1898), appear to be key in unraveling the tectonic significance of K_2O. These regions lie within a latitudinal transition between relatively low-K_2O volcanics of the Lassen area to the north, and ultrapotassic rocks in the "high" Sierra Nevada to the south. Though volcanism was not contemporaneous across all these areas, there is a strong latitudinal gradient in K_2O, which bears greatly on the magmatic history of the Cascade and the Sierra Nevada provinces in particular, and the tectonic significance of K_2O in general.

Although there has been much discussion of K_2O as an indicator of depth to a subducted slab, recent interest in the Cordillera has turned to the possibility that ultrahigh K_2O may reflect delamination of mantle lithosphere. Feldstein and Lange (1999) were the first to propose that high-K_2O volcanism in the southern Sierra Nevada was due to a dual process involving subduction-related enrichment of the mantle source in large ion lithophile elements (LILE, i.e., K and Ba) and subsequent mantle partial melting due to delamination of the mantle lithosphere, or Basin and Range extension. Manley et al. (2000) and Farmer et al. (2002) provided additional geochemical data to demonstrate the temporal plausibility of a delamination-induced melting event in the southern Sierra Nevada and suggested that Pliocene uplift of the Sierra Nevada was coincident with renewed high-K_2O volcanism. Our preliminary geochemical study suggests that the supposed linkage between K_2O and delamination is at best coincidental, and not causal. We tentatively propose an alternative, testable hypothesis for the generation of K_2O variations in the Cordillera.

Central Sierra Nevada Ancestral Cascade (CSNAC) Geochemistry

The nature of the Sierra Nevada changes dramatically as one moves south of 38°23′N. South of that latitude is the "high Sierra," which has mountain peaks that regularly top 4000 m and a bedrock geology consisting largely of granitoids. North of that latitude, the Sierra Nevada is high, but much more subdued, with few peaks rising above 3500 m, and the bedrock geology is largely volcanic. As voluminous and important as these volcanics of the central Sierra Nevada are, only two unpublished Ph.D. theses (Priest, 1979; Brem, 1977) and a single publication (Noble et al., 1976) have discussed their geochemistry (and only partially), and these studies largely dealt with the geographically restricted Little Walker caldera region, just east of Sonora pass (Figs. 3 and 14). Here, we discuss whole-rock major-element data for rocks collected from the Sonora and Carson pass regions (Fig. 3; Table 3; analytical methods in Appendix 1).

Using the inferred paleolatitude of the Mendocino triple junction (Fig. 1), the Sonora and Carson Pass volcanics were erupted in a subduction, or arc setting. The predominance of

TABLE 3. GEOCHEMICAL DATA

Sample name	SiO_2	TiO_2	Al_2O_3	Fe_2O_3	MnO	MgO	CaO	Na_2O	K_2O	P_2O_5	Cr (ppm)	Sum
Stanislaus Formation												
PC043–2	57.06	1.04	16.28	6.88	0.09	5.19	6.92	3.89	1.56	0.314	224.5	99.224
BP007–1	50.01	1.64	14.82	9.42	0.1	10.07	9.11	2.63	1.9	0.463	640.9	100.163
BP020–1	55.59	0.88	16.28	6.98	0.07	6.5	7.27	3.64	1.59	0.241	269.6	99.041
BP046–1	60.2	0.71	17.71	5.48	0.03	2.41	6	3.87	2.12	0.366	8.1	98.896
BP046–2	53.29	1.21	18	8.67	0.09	4.07	7.37	3.67	2.85	0.714	1.8	99.934
DC036–1	49.74	1.14	15.72	9.36	0.13	9.73	9.09	2.61	1.87	0.442	548.8	99.832
DC064–1	60.53	1.38	16.15	6.09	0.08	1.6	3.85	3.71	5.01	0.493		98.893
DC065–1	59.57	1.49	16.42	6.37	0.05	1.72	3.93	3.65	5.22	0.604		99.024
DCO16–1	58.01	1.14	16.99	6.84	0.06	3.7	6.09	3.54	3.62	0.417	78.6	100.407
PC005–1	57.13	1.38	18.69	6.8	0.04	1.29	6.47	4.12	3.44	0.685	101.9	100.045
PC032–1	50.96	1.49	17.44	9.97	0.12	4.17	9.64	3.29	1.89	0.376	21.1	99.346
PC065–1	61.61	0.79	16.83	5.42	0.06	3.12	5.07	3.33	3.66	0.311	43.8	100.201
PC066–1	59.48	0.94	19.83	4.78	0.04	1.24	6	4.11	3.14	0.386	0.3	99.946
PC006–2	54.83	1.28	16.25	7.2	0.11	3.96	8.5	3.68	2.92	0.569	165	99.299
PC007–1	57.54	1.33	16.88	8.4	0.03	1.87	6.03	3.75	3.07	0.603	165	99.503
PC007–2	56.91	1.33	16.71	8.2	0.03	1.85	5.97	3.75	3.08	0.595	164	98.425
PC008–2	54.46	1.26	16.13	7.53	0.1	4.12	7.94	3.68	2.96	0.57	170	98.750
PC010–1	54.46	1.27	16.34	7.83	0.1	4.25	8.53	3.5	2.59	0.592	174.8	99.462
PC010–2	54.42	1.29	16.28	7.87	0.09	4.23	8.42	3.47	2.58	0.59	172.4	99.240
PC015–2	54.74	1.33	15.8	8.41	0.2	4.27	7.53	3.35	2.73	0.605	341.9	98.965
PC016–1	54.57	1.83	16.84	7.52	0.09	2.45	5.93	3.91	3.43	1.074	82.4	97.644
LW-101 CMS 1.1 4–6-0	70.09	0.44	15.97	2.16	0.06	0.48	1.32	3	6.21	0.098		99.828
LW-107 CMS 1.1 4–6-0	63.68	1.14	16.87	4.37	0.07	1.21	2.89	4.3	4.82	0.314		99.664
LW-108 SI-1 3–29–04	55.53	1.02	17.36	7.34	0.08	3.74	7.24	3.49	2.48	0.453	46.1	98.733
LW-110 MO-1 3–25–04	63.59	0.88	16.43	6.58	0.1	1.8	5.79	2.17	2.98	0.195	76.4	100.515
LW-111 CMS 1.2 4–1	58.29	0.97	17.83	6. 77	0.07	3.42	6.04	3.62	3.02	0.354	12.1	100.384
LW-112 MO-1 3–25–04	57.46	1.03	17.48	6.85	0.07	4.56	6.48	4.37	1.94	0.282	58.7	100.522
LW-112 XM CMS 1.1 3-	66.86	0.77	15.61	4.17	0.03	1.66	4.27	3.25	3.15	0.39	15.8	100.160
LW-113 CMS 1.1	58.35	0. 97	17.86	6.71	0.07	3.47	6.05	3.64	3.01	0.352	11.5	100.482
LW114 RM-1 4–1-04	62.26	0.71	17.65	4. 54	0.01	1.37	4.31	3.92	4.16	0.259	31.9	99.189
LW-115 CMS 1.1 4–1	61.94	1	18.3	4. 77	0.05	1.49	4.08	5.21	2.3	0.412		99.552
LW-116 SL-1 3–29–04	58.9	1.02	18.47	5. 26	0.06	1.82	4.04	4.72	3.57	0.44		98.300
LW-117 CMS 1.1 4/7/0	60.08	0.94	18.63	4.65	0.03	1.5	4.07	4.32	3.84	0.399		98.459
LWK 103 Rm1 4–1-04	58.89	0.87	18.18	6.75	0.09	2.32	6.07	3.96	2.77	0.453	26.2	100.353
LW-K102 SL-1 3–29–04	58.69	0.88	17.64	6.39	0.05	2.41	5.94	3.86	2.8	0.429	19.8	99.089
Relief Peak Formation												
TMOB 1-SP-05	50.95	1.521	15.54	11.22	0. 13	7.58	8.86	2.1	1.25	0.477		99.628
TMOB 2.1-SP-05	51.09	1.512	15.65	11.34	0.13	7.31	9.1	1.92	1.28	0.455		99.787
TMOB 2 TOP? 1-SP-05	51.25	1.516	15.82	11.49	0.13	6.77	9.22	1.93	1.17	0.46		99.756
TMOB 3.1-SP-05	49.67	1.401	15.89	12.01	0.16	8.06	9.35	1.88	0.85	0.346		99.617
TMOB 4-SP-05	50.34	1.342	16.11	12.5	0.13	7.48	9.4	1.55	0.77	0.322		99.944
TMOB 4 TOP-SP-05	50.11	1.286	16.11	12. 3	0.12	7.77	9.41	1.55	0.57	0.303		99.529
TMOB 5-SP-05	50.66	1.404	16.1	12.11	0.14	7.38	9.46	2.08	0.74	0.309		100.383
TMOB 6-SP-05	50.05	1.37	16.11	12.14	0.15	7.26	9.58	2	0.59	0.298		99.548
TMOB 7-SP-05	50.45	1.323	16.08	11.98	0.14	7.76	9.47	1.95	0.62	0.291		100.064
TMOB 8-SP-05	50.56	1.284	15.73	11.98	0.12	8.18	9.2	1.62	0.71	0.281		99.665
TMOB9 NB-SP-05	49.84	1.31	16.02	11.73	0.19	8.06	9.34	2.61	0.6	0.287		99.987
TMOB 10-SP-05	50.15	1.283	15.6	12.04	0.11	8.72	9.25	1.57	0.62	0.278		99.621
TMOB11 NB-SP-05	49.72	1.32	16.04	12.12	0.18	7.31	9.48	2.42	0.66	0.282		99.532
TMOB11b NB-SP-05	49.79	1.29	15.85	11.8	0.17	7.91	9.33	2.58	0.69	0.26		99.670
TMOB12 NB-SP-05	50.44	1.39	17.32	12.55	0.18	5.24	7.74	1.88	3.16	0.288		100.188
TMOB W-L-SP-05	50.16	1.288	15.66	11.86	0.12	8.2	9	2.15	0.85	0.254		99.542
TMOBWM NB-SP-05	49.13	1.31	16.57	12.35	0.19	8.46	8.77	2.02	1.29	0.262		100.352
DC067–1	49.42	1.23	16.47	11.68	0.14	7.44	9.54	2.7	0.57	0.197	232.2	99.387
PC-BA-1	54.54	1.32	16.51	7.05	0.06	4.75	8.65	3.09	2.35	0.382	116.8	98.702
RP-1 KT-1 3–25–04	56.5	0.95	17.99	7.39	0.09	3.63	6.98	3.83	2.2	0.496	33.9	100.056
RP-4 KAT 3–31–04	53.83	1.11	18.44	8.99	0. 13	2.91	8.8	3.67	2.23	0.536	2.1	100.646
RP-7 VS-1 3–25–04	52.32	1.35	17.28	8.85	0.09	5.7	8.4	3.43	2.31	0.539	78.5	100.269
RP-8 CMS 1.1 3–30	73.38	0.59	13.92	4.77	0.02	2.34	1.6	2.27	2.85	0.11	10	101.850
RP-9 KT-1 3–25–04	55.91	0.96	17.81	7.22	0.08	3.8	6.34	4.43	2.25	0.441	24.3	99.241
RP-DP CMS-1.1 4/5/04	55.56	1.49	17.1	7.75	0.08	3.4	5.95	4.07	3.56	0.662	60.7	99.622
EH K105 3–25	63.98	1.11	17.02	4.35	0.06	1.16	2.81	4.27	5.26	0.322		100.342
EH K109 3–29	70.46	0.38	16.14	2.22	0.03	0.44	1.36	4.68	5.1	0.1		100.910
RLBA NB-SP-05	66.9	0.69	14.23	5.14	0.06	2.06	4.65	3.33	2.21	0.376		99.646
RP DIKE-SP-05	60.44	0.974	18.09	6.36	0.06	1.27	6.53	3	2.37	0.48		99.574
HBL AND PLUG-SP-05	57.52	0.98	17.58	7. 11	0.1	3.51	7.27	2.92	2.26	0.341		99.591

(*continued.*)

TABLE 3. GEOCHEMICAL DATA (*continued.*)

Sample name	SiO_2	TiO_2	Al_2O_3	Fe_2O_3	MnO	MgO	CaO	Na_2O	K_2O	P_2O_5	Cr (ppm)	Sum
Carson Pass												
SBDCP16a-1	56.24	0.98	17.69	7.34	0.1	3.87	7.31	3.57	2.29	0.352	28.3	99.742
SBDCP19–2	54.95	1.05	18.12	7.7	0.09	3.69	8.63	3.27	1.85	0.289	19.3	99.639
SBDCP75–2	58.43	0.82	17.91	7.07	0.09	3.07	6.43	3.31	2.3	0.271	4.3	99.701
SBDCP62–1	51.11	1.03	15.71	8.99	0.12	8.58	9.36	2.96	1.7	0.328		99.888
RL1 NB-SP-05	52.46	1.04	16.16	8.99	0.09	7.32	8.82	3	1.89	0.337		100.107
RL 2-SP-05	52.67	1.039	15.69	8.55	0.08	9.03	8.38	1.99	1.96	0.378		99.767
RL3 NB-SP-05	52.82	1.12	16.51	8.49	0.09	6.73	8.4	3.29	2.11	0.56		100.120
RL4 NB-SP-05	52.28	1.09	16.11	8.49	0.11	7.68	8.23	3.2	2.08	0.37		99.640
RL5 NB-SP-05	53.66	1.11	16.83	8.09	0.12	6.19	8.14	3.67	2.13	0.4		100.340
SBDCP45–2	52.18	1.2	18.36	9.09	0.21	3.72	10.32	3.1	1.28	0.327	40.7	99.787
SBDCP67–1	58.6	0.81	17.53	6.93	0.09	3.63	6.82	4.15	2.45	0.279		101.289
SBDCP67–2	55.98	1.06	17.75	7.36	0.05	3.85	8.05	3.68	1.98	0.248		100.008
SBDCP46–2	58.43	0.85	17.05	6.04	0.05	3.08	6.02	3.88	2.56	0.433	29.6	98.393
SBDCP22–1	55.77	1	17.73	7.11	0.06	4	8	3.54	1.83	0.259	55.7	99.299
SBDCP27–1	61.73	0.56	18.37	5.42	0.04	1.58	5.73	4.09	2.02	0.329		99.869
SBDCP63–2	56.94	0.96	17.57	6.57	0.09	3.6	6.95	3.16	2.64	0.334	24.3	98.814
SBDCP23–1	55.47	0.94	18.46	7.6	0.09	3.99	7.67	3.82	1.5	0.3		99.840

block-and-ash-flow tuffs, debris-flow deposits, lahars, and intermediate-composition lava flows and plugs shows an affinity to Cascade activity, as opposed to the "fundamentally basaltic" and bimodal volcanism the dominates the Basin and Range (Christiansen and Lipman, 1972). Based on analogy with Lassen, it may be likely that volcanic centers were preferentially eroded due to the pervasiveness of hydrothermal alteration of near-vent materials. Because of the clear association with the Cascades, the rocks of the region are herein referred to as the Central Sierra Nevada Ancestral Cascade (CSNAC) province.

The major-element compositions of Central Sierra Nevada Ancestral Cascade province volcanic rocks are in some respects intermediate, or perhaps transitional, between Basin and Range, and Cascade volcanism. For purposes of geochemical comparisons, the Carson Pass volcanics (14.7–6 Ma) are undivided, as they are internally geochemically similar and, as noted already, have no direct stratigraphic relationship to the latites of the Stanislaus Formation. At Sonora Pass, also already noted, the volcanics are divided into Relief Peak Formation (pre–10.2 Ma), the Stanislaus Formation (9–10.2 Ma), and the poorly dated 9(?) to 6 Ma Disaster Peak Formation (Fig. 4B). Results from the Disaster Peak Formation are not presented in this study. The Central Sierra Nevada Ancestral Cascade province rocks are calc-alkaline on the AFM diagram but plot as mildly trachytic on an alkali-silica diagram (Figs. 15A and 15B). The most mafic rocks are basalts (7.3%–8.7% MgO) from the Relief Peak Formation, which are similar to primitive Cascade basalts (Figs. 15A and 15B), but most rocks are intermediate in composition. More interesting is the comparison to Lassen (Fig. 15C), where basalts of similar composition evolve to high-SiO_2 compositions, but which have lower alkali contents than in the Central Sierra Nevada Ancestral Cascade province, where intermediate compositions have higher K_2O at a given SiO_2 content; when the southern Sierra volcanics are considered, there appears to be a trend of increasing K_2O from north to south.

Farmer et al. (2002) suggested that high-K_2O values in the Sierra may have resulted from K-metasomatism of the upper mantle lithosphere due to slab-related fluid inputs; they suggested that this K-enriched region was exposed to the asthenosphere and partially melted during lithosphere delamination. However, an association between K_2O and slab-related components is unclear. At Lassen, Borg et al. (2000, 2002) have demonstrated that Sr/P ratios provide a positive index of slab-derived fluids. However, high-K_2O values are not associated with high Sr/P_2O_5 for any of the volcanic rocks from the Sierra Nevada, whether from Lassen or elsewhere (Fig. 15C). Sr/P ratios do not vary with MgO in the Central Sierra Nevada Ancestral Cascade province and so are not controlled by fractional crystallization. Also, K_2O is similarly uncorrelated with Ba contents, or Ba/Rb or Ba/Nb ratios, which are thought to relate to subducted fluid input (e.g., Feldstein and Lange, 1999). With no clear relationship between K_2O and putative slab-derived components, it is unlikely that elevated K_2O reflects a subduction component.

One rather striking relationship however, is the latitudinal increase in K_2O at a given SiO_2 content as one moves south along the Sierra Nevada (Fig. 15C). The K_2O-SiO_2 diagram clearly illustrates the transitional nature of the Central Sierra Nevada Ancestral Cascade province and suggests a spatial control that is independent of time of eruption. Together, these relationships, or lack thereof, in Figures 15B and 15C cast doubt upon the role of K_2O as an index of subducted fluid input, or a signal of lithosphere delamination.

High-K_2O Volcanism as a Product of High-Pressure Fractional Crystallization

If K_2O is not an index of subduction-related fluid input, nor an indicator of delamination, what then are the controls of K_2O contents in Sierra Nevada, and more generally, Cordilleran magmas? In an experimental study, Meen (1990) demonstrated that the pressure of fractional crystallization affects K_2O-SiO_2 covariations. At pressures above ~8–10 kbar, most basaltic magmas have clinopyroxene on the liquidus, in place of olivine and plagioclase (Meen, 1990; Putirka et al., 1996).

Clinopyroxenes have SiO_2 contents of ~49–50 wt% and so have similar SiO_2 contents compared to the primitive basaltic liquids from which they crystallize. The effective bulk partition coefficient of SiO_2 is thus ~1, when clinopyroxene is the dominant precipitate, and may even be slightly greater than 1, depending upon the precise composition of the clinopyroxene and coexisting liquid. However, even at pressures as high as 30 kbar, K_2O is still nearly perfectly incompatible in clinopyroxene (Putirka et al., 1996). Meen (1990) proposed that high-pressure, clinopyroxene-dominated fractional crystallization would thus cause K_2O contents to increase steeply with only modest increases in SiO_2. At lower pressures, olivine and plagioclase replace clinopyroxene as fractionating phases. Thus, with decreased pressure the amount of clinopyroxene will progressively decrease relative to olivine and plagioclase. We propose that the K_2O-SiO_2 trends in Figure 15B reflect precisely this process and are controlled by an increase in the thickness of the granitic crust in the Sierra Nevada toward the south, as illustrated in Figure 16. Simple mass-balance calculations illustrate the plausibility of this effect on K_2O-SiO_2 systematics (Fig. 15C).

Our model of high-pressure fractional crystallization (i.e., high modal clinopyroxene) as the cause of high K_2O finds support in two observations. First, clinopyroxene is common as a phenocryst phase in the Central Sierra Nevada Ancestral Cascade province and as microphenocryst and groundmass phases in the southern Sierra Nevada volcanics, but it is nearly absent at the Lassen volcanic center, where plagioclase and olivine dominate the phenocryst mineralogy. Of course, the precise modal ratios of phenocryst phases observed in volcanic rocks at the surface might only reflect the latest phase of partial crystallization prior to eruption, but if nothing else, there is clear petrologic evidence for an absence of low-pressure (olivine + plagioclase dominated) fractional crystallization in the Central Sierra Nevada Ancestral Cascade province and southern Sierra. In addition, Mavko and Thompson (1983) showed an increase in crustal thickness moving south from Lassen to Mt. Whitney. An increase in crustal thickness to the south is perhaps also to be expected given the increase in peak elevations in the southern Sierra Nevada.

Finally, the seemingly abrupt increase in elevation south of 38°23′N, and the rapid southward changeover from volcanic to granitic basement suggests an additional crustal control on volcanic activity. We postulate that at 38°23′N, the Sierra Nevada granitic crust reaches a threshold value in thickness, such that south of this latitude, the crust acts as a low-density "cap" and is sufficiently thick to inhibit upward magma transport and voluminous surface magmatism. North of this latitude, the granitic crust is sufficiently thin to allow effective magma transport. Highly alkaline, K_2O-rich magmas in the south thus might not only reflect clinopyroxene fractionation, but might also reflect a requirement that beneath thick crust, magmas must achieve very low melt fractions—and high volatile contents (Feldstein and Lange, 1999)—to allow sufficient positive buoyancy for magmas to reach the surface. We emphasize that these hypotheses are tentative, pending more complete geochemical analyses of the Central Sierra Nevada Ancestral Cascade province volcanics, which are currently under way. Nonetheless, the model is testable. If valid, clinopyroxene thermobarometry of volcanic rocks from the Central Sierra Nevada Ancestral Cascade province should yield lower pressures compared to those of ultrapotassic rocks from southern Sierra Nevada, and trace-element compositions in the Central Sierra Nevada Ancestral Cascade province should be consistent with greater removal of those elements that are highly compatible in clinopyroxene, but less compatible in olivine or plagioclase (i.e., Cr, Sc). We also suspect that the model illustrated in Figure 16 may be generally applicable to explain K_2O variations across the Cordillera and suggest that the model can be further tested by examining crystallization conditions in volcanic rocks of the Great Basin.

The 10 Ma to ca. 9 Ma high-K_2O latite and quartz latite volcanism in the Sonora Pass area of the central Sierra represents a local excursion to higher alkalinity, relative to the more "normal" andesites and trachyandesites that dominated this segment throughout its life (15 Ma to 6 Ma). We propose that this brief excursion was triggered by deep-seated faulting at a pull-apart (releasing stepover) structure at the inception of West Walker Lane faulting. This fault system penetrated a lithospheric plate with a thick crustal section, tapping magmas generated at relatively great depths.

PRELIMINARY PALEOGEOGRAPHIC AND TECTONIC MODELS: SUMMARY AND CONCLUSIONS

Prior to our study, very little was known about the Tertiary paleogeographic and tectonic evolution of the central Sierra Nevada. We use the initial results of our multidisciplinary study to present preliminary models (Table 4), to be tested or modified by future work.

Arc Stratigraphy and Paleogeography

The new $^{40}Ar/^{39}Ar$ dates described here, combined with our new $^{40}Ar/^{39}Ar$ dates reported elsewhere (Busby et al., 2007), indicate that andesite volcanism occurred along the present-day central Sierran crest from ca. 14 to 6 Ma. In the Sonora Pass area, andesite volcanism as young as 10.10 ± 0.06 Ma was interrupted by high-K volcanism, including eruption of Table Mountain Latite lava flows at Sonora Peak at 10.25 ± 0.06 Ma, followed by eruption of all three members of the Eureka Valley Tuff quartz latite ignimbrites between 9.30 ± 0.03 Ma and 9.16 ± 0.03 Ma. Andesitic volcanism in the Sonora Pass area resumed by 7.12 ± 0.06 Ma. The paleomagnetism results from Table Mountain Latites of the Sonora Pass region are consistent with $^{40}Ar/^{39}Ar$ geochronology and likely constrain the two reversed polarity flows at Sonora Pass to a very precisely dated cryptochron during chron C5n, where one of the reversed flows correlates with the classic Stanislaus Table Mountain Latite of Ransome (1898) in the Sierra Nevada Foothills. The reversed polarity flows within

TABLE 4. PRELIMINARY SUMMARY OF EVENTS IN THE CENTRAL NEVADA SIERRA ANCESTRAL CASCADES (CSNAC) PROVINCE

Oligocene (33.7–23.8)	Deposition of multiple ignimbrites within paleocanyons inherited from Cretaceous time; erupted from calderas in central Nevada.
Early Miocene (23.8–16.4)	Deep dissection of Oligocene ignimbrite (reincision 1, Figs. 4 and 17) due to uplift triggered by onset of arc magmatism in present-day Sierra Nevada.
Middle Miocene (16.4–11.2)	Andesite/trachyandesite volcanism begins ca. 15 Ma. Numerous, small centers form along faults. Western Walker Lane transtensional faulting begins within the CSNAC at ca. 11 Ma at Sonora Pass (reincision 2, Figs. 4 and 17); releasing stepover produces pull-apart basin at ca. 10–9 Ma high-K volcanism at a large center (Little Walker center, Fig. 14).
Late Miocene (11.2–5.3)	Andesite/trachyandesite volcanism at small fault-controlled centers continues to 6 Ma. Uplift event at ca. 7 Ma (reincision 3, Figs. 4 and 17) due to northward sweep of triple junction (Fig. 1), and/or second episode of faulting (Hope Valley graben, Fig. 13).
Pliocene–Holocene (5.3–0)	CSNAC arc magmatism ceases by ca. 6 Ma, within ~10 m.y. of its birth, with minimal overprinting by intrusions or alteration, due to northward sweep of triple junction (Fig. 1). Range front faulting continues to present, associated with Basin and Range volcanism.

Note: Ages are in Ma, using time scale of Geological Society of America (1999).

the dominantly normal polarity latite provide: (1) paleomagnetically distinctive horizons useful for stratigraphic correlation to other localities, and (2) a recognizable datum against which we can paleomagnetically measure differential vertical-axis rotations between tectonic blocks containing these flows.

Subvolcanic and vent-proximal deposits occur along the modern Sierra crest, in close spatial association with the range front faults. These rocks include subvolcanic intrusions, dikes, plugs, lava flows, and block-and-ash-flow tuffs. Subvolcanic andesite intrusions are small in the Ebbetts Pass to Carson Pass areas, and they are even smaller in the Sonora Pass area, where alteration products are correspondingly limited in area. Furthermore, andesitic lava domes appear to be absent from the Sonora Pass area, but they are common in the Carson Pass area, although small (Busby et al., 2007; Fig. 13). This suggests that the arc front was not well defined. We find no large stratovolcanoes like those of the modern Cascades arc; instead, the eruptive centers are small.

Andesite lithofacies considered to record deposition at sites medial to distal from Miocene volcanic centers include volcanic lithic lapilli tuffs, debris-flow deposits, and streamflow deposits. These generally lie 5–25 km west of the modern crest in the Carson Pass area (Busby et al., 2007), but they occur at the crest in the Sonora Pass area, again suggesting a diffuse volcanic front. Debris-flow deposits are interpreted as the distal equivalents of block-and-ash-flows, and streamflow deposits represent reworked equivalents of debris flows.

Numerous workers have suggested that the high-K volcanic rocks (Stanislaus Group) were erupted from the Little Walker center (Figs. 3B and 14; Noble et al., 1974; Brem, 1977; King et al., 2006), although none of the eruptive products of the Stanislaus Group has been identified there, by previous workers or by us. Our reconnaissance field and geochemical work there suggests that the center consists of high-K intrusions and bedded volcaniclastic rocks, many of which are too altered to be suitable for geochemical analysis or dating. We do not find the key diagnostic feature of calderas, which is a very thick accumulation of welded ignimbrite enclosing avalanche blocks, nor is there evidence of resurgent doming of strata around a central intrusion. However, the center does form a roughly circular feature at least partly rimmed by intrusions, so it may represent a buried caldera. The Little Walker center remains the only candidate in the region for the source of the high-K volcanic rocks.

The high-K volcanic strata show extremely rapid variation in thickness, which we attribute to topographic controls of the paleocanyons and reincision events within those paleocanyons, as well as the topographic effects of developing range front faults. For example, the Table Mountain Latite is 400 m thick, with ~26 flow units, along the present-day Sierran crest at Sonora Peak, and it is less than half as thick (180 m), with half as many flows (13) ~20 km to the east, closer to the inferred source at Grouse Meadow (Fig. 10). About 25 km to the west of Sonora Peak, at Dardanelles Cone, the Table Mountain Latite is only 83 m thick, with just two flow units, yet our magnetostratigraphic data suggest that one flow can be correlated all the way from the crest to the western edge of the Sierra. Thus, the sheer volume of the magmatism apparently allowed the lava flows to overwhelm topography within pre-existing canyons, as well as on growing faults. Pyroclastic flows are more mobile by nature, so the presence of Eureka Valley Tuff in paleocanyons far from the inferred source area is less surprising. However, our detailed mapping in progress shows that erosional unconformities exist between the members of the tuff (not shown in Fig. 4A), in addition to erosional unconformities between the high-K formations (Fig. 4A), and deep, widespread unconformities that bound the high-K section (reincision events 2 and 3, Fig. 4A).

Paleochannels and Sierran Landscape Evolution

Early workers concluded that almost all of the present-day topography in the Sierra Nevada Range was created by late Cenozoic uplift (Lindgren, 1911; Ransome, 1898), but later workers have made a distinction between basement topography and river canyons that have been rapidly incised since the Pleistocene (e.g., Bateman and Wahrhaftig, 1966; Huber, 1981, 1990; Stock et al., 2004; Wakabayashi and Sawyer, 2001). "Paleorelief" in the Sierra Nevada is defined as relief that predates late Cenozoic deposits, which can be determined by comparing the elevation of local basement highs to the local base of Cenozoic strata (Fig. 17; Bateman and Wahrhaftig, 1966; Wakabayashi and Sawyer, 2001). Our new mapping shows that paleorelief in the Carson Pass–Kirkwood area is ~650 m (Busby et al., 2007), consistent with previous estimates for the central Sierra (Bateman and Wahrhaftig, 1966). Our finding also agrees with Wakabayashi and Sawyer's (2001) observation of low (<200 m) paleorelief values in the northern Sierra Nevada, high (>1000 m) in the southern Sierra, and intermediate values in the central part of the range.

Our new findings differ from that of previous workers in a few important ways. We find evidence for greater local paleorelief, and higher axial paleo-gradients, than are inferred by previous workers (Busby et al., 2007). To emphasize this difference, we refer to the central Sierran features we have studied as paleocanyons, rather than paleochannels. This terminology contrasts with Wakabayashi and Sawyer's (2001, p. 550–551) interpretation of low Tertiary stream gradients, referring to the "broad alluviated nature of the paleovalleys compared with narrow, bedrock-floored modern canyon (Bateman and Wahrhaftig, 1966; Christensen, 1966; Huber, 1981, 1990) ...consistent with low Eocene-Miocene incision rates." On the basis of work completed so far, we suggest that the central Sierran paleocanyons may not be any broader than the modern canyons (Busby et al., 2007). Furthermore, the paleocanyons in the central Sierra appear to be steep-walled. They are filled with braided stream deposits containing abundant large boulders, and they lack meandering stream deposits, suggesting reasonably high axial gradients. Although our estimates of "local relief" are similar to those made by Clark et al. (2005) for the central Sierra (they estimated <500 m, and we estimate 650 m), our estimates of "local slopes" are much greater. They estimated this slopes <10° for the central Sierra, whereas we map "local slopes" (maximum gradients of unconformities) of up to 50° on granitic basement and up to 70° on metamorphic basement, and up to 48° on unconformities within the Tertiary paleocanyon fill. We also report deeper incisions within the Tertiary section than those reported by Wakabayashi and Sawyer (2001): they reported maximum Eocene-Miocene reincision of 150 m, whereas we propose that paleocanyon fills of the central Sierra record reincision events of 300–650 m. The deepest, highest-gradient unconformities, labeled reincision events 1, 2, and 3 in Figure 4, are interpreted to record previously unrecognized tectonic events (Fig. 17).

The first major reincision event (Figs. 4 and 17B) is represented by up to 650 m of erosion of Oligocene ignimbrites in early Miocene time. These ignimbrites are commonly preserved as thin erosional remnants on the deepest part of the paleocanyon floors, but also occur on paleobenches in granitic basement on the highest parts of paleocanyon walls, indicating that ignimbrites filled the canyons (Fig. 17A) before being largely removed by erosion in the early Miocene (Fig. 17B). This reincision event coincides with the onset of Tertiary arc magmatism.

The second major reincision event (Figs. 4 and 17D) is represented by up to 650 m of erosion of middle Miocene and older volcanic rocks in middle Miocene time (at ca. 11 Ma). This coincides with the onset of faulting, recorded by avalanche deposits and fanning dips in the Sonora Pass area, and immediately precedes eruption of high-K volcanic rocks there.

The third major reincision event (Figs. 4 and 17F) is represented by up to 650 m of erosion of late Miocene and older volcanic rocks in late Miocene time (by ca. 7 Ma). This may record uplift attendant with the northward sweep of the triple junction through the latitude of the central Sierra (Fig. 1), since arc magmatism ceased soon after (by ca. 6 Ma, Fig. 4). Alternatively, reincision event 3 could correspond to a second episode of range front faulting, recorded by development of the Hope Valley graben during the last gasp of arc magmatism there.

Tectonic Controls on Volcanic Styles and Composition

High-K_2O volcanic rocks from the central Sierra Nevada reveal a potential tectonic significance to K_2O contents that has not yet been fully recognized in the Cordillera. Earlier interpretations of K_2O in the Cordillera have emphasized either depth to the subducted slab (Lipman et al., 1972), input of subduction-related fluids (Feldstein and Lange, 1999), or subducted fluid-input combined with delamination of the mantle lithosphere (Manley et al., 2000; Farmer et al., 2002). However, the Central Sierra Nevada Ancestral Cascade (CSNAC) province volcanics, when compared to other volcanics in the region, are interestingly intermediate between the ultrapotassic volcanics of the southern Sierra Nevada and the low-K_2O volcanics that characterize the Lassen region. We propose that this latitudinal gradient to higher K_2O in the southern Sierra Nevada reflects increases in the depths of fractional crystallization to the south, controlled by increases in crustal thickness to the south, which cause clinopyroxene to replace olivine at the liquidus. Experiments and mass-balance calculations further show that clinopyroxene-dominated fractional crystallization will yield elevated K_2O with only moderate increases in SiO_2.

We further propose that crustal thickness variations control the volume of liquid erupted. North of latitude 38°23′N, volcanic rocks dominate the landscape, while south of this latitude, volcanic rocks are rare. We suggest that at 38°23′N, the low-density granitic crust reaches a threshold value such that south of this latitude, the density cap is too thick to allow efficient magma transport to the surface.

We speculate that variations in the composition of volcanic rocks in the central Sierra Nevada are controlled by structural styles. The high-K rocks (Stanislaus Group) probably erupted at the Little Walker center. We infer that this center formed at a right stepover in a dextral transtensional fault zone, along the longest fault we have mapped in the central Sierra, thus producing a pull-apart basin with faults that tapped magmas at relatively deep levels. In contrast, the andesites and trachyandesites (Merhten, Relief, and Disaster Peal Formations) lie along shorter faults with normal to weakly transtensional offset, thus producing half grabens (Sonora Pass) and a full graben (Carson Pass) with faults that tapped magmas at somewhat shallower depths. Transtension is important in convergent margins, but its effects are still poorly understood (Dewey, 2002); our study shows how transtension may affect volcanic styles and compositions. We tentatively suggest that the closest modern structural (not compositional) analogue may be the Sumatra volcanic arc in Indonesia, where small volcanic centers (in Sumatra, mainly rhyolite domes) occur at numerous small faults, whereas larger volcanic centers (in Sumatra, rhyolite caldera complexes) form along releasing stepovers, in pull-apart basins (Bellier and Sebrier, 1994; Chesner, 1998; Bellier et al., 1999). The pull-apart basin at Sonora Pass, and its high-K magmatism, may thus signal the inception of transtensional faulting in the western Walker Lane belt, thus recording the birth of the new plate margin.

APPENDIX 1

Analytical Methods: Wavelength Dispersive X-Ray Fluorescence Spectroscopy

For analysis of the major oxides (SiO_2, TiO_2, Al_2O_3, Fe_2O_3, MgO, MnO, CaO, Na_2O, K_2O, and P_2O_5), we prepared fused glass beads. Sample powders were ground for 3–5 min in a shatterbox, inside a tungsten carbide vessel. Following grinding, powders were calcined overnight at 1000 °C (850–950 °C for high-SiO_2 samples), then ground again in an agate mortar and pestle. Fused beads were prepared from calcined powders using a "prefused" flux from Claisse, which had a composition of 35% Li-tetraborate + 65% Li-metaborate and a sample:flux ratio of 1:6, and then samples were fused into glass beads using the Claisse Fluxy fusion machine; LiI was used as a release agent. Calibrations are based on U.S. Geological Survey (USGS) rock powders: AGV-2, RGM-1, STM-1, SDC-1, BHVO-2, BCR-2, W-2, QLO-1, GSP-2, and DTS-2, and synthetic standards were made up of various proportions of the following oxides: Al_2O_3, SiO_2, Fe_2O_3, MgO, and $NaH_2PO_4(H_2O)$ and KH_2PO_4. Pressed powder pellets (40 mm diameter) were used for the analysis of the following trace elements: V, Cr, Co, Ni, Zn, Rb, Sr, Zr, Nb, Ba, La, Sm, Hf, and Sc. Trace-element calibrations reproduced USGS standard concentrations to 10%–15% relative error. Major-oxide analyses conducted by X-ray fluorescence at California State University–Fresno were compared to reported values for the USGS standards BCR-2 and GSP-2 (Table A1).

TABLE A1. REPRODUCTION OF MAJOR OXIDES FOR USGS STANDARDS BCR-2 AND GSP-2, IN WEIGHT %.

	BCR-2[†]			GSP-2[†,‡]		
	USGS	XRF CSU Fresno[§]		USGS	XRF CSU Fresno	
	COA[#]	Avg.	Std. dev.	COA	Avg.	Std. dev.
SiO_2	54.1	53.8	0.045	67.3	67.4	0.033
TiO_2	2.26	2.28	0.004	0.67	0.68	0.004
Al_2O_3	13.5	13.41	0.015	15.06	15.06	0.015
Fe_2O_3	13.8	13.75	0.005	4.95	4.94	0.004
MnO	-	0.17	0	-	0.01	0
MgO	3.59	3.6	0.005	0.97	1.01	0
CaO	7.12	7.1	0.006	2.12	2.1	0.004
Na_2O	3.16	3.16	0.008	2.81	2.87	0.01
K_2O	1.79	1.8	0.005	5.44	5.46	0.004
P_2O_5	0.35	0.35	0.001	0.29	0.29	0.001

[†]BCR—Basalt, Columbia River; GSP—Granodiorite, Silver Plume (Colorado);
[‡]Renormalized to anhydrous basis.
[§]XRF CSU Fresno—X-ray fluorescence, conducted at California State University, Fresno (Avg. and Std. dev. represent mean and 1 σ on multiple analyses of U.S. Geological Survey standards, when run as unknowns).
[#]COA—Certificate of Analysis, reported by the U.S. Geological Survey (USGS).

ACKNOWLEDGMENTS

Funding for this project was provided by the National Science Foundation (NSF) grants EAR-0125179 (to Busby and Gans), EAR-0337345 and MRI-421272, -0313688 (to Putirka), by the U.S. Geological Survey National Cooperative Geologic Mapping Program, award no. 03HQAG0030 (to Busby) and award no. 05GQAG0010 (to Busby), by University of California–Santa Barbara General Research Grants (to Busby), and by a Geological Society of America research grant (to Hagan). Field assistance from Austin Zinssler, Daisy Pataki, and Carolyn Gorny is gratefully acknowledged. The field area is highly accessible, so we have benefited from field discussions with many people, only some of whom can be listed here for space reasons; these include all 55 participants of the 2004 Volcanological Society of Sacramento field trip, especially field trip honorees Garniss Curtis and Burt Slemmons, as well as additional field discussions with George Bergantz, Larry Garside, Brian Hausback, Chris Henry, Angela Jayko, Nathan King, and George Saucedo.

REFERENCES CITED

Armin, R.A., John, D.A., Moore, W.J., and Dohrenwend, J.C., 1984, Geologic Map of the Markleeville 15 Minute Quadrangle, Alpine County, California: U.S. Geological Survey Miscellaneous Investigations Series Report I-1474, scale 1:62,500.

Atwater, T., and Stock, J., 1998, Pacific–North America plate tectonics of the Neogene Southwestern United States—An update: International Geological Review, v. 40, p. 375–402.

Axelrod, D.L., 1980, Contributions to the Neogene Paleobotany of Central California: Berkeley, University of California Press, 212 p.

Bassett, K.N., and Busby, C., 2005, Structure and tectonic setting of an intra-arc strike-slip basin (Bisbee Basin, southern Arizona), *in* Anderson, T.H., Nourse, J.A., Mckee, J.W., and Steiner, M.B., eds., The Mojave-Sonora Megashear Hypothesis: Development, Assessment, and Alternatives: Geological Society of America Special Paper 393, p. 359–376.

Bateman, P.C., and Wahrhaftig, C., 1966, Geology of the Sierra Nevada, *in* Bailey, E.H., ed., Geology of Northern California: California Division of Mines Bulletin 190, p. 107–172.

Bellier, O., and Sebrier, M., 1994, Relationship between tectonism and volcanism along the Great Sumatran fault zone deduced by SPOT image analysis: Tectonophysics, v. 233, p. 215–231, doi: 10.1016/0040-1951(94)90242-9.

Bellier, O., Bellon, H., Sebrier, M., and Sutanto, M.R.C., 1999, K-Ar age of the Ranau tuffs; implications for the Ranau caldera emplacement and slip-partitioning in Sumatra (Indonesia): Tectonophysics, v. 312, p. 347–359, doi: 10.1016/S0040-1951(99)00198-5.

Bennett, R.A., Wernicke, B.P., and Davis, J.L., 1998, Continuous GPS measurements of contemporary deformation across the northern Basin and Range Province: Geophysical Research Letters, v. 25, p. 563–566, doi: 10.1029/98GL00128.

Bennett, R.A., Davis, J.L., and Wernicke, B.P., 1999, Present-day pattern of Cordilleran deformation in the western United States: Geology, v. 27, p. 371–374, doi: 10.1130/0091-7613(1999)027<0371:PDPOCD>2.3.CO;2.

Borg, L.E., Brandon, A.D., Clynne, M.A., and Walker, R.J., 2000, Re-Os isotopic systematics of primitive lavas from the Lassen region of the Cascade arc, California: Earth and Planetary Science Letters, v. 177, p. 301–317, doi: 10.1016/S0012-821X(00)00051-0.

Borg, L.E., Blichert-Toft, J., and Clynne, M.A., 2002, Ancient and modern subduction zone contributions to the mantle sources of lavas from the Lassen region of California inferred from Lu-Hf isotope systematics: Journal of Petrology, v. 43, p. 705–723, doi: 10.1093/petrology/43.4.705.

Brem, G.F., 1977, Petrogenesis of Late Tertiary Potassic Volcanic Rocks of the Sierra Nevada and Western Great Basin [Ph.D. thesis]: Riverside, University of California, 361 p.

Busby, C.J., and Bassett, K., 2007, Volcanic facies architecture of an intra-arc strike-slip basin, Santa Rita Mountains, Arizona: Bulletin of Volcanology, v. 70, no. 1, p. 85–103.

Busby, C., Wagner, D., Hagan, J., Putirka, K., Pluhar, C., Gans, P., Rood, D., and Skilling, I., 2006, Mapping of Cenozoic Volcanic Rocks in the Central High Sierra: Clues to Understanding Landscape Evolution and Range-Front Faulting: Sonora, California, National Association of Geoscience Teachers Guidebook, Far Western Section, 29 September–1 October 2006, 60 p.

Busby, C., DeOreo, S., Skilling, I., Gans, P, and Hagan, J., 2007, Carson Pass–Kirkwood paleocanyon system: Implications for the Tertiary evolution of the Sierra Nevada, California: Geological Society of America Bulletin (in press).

Camus, G., Gourgaud, A., Moussand-Berthommier, P.-C., and Vincent, P.-M., 2000, Merapi (Central Java, Indonesia): An outline of the structural and magmatological evolution, with a special emphasis to the major pyroclastic events: Journal of Volcanology and Geothermal Research, v. 100, p. 139–163, doi: 10.1016/S0377-0273(00)00135-9.

Cande, S.C., and Kent, D.V., 1995, Revised calibration of the geomagnetic polarity timescale for the Late Cretaceous and Cenozoic: Journal of Geophysical Research, v. 100, p. 6093–6095, doi: 10.1029/94JB03098.

Castor, S.B., Garside, L.J., Henry, C.D., Hudson, D.M., McIntosh, W.C., and Vikre, P.G., 2002, Multiple episodes of magmatism and mineralization in the Comstock District, Nevada: Geological Society of America Abstracts with Programs, v. 34, no. 6, p. 185.

Cecil, M.R., Ducea, M.N., Reiders, P.W., and Chase, C.G., 2006, Cenozoic exhumation of the northern Sierra Nevada, California, from (U-Th)/He thermochronology: Geological Society of America Bulletin, v. 118, p. 1481–1488.

Chase, C.G., and Wallace, T.C., 1988, Flexural isostasy and uplift of the Sierra Nevada of California: Journal of Geophysical Research, v. 93, p. 2795–2802.

Chesner, C.A., 1998, Petrogenesis of the Toba Tuffs, Sumatra, Indonesia: Journal of Petrology, v. 39, p. 397–438, doi: 10.1093/petrology/39.3.397.

Christiansen, M.N., 1966, Late Cenozoic crustal movements in the Sierra Nevada of California: Geological Society of America Bulletin, v. 77, p. 163–182, doi: 10.1130/0016-7606(1966)77[163:LCCMIT]2.0.CO;2.

Christiansen, R.L., and Lipman, P.W., 1972, Cenozoic volcanism and plate tectonic evolution of the western United States: Part 2. Late Cenozoic: Proceedings of the Royal Society of London, v. 271, p. 249–284, doi: 10.1098/rsta.1972.0009.

Christiansen, R.L., Yeats, R.S., Graham, S.A., Niem, W.A., Niem, A.R., and Snavely, P.D., Jr., 1992, Post-Laramide geology of the U.S. Cordilleran region, *in* Burchfiel, B.C., Lipman, P.W., and Zoback, M.L., eds., The Cordilleran Orogen: Conterminous U.S.: Boulder, Colorado, The Geological Society of America, The Geology of North America, v. G-3, p. 261–406.

Clark, M.K., Maheo, G., Saleeby, J., and Farley, K.A., 2005, The non-equilibrium landscape of the southern Sierra Nevada, California: GSA Today, v. 15, no. 9, p. 4–10, doi: 10.1130/1052-5173(2005)015[4:TNLOTS]2.0.CO;2.

Clement, B.M., 2004, Dependence of the duration of geomagnetic polarity reversals on site latitude: Nature, v. 428, p. 637–640.

Cogné, J.P., 2003, PaleoMac: A MacIntosh application for treating paleomagnetic data and making plate reconstructions: Geochemistry, Geophysics, Geosystems, v. 4, p. 1007, doi: 10.1029/2001GC000227.

Curtis, G.H., 1951, The Geology of the Topaz Lake Quadrangle and the Eastern Half of the Ebbetts Pass Quadrangle, scale 1:125,000 [Ph.D. thesis]: Berkeley, University of California, 280 p.

Curtis, G.H., 1954, Mode of origin of pyroclastic debris in the Merhten Formation of the Sierra Nevada: University of California Publications in Geological Sciences, v. 29, p. 453–502.

Dalrymple, G.B., 1963, Potassium-argon dates of some Cenozoic volcanic rocks of the Sierra Nevada: Geological Society of America Bulletin, v. 74, p. 379–390, doi: 10.1130/0016-7606(1963)74[379:PDOSCV]2.0.CO;2.

Davis, D.A., Henry, C.D., Garside, L.J., Faulds, J.E., and Goldstrand, P.M., 2000, Eocene-Oligocene paleovalleys cross the Sierra Nevada–Basin and Range boundary, western Nevada and eastern California: Geological Society of America Abstracts with Programs, v. 32, no. 6, p. 167.

Dewey, J.F., 2002, Transtension in arcs and orogens: International Geology Review, v. 44, p. 402–439.

Dickinson, W.R., 1997, Tectonic implications of Cenozoic volcanism in coastal California: Geological Society of America Bulletin, v. 109, p. 936–934, doi: 10.1130/0016-7606(1997)109<0936:OTIOCV>2.3.CO;2.

Dickinson, W.R., and Snyder, W.S., 1979, Geometry of triple junctions related to San Andreas transform: Journal of Geophysical Research, v. 84, p. 561–572.

Dixon, T.H., Robaudo, S., Lee, J., and Reheis, M.C., 1995, Constraints on present-day Basin and Range deformation from space geodesy: Tectonics, v. 14, p. 755–772, doi: 10.1029/95TC00931.

Dixon, T.H., Miller, M., Farina, F., Wang, H., and Johnson, D., 2000, Present-day motion of the Sierra Nevada block and some tectonic implications for the Basin and Range Province: North American Cordillera: Tectonics, v. 19, p. 1–24, doi: 10.1029/1998TC001088.

Dokka, R.K., and Travis, C.J., 1990, Role of the Eastern California shear zone in accommodating Pacific–North American plate motion: Geophysical Research Letters, v. 17, p. 1323–1326.

Ducea, M.N., and Saleeby, J.B., 1996, Buoyancy sources for a large, unrooted mountain range, the Sierra Nevada, California: Evidence from xenolith thermobarometry: Journal of Geophysical Research, v. 101, p. 8229–8244, doi: 10.1029/95JB03452.

Ducea, M.N., and Saleeby, J.B., 1998, A case for delamination of the deep batholithic crust beneath the Sierra Nevada, California: International Geology Review, v. 40, p. 78–93.

Duffield, W.A., and Dalrymple, G.B., 1990, The Taylor Creek Rhyolite of New Mexico—A rapidly emplaced field of lava domes and flows: Bulletin of Volcanology, v. 52, p. 475–487.

Eddington, P.K., Smith, R.B., and Renggli, C., 1987, Kinematics of Basin and Range intraplate extension, *in* Coward, M.P., Dewey, J.F., and Hancock, P.L., eds., Continental extensional tectonics: Geological Society [London] Special Publication 28, p. 371–392.

Farmer, G.L., Glazner, A.F., and Manley, C.R., 2002, Did lithospheric delamination trigger late Cenozoic potassic volcanism in the southern Sierra Nevada, California: Geological Society of America Bulletin, v. 114, p. 754–768, doi: 10.1130/0016-7606(2002)114<0754:DLDTLC>2.0.CO;2.

Faulds, J.E., Henry, C.D., and Hinz, N.H., 2005, Kinematics of the northern Walker Lane; an incipient transform fault along the Pacific–North American plate boundary: Geology, v. 33, p. 505–508, doi: 10.1130/G21274.1.

Feldstein, S.N., and Lange, R.A., 1999, Pliocene potassic magmas from the King's River region, Sierra Nevada, California: Evidence of melting of a subduction-modified mantle: Journal of Petrology, v. 40, p. 1301–1320, doi: 10.1093/petrology/40.8.1301.

Fisher, R.A., 1953, Dispersion on a sphere: Proceedings of the Royal Society of London, v. A217, p. 295–305.

Fisher, R.V., 1984, Submarine volcaniclastic rocks, *in* Kokelaar, B.P., and Howells, M.F., eds., Marginal basin geology; volcanic and associated sedimentary and tectonic processes in modern and ancient marginal basins: Geological Society [London] Special Publication 16, p. 5–27.

Fisher, R.V., and Heiken, G., 1982, Mt. Pelee, Martinique: May 8 and 20, 1902, pyroclastic flows and surges: Journal of Volcanology and Geothermal Research, v. 13, p. 339–371, doi: 10.1016/0377-0273(82)90056-7.

Fisher, R.V., and Schmincke, H.U., 1984, Pyroclastic Rocks: Berlin, Springer-Verlag, 472 p.

Fisher, R.V., Smith, A.L., and Roobol, J.M., 1980, Destruction of St. Pierre, Martinique, by ash-cloud surges, May 8 and 20, 1902: Geology, v. 8, p. 472–476, doi: 10.1130/0091-7613(1980)8<472:DOSPMB>2.0.CO;2.

Freundt, A., Wilson, C.J.N., and Carey, S., 2000, Ignimbrites and block-and-ash flow deposits, *in* Sigurdsson, H., Houghton, B.F., McNutt, S.R., Rymer, H., and Stix, J., eds., Encyclopedia of Volcanoes: San Diego, Academic Press, p. 581–599.

Gans, P., 1997, Large-magnitude Oligo-Miocene extension in southern Sonora; implications for the tectonic evolution of northwest Mexico: Tectonics, v. 16, p. 388–408.

Garrison, N.J., Busby, C.J., Gans, P., and Wagner, D., 2008, this volume, A mantle plume beneath California? The Mid-Miocene Lovejoy flood basalt, northern California, *in* Wright, J., and Shervais, J., eds., Ophiolites, Arcs, and Batholiths: Geological Society of America Special Paper 438, doi: 10.1130/2008.2438(20).

Garside, L.J., Henry, C.D., Faulds, J.E., and Hinz, N.H., 2005, The upper reaches of the Sierra Nevada auriferous gold channels, *in* Rhoden, H.N., Steininger, R.C., and Vikre, P.G., eds., Window to the World: Reno, Nevada, Geological Society of Nevada Symposium Proceedings, p. 209–235.

Geological Society of America, 1999, Geological Society of America Time Scale.

Giusso, J.R., 1981, Preliminary Geologic Map of the Sonora Pass 15-Minute Quadrangle, California: U.S. Geological Survey Open-File Report 81-1170, scale 1:62,500.

Glazner, A.F., and Supplee, J.A., 1982, Migration of Tertiary volcanism in the southwestern United States and subduction of the Mendocino fracture zone: Earth and Planetary Science Letters, v. 60, p. 429–436, doi: 10.1016/0012-821X(82)90078-4.

Golia, R.T., and Stewart, J.H., 1984, Depositional environments and paleogeography of the Upper Miocene Wassuk Group, west-central Nevada: Sedimentary Geology, v. 38, p. 159–180, doi: 10.1016/0037-0738(84)90078-2.

Grunewald, U., Sparks, R.S.J., Kearns, S., and Komorowski, J.C., 2000, Friction marks on blocks from pyroclastic flows at the Soufriere Hills volcano, Montserrat: Implications for flow mechanisms: Geology, v. 28, p. 827–830, doi: 10.1130/0091-7613(2000)28<827:FMOBFP>2.0.CO;2.

Hamilton, W., and Myers, W.B., 1966, Cenozoic tectonics of the western United States: Reviews of Geophysics, v. 4, p. 509–549.

Hatherton, T., and Dickenson, W.R., 1969, The relationship between andesitic volcanism and seismicity in Indonesia, the Lesser Antilles, and other island arcs: Journal of Geophysical Research, v. 74, p. 5301–5310.

Heiken, G., and Wohletz, K., 1985, Volcanic Ash: Berkeley, University of California Press, 246 p.

Henry, C.D., and Perkins, M.E., 2001, Sierra Nevada–Basin and Range transition near Reno, Nevada: Two-stage development at 12 and 3 Ma: Geology, v. 29, p. 719–722, doi: 10.1130/0091-7613(2001)029<0719:SNBART>2.0.CO;2.

Hinz, N.H., Faulds, J.E., and Henry, C.D., 2003, Dextral displacement on the Honey Lake fault zone, northern Walker Lane, northeast California and westernmost Nevada; preliminary constraints inferred from Oligocene ash-flow tuff stratigraphy: Geological Society of America Abstracts with Programs, v. 35, no. 6, p. 347.

Horton, T.W., Sjostrom, D.J., Abruzzese, M.J., Poage, M.A., Waldbauer, J.R., Hren, M.T., Wooden, J.L., and Chamberlain, C.P., 2004, Spatial and temporal variation of Cenozoic surface elevation in the Great Basin and Sierra Nevada: American Journal of Science, v. 304, p. 862–888.

House, M.A., Wernicke, B.P., and Farley, K.A., 1998, Dating topography of the Sierra Nevada, California, using apatite (U-Th)/He ages: Nature, v. 396, p. 66–69, doi: 10.1038/23926.

House, M.A., Wernicke, B.P., and Farley, K.A., 2001, Paleo-geomorphology of the Sierra Nevada, California, from (U-Th)/He ages in apatite: American Journal of Science, v. 301, p. 77–102, doi: 10.2475/ajs.301.2.77.

Huber, N.K., 1981, Amount and timing of late Cenozoic uplift and tilt of the central Sierra Nevada, California—Evidence from the upper San Joaquin River basin: U.S. Geological Survey Professional Paper 1197, 28 p.

Huber, N.K., 1990, The late Cenozoic evolution of the Tuolumne River, central Sierra Nevada, California: Geological Society of America Bulletin, v. 102, p. 102–115.

Irvine, T.N., and Baragar, W.R., 1971, A guide to the chemical classification of the common volcanic rocks: Canadian Journal of Earth Sciences, v. 8, p. 523–548.

John, D.A., Garside, L.J., and Wallace, A.R., 1999, Magmatic and tectonic setting of late Cenozoic epithermal gold-silver deposits in northern Nevada, with an emphasis on the Pah Rah and Virginia Ranges and the northern Nevada Rift, *in* Kizis, J.A., ed., Low-Sulfidation Gold Deposits in Northern Nevada; Olinghouse Deposit, Mule Canyon Deposit, Midas Deposit: Geological Society of Nevada Special Publication 29, p. 65–158.

Jones, C.H., and Dollar, R.S., 1986, Evidence of Basin and Range extensional tectonics in the Sierra Nevada: The Durrwood Meadows swarm, Tulare County, California (1983–1984): Bulletin of the Seismological Society of America, v. 76, p. 439–461.

Jones, C.H., Kanamori, H., and Roecker, S.W., 1994, Missing roots and mantle "drips": Regional Pn and teleseismic arrival times in the southern Sierra Nevada and vicinity, California: Journal of Geophysical Research, v. 99, p. 4567–4601, doi: 10.1029/93JB01232.

Jones, C.H., Farmer, G.L., and Unruh, J.R., 2004, Tectonics of Pliocene removal of lithosphere of the Sierra Nevada, California: Geological Society of America Bulletin, v. 116, p. 1408–1422, doi: 10.1130/B25397.1.

Keith, W.J., Dohrenwend, J.C., Guisso, J.R., and John, D.A., 1982, Geologic Map of the Carson-Iceberg and Leavitt Lake Roadless Areas, Central Sierra Nevada, California: U.S. Geological Survey Report MF-1416-A, scale 1:62,500.

King, N.M., Hillhouse, J.W., Gromme, S., and Hausback, B.P., 2006, Stratigraphy, paleomagnetism, and anisotropy of magnetic susceptibility of the Miocene Stanislaus Group, central Sierra Nevada and Sweetwater Mountains, California and Nevada: Eos (Transactions, American Geophysical Union), v. 87, no. 52, Fall Meeting, Abstract GP11A-0063.

Kirschvink, J.L., 1980, The least-squares line and plane and the analysis of palaeomagnetic data: Geophysical Journal of the Royal Astronomical Society, v. 62, p. 699–718.

Lahren, M.M., and Schweickert, R.A., 1995, Lake Tahoe Field Trip Guide of the AAPG Rocky Mountain Section Meeting, Reno, Nevada: Tulsa, Oklahoma, American Association of Petroleum Geologists, p. 23.

Le Bas, M.J., Le Maitre, R.W., Streckeisen, A., and Zanettin, B., 1986, A chemical classification of volcanic rocks based on the total alkali-silica diagram: Journal of Petrology, v. 27, p. 745–750.

Le Pourhiet, L., Gurnis, M., and Saleeby, J., 2006, Mantle instability beneath the Sierra Nevada Mountains and Death Valley extension (California, USA): Earth and Planetary Science Letters, v. 251, p. 104–119, doi: 10.1016/j.epsl.2006.08.028.

Lindgren, W., 1911, The Tertiary Gravels of the Sierra Nevada of California: Washington, D.C., U.S. Geological Survey, 222 p.

Lipman, P.W., Prostka, H.J., and Christiansen, R.L., 1972, Cenozoic volcanism and plate-tectonic evolution of the western United States: Part I. Early and middle Cenozoic: Philosophical Transactions of the Royal Society of London, ser. A, v. 271, p. 217–248, doi: 10.1098/rsta.1972.0008.

Manley, C.R., Glazner, A.F., and Farmer, G.L., 2000, Timing of volcanism in the Sierra Nevada of California: Evidence for Pliocene delamination of the batholithic root?: Geology, v. 28, p. 811–814, doi: 10.1130/0091-7613(2000)28<811:TOVITS>2.0.CO;2.

Mavko, B.B., and Thompson, G.A., 1983, Crustal and upper mantle structure of the northern and central Sierra Nevada: Journal of Geophysical Research, v. 88, p. 5874–5892.

McKee, E.H., and Noble, D.C., 1976, Age of the Cardenas lavas, Grand Canyon, Arizona: Geological Society of America Bulletin, v. 87, p. 1188–1190, doi: 10.1130/0016-7606(1976)87<1188:AOTCLG>2.0.CO;2.

Meen, J.K., 1990, Elevation of potassium content of basaltic magma by fractional crystallization: The effect of pressure: Contributions to Mineralogy and Petrology, v. 104, p. 309–331, doi: 10.1007/BF00321487.

Miyabuchi, Y., 1999, Deposits associated with the 1990–1995 eruption of Unzen volcano, Japan: Journal of Volcanology and Geothermal Research, v. 89, p. 139–158, doi: 10.1016/S0377-0273(98)00129-2.

Morton, J.L., Silberman, M.L., Bonham, H.F., Garside, L.J., and Noble, D.C., 1977, K-Ar ages of volcanic rocks, plutonic rocks, and ore deposits in Nevada and eastern California—Determinations run under the USGS-NBMG cooperative program: Isochron/West, v. 20, p. 19–29.

Mosier, D.L., 1991, Tertiary Volcanic History of the Markleeville Peak Area, Alpine County, California [M.S. thesis]: Hayward, California State University, 95 p.

Noble, D.C., Slemmons, D.B., Korringa, M.K., Dickinson, W.R., Al-Rawi, Y., and McKee, E.H., 1974, Eureka Valley Tuff, east-central California and adjacent Nevada: Geology, v. 2, p. 139–142, doi: 10.1130/0091-7613(1974)2<139:EVTECA>2.0.CO;2.

Noble, D.C., Korringa, M.K., Church, S.E., Bowman, H.R., Silberman, M.L., and Heropoulos, C., 1976, Elemental and isotopic geochemistry of nonhydrated quartz latite glasses from the Eureka Valley Tuff, east-central California: Geological Society of America Bulletin, v. 87, p. 754–762, doi: 10.1130/0016-7606(1976)87<754:EAIGON>2.0.CO;2.

Oldow, J.S., 2000, Displacement transfer and differential block motion in the central Walker Lane, western Great Basin: Eos (Transactions, American Geophysical Union), v. 81, p. 1174.

Oldow, J.S., 2003, Active transtensional boundary zone between the western Great Basin and Sierra Nevada block, western U.S. Cordillera: Geology, v. 31, p. 1033–1036, doi: 10.1130/G19838.1.

Pekar, S.F., Christie-Blick, N., Miller, K.G., and Kominz, M.A., 2003, Quantitative constraints on the origin of stratigraphic architecture at passive continental margins; Oligocene sedimentation in New Jersey, U.S.A.: Journal of Sedimentary Research, v. 72, p. 227–245.

Piper, A.M., Gale, H.S., Thomas, H.E., and Robinson, T.W., 1939, Geology and Ground Water Hydrology of the Mokelumne Area, California: U.S. Geological Survey Water-Supply Paper 780, 230 p.

Pluhar, C.J., and Coe, R.S., 1996, Paleomagnetism of the Stanislaus Group, Table Mountain Latite Member, Sierra Nevada, California: Eos (Transactions, American Geophysical Union), v. 77, p. 158.

Poage, M.A., and Chamberlain, C.P., 2002, Stable isotopic evidence for a pre–middle Miocene rain shaddow in the western Basin and Range; implications for the paleotopography of the Sierra Nevada: Tectonics, v. 21, p. 10.

Priest, G.R., 1979, Geology and Geochemistry of the Little Walker Volcanic Center, Mono County, California [Ph.D. thesis]: Corvallis, Oregon, Oregon State University, 315 p.

Putirka, K., Johnson, M., Kinzler, R., and Walker, D., 1996, Thermobarometry of mafic igneous rocks based on clinopyroxene-liquid equilibria, 0–30 kbar: Contributions to Mineralogy and Petrology, v. 123, p. 92–108, doi: 10.1007/s004100050145.

Ransome, F.L., 1898, Some Lava Flows on the Western Slope of the Sierra Nevada, California: U.S. Geological Survey Bulletin 89, p. 71.

Roelofs, A., and Glazner, A.F., 2004, Tertiary volcanic activity at Sonora Pass, CA: Arc and non-arc magmatism in the central Sierra Nevada: Eos (Transactions of the American Geophysical Union), abstract V13B-1476.

Rood, D., Busby, C., Jayko, A., and Luyendyk, B., 2005, Neogene to Quaternary kinematics of the central Sierran frontal fault system in the Sonora Pass region: Preliminary structural, paleomagnetic and neotectonic results: Geological Society of America Abstracts with Programs, v. 37, no. 4, p. 65.

Roullet, F., 2006, The Miocene Dixie Mountain Volcanic Center, Northern Sierra Nevada: Eroded Stratovolcano or Polygenetic Cryptodome Complex? [M.S. thesis]: Santa Barbara, University of California, 67 p.

Saleeby, J.B., and Foster, Z., 2004, Topographic response to mantle lithosphere removal in the southern Sierra Nevada region, California: Geology, v. 32, p. 245–248, doi: 10.1130/G19958.1.

Sauber, J., Thatcher, W., Solomon, S.C., and Lisowski, M., 1994, Geodetic slip rate for the Eastern California shear zone and recurrence time of Mojave Desert earthquakes: Nature, v. 367, p. 264–266, doi: 10.1038/367264a0.

Savage, J.C., Lisowski, M., and Prescott, W.H., 1990, An apparent shear zone trending north-northwest across the Mojave Desert into Owens Valley, eastern California: Geophysical Research Letters, v. 17, p. 2113–2116.

Schweickert, R.A., Lahren, M.M., Smith, K.D., and Karlin, R.D., 1999, Preliminary map of active faults of the Lake Tahoe basin: Seismological Research Letters, v. 70, p. 306–312.

Schweickert, R.A., Lahren, M.M., Karlin, R.D., and Howle, J., 2000, Lake Tahoe active faults, landslides, and tsunamis, *in* Lageson, D.R., Peters, S.G., and Lahren, M.M., eds., Great Basin and Sierra Nevada: Boulder, Colorado, Geological Society of America Field Guide 2, p. 1–22.

Schweickert, R.A., Lahren, M.M., Smith, K.D., Howle, J.F., and Ichinose, G., 2004, Transtensional deformation in the Lake Tahoe region, California and Nevada, USA: Tectonophysics, v. 392, p. 303–323, doi: 10.1016/j.tecto.2004.04.019.

Sigurdsson, H., Houghton, B.F., McNutt, S.R., Rymer, H., and Stix, J., 2000, Encyclopedia of Volcanoes: San Diego, Academic Press, 1471 p.

Skilling, I., Busby, C.J., and Imai, T., 2004, Andesitic peperite-bearing debris flows; physical volcanology and paleoenvironment of the Miocene Merhten Formation, California: Geological Society of America Abstracts with Programs, v. 36, no. 4, p. 85.

Slemmons, D.B., 1953, Geology of the Sonora Pass Region [Ph.D. thesis]: Berkeley, University of California, 201 p.

Slemmons, D.B., 1966, Cenozoic Volcanism of the Central Sierra Nevada, California: Geology of Northern California: California Division of Mines and Geology Bulletin, v. 170, p. 199–208.

Slemmons, D.B., 1975, Cenozoic deformation along the Sierra Nevada Province and Basin and Range Province boundary: California Geology, v. 28, p. 99–105.

Stock, G.M., Anderson, R.S., and Finkel, R.C., 2004, Pace of landscape evolution in the Sierra Nevada, California, revealed by cosmogenic dating of cave sediments: Geology, v. 32, p. 193–196, doi: 10.1130/G20197.1.

Surpless, B.E., Stockli, D.F., Dumitru, T.A., and Miller, E.L., 2002, Two-phase westward encroachment of Basin and Range extension into the northern Sierra Nevada: Tectonics, v. 21, p. 1002, doi: 10.1029/2000TC001257.

Thatcher, W., Foulger, G.R., Julian, B.R., Svarc, J.L., Quily, E., and Bawden, G.W., 1999, Present-day deformation across the Basin and Range Province, western United States: Science, v. 283, p. 1714–1718, doi: 10.1126/science.283.5408.1714.

Trexler, J.H., Jr., Cashman, P.H., Muntean, T., Schwartz, K., Ten Brink, A., Faulds, J.E., Perkins, M., and Kelly, T., 2000, Neogene basins in western Nevada document the tectonic history of the Sierra Nevada–Basin and Range transition zone for the last 12 Ma, *in* Lageson, D.R., Peters, S.G., and Lahren, M.M., eds., Great Basin and Sierra Nevada: Boulder, Colorado, Geological Society of America Field Guide 2, p. 97–116.

Unruh, J.R., 1991, The uplift of the Sierra Nevada and implications for late Cenozoic epeirogeny in the western Cordillera: Geological Society of America Bulletin, v. 103, p. 1395–1404, doi: 10.1130/0016-7606(1991)103<1395:TUOTSN>2.3.CO;2.

Unruh, J.R., Humphrey, J., and Barron, A., 2003, Transtensional model for the Sierra Nevada frontal fault system, eastern California: Geology, v. 31, p. 327–330, doi: 10.1130/0091-7613(2003)031<0327:TMFTSN>2.0.CO;2.

Voight, B., Constantine, E.K., Siswowidjoyo, S., and Torley, R., 2000, Historical eruptions of Merapi Volcano, Central Java, Indonesia, 1768–1998: Journal of Volcanology and Geothermal Research, v. 100, p. 69–138, doi: 10.1016/S0377-0273(00)00134-7.

Wagner, D.L., Saucedo, G.J., and Grose, T.L.T., 2000, Tertiary Volcanic Rocks of the Blairsden Area, Northern Sierra Nevada, California, *in* Brooks, E.R., and Dida, L.T., eds., Field Guide—Geology and Tectonics of the Northern Sierra Nevada: California Division of Mines and Geology Special Publication, v. 122, p. 155–172.

Wakabayashi, J., and Sawyer, T.L., 2001, Stream incision, tectonics, uplift, and evolution of topography of the Sierra Nevada, California: The Journal of Geology, v. 109, p. 539–562, doi: 10.1086/321962.

Wallace, R.E., Davis, J.F., and McNally, K.C., 1984, Terms for expressing earthquake potential, prediction, and probability: Bulletin of the Seismological Society of America, v. 74, p. 1819–1825.

Wernicke, B.P., Clayton, R., Ducea, M., Jones, C.H., Park, S., Ruppert, S., Saleeby, J., Snow, J.K., Squires, L., Fliedner, M, Jiracek, G., Keller, R., Klemperer, S., Luetgert, J., Malin, P., Miller, K., Mooney, W., Oliver, H. and Phinney, R., 1996, Origin of high mountains in the continents: The southern Sierra Nevada: Science, v. 271, p. 190–193, doi: 10.1126/science.271.5246.190.

Whitney, J.D., 1880, The Auriferous Gravels of the Sierra Nevada of California, Contributions to American Geology: Memoirs of the Museum of Comparative Zoology, Volume 1: Cambridge, Massachusetts, Harvard University Press, 659 p.

Wolfe, J.A., Schorn, H.E., Forest, C.E., and Molnar, P., 1997, Paleobotanical evidence for high altitudes in Nevada during the Miocene: Science, v. 276, p. 1672–1675.

Manuscript Accepted by the Society 16 July 2007